Spectrum Sharing for Multi-User Massive MIMO Networks

by

Rosa Saif

A thesis submitted to the
School of Graduate and Postdoctoral Studies in partial
fulfillment of the requirements for the degree of

Doctor of Philosophy
in
Electrical and Computer Engineering

Faculty of Engineering and Applied Science
University of Ontario Institute of Technology (Ontario Tech University)
Oshawa, Ontario, Canada

December, 2023

THESIS EXAMINATION INFORMATION

Submitted by: **Rosa Saif**

Doctor of Philosophy in **Electrical and Computer Engineering**

Thesis Title: Spectrum Sharing for Multi-User Massive MIMO Networks

An oral defense of this thesis took place on November 27, 2023 in front of the following examining committee:

Examining Committee:

Chair of Examining Committee:	Prof. Ali Gerami
Research Supervisor:	Prof. Shahram ShahbazPanahi
Examining Committee Member:	Prof. Min Dong
Examining Committee Member:	Prof. Shahram Shah Heydari
University Examiner:	Prof. Ying Wang
External Examiner:	Prof. Shahrokh Valaee (University of Toronto)

The above committee determined that the thesis is acceptable in form and content and that a satisfactory knowledge of the field covered by the thesis was demonstrated by the candidate during an oral examination. A signed copy of the Certificate of Approval is available from the School of Graduate and Postdoctoral Studies.

ABSTRACT

In this dissertation, we propose a creative approach to advance 5G network technologies by investigating the impact of employing an underlay spectrum sharing (USS) scheme on the performance of two massive multi-input-multi-output (MIMO) networks. We explore an USS approach where a multi-user massive MIMO network (primary network (PN)), i.e., the owner of the frequency spectrum, allows another multi-user massive MIMO network, the secondary network (SN), to utilize its allocated spectrum to serve secondary users (SUs). Within this context, we devise joint power allocation and beamforming techniques at the SN for both conventional time-division duplexing (C-TDD) and reverse time-division duplexing (R-TDD) protocols. In the C-TDD approach, both the PN and SN operate concurrently in either the uplink (UL) or downlink (DL) modes. In the R-TDD protocol, the PN and SN do not simultaneously operate in the UL or DL modes. It is worth noting that, during the training phase of the PN (learning phase of the SN), all the SN's nodes remain silent and listen to the PN to acquire as much information as possible about the PN. The optimization problems aim to maximize the SN's achievable sum-rate in both UL and DL, while guaranteeing the minimum acceptable individual rate for each primary user (PU) and satisfying the SN's power constraints. Effective solutions are proposed for both the C-TDD and R-TDD protocols, including novel methods to mitigate interference caused by the SN's nodes to the PN's nodes during UL and DL phases. We assume that the PN parameters are set by the PN independently, without considering the presence of the SN, to minimize the SN's potential impact on the PN's frame structure and system design. Our simulation results demonstrate that for a moderate-scale SN coverage area, both C-TDD and R-TDD approaches reveal almost comparable performance. Additionally, changes in the SN's settings have a small effect on the total sum-rate of the PN when our proposed method is employed. Finally, for all tested values of the number of antennas at the secondary base stations (SBS), the R-TDD approach outperforms the C-TDD approach when the SN coverage area is large, and vice versa.

Keywords: *underlay spectrum sharing (USS); time-division duplexing (TDD); multi-user massive MIMO networks; beamforming; interference mitigation*

AUTHOR'S DECLARATION

I hereby declare that this thesis consists of original work of which I have authored. This is a true copy of the thesis, including any required final revisions, as accepted by my examiners.

I authorize the University of Ontario Institute of Technology (Ontario Tech University) to lend this thesis to other institutions or individuals for the purpose of scholarly research. I further authorize University of Ontario Institute of Technology (Ontario Tech University) to reproduce this thesis by photocopying or by other means, in total or in part, at the request of other institutions or individuals for the purpose of scholarly research. I understand that my thesis will be made electronically available to the public.

Rosa Saif

STATEMENT OF CONTRIBUTIONS

Part of this dissertation (described in Chapters 3 and 4) has been published as:

- R. Saif, Z. Pourgharehkhan, S. ShahbazPanahi, M. Bavand, and G. Boudreau, "Underlay Spectrum Sharing in Massive MIMO Systems," IEEE Transactions on Cognitive Communications and Networking, vol.9, no.3, pp.647-663, 2023.

I hereby certify that I am the sole author of this thesis. I have used standard referencing practices to acknowledge ideas, research techniques, or other materials that belong to others. Furthermore, I hereby certify that I am the sole source of the creative works and/or inventive knowledge described in this thesis.

ACKNOWLEDGEMENTS

First and foremost, I would like to express my deep and sincere appreciation to my supervisor, Prof. Shahram ShahbazPanahi, for his unwavering support, patience, guidance, enthusiasm, and immense knowledge throughout this journey. I am profoundly grateful for his teachings, insightful feedback, and constructive advice, all of which have been invaluable to my research. This endeavor would not have been possible without his assistance.

I would also like to extend my heartfelt gratitude to my cherished husband, Soroush, for his unwavering love, support, patience, and wholehearted belief in me. To my beloved daughter, Sophia, I am thankful for her encouraging presence in my life. My heartfelt thanks go to my parents for their unconditional love and for providing me with the strength to pursue my dreams. To my sisters and my brother, I express my gratitude for their encouragement and love. Lastly, I am deeply appreciative of all my caring friends for their support and kindness.

Contents

List of Acronyms

5G	5 Generation
4G	4 Generation
GSM	Global System for Mobile Communications
LTE	Long-Term Evolution
3GPP	3rd Generation Partnership Project
MIMO	Multi-Input-Multi-Output
USS	Underlay Spectrum Sharing
PN	Primary Network
SN	Secondary Network
BS	Base Station
PBS	Primary Base Station
SBS	Secondary Base Station
PU	Primary User
SU	Secondary User
UL	Uplink
DL	Downlink

QoS	Quality of Service
CSI	Channel State Information
SINR	Signal-to-Interference-plus-Noise Ratio
FDD	Frequency-Division Duplexing
TDD	Time-Division Duplexing
C-TDD	Conventional Time-Division Duplexing
R-TDD	Reverse Time-Division Duplexing
BF	Beamforming
ZF	Zero-forcing
MZF	Modified Zero-forcing
ZF BF	Zero-forcing Beamforming
SoI	Source of Interference
APAR	Average Per-User Achievable Rate

List of Figures

List of Tables

Chapter 1

Introduction

1.1 Motivation

1.1.1 5G Technology

Over the past few decades, cellular communication has undergone a continuous evolution characterized by the introduction of various network architectures [2], multiple access techniques [3, 4], and emerging technologies [5]. This evolution has been driven by the ever-growing demand for improved quality of service, higher data rates, superior spectral efficiency, increased capacity, and reduced latency [6–8]. In response to these expectations, significant strides have been taken in the design of cellular systems to meet the growing needs and demands of users [9, 10]. Among these advancements, 5G technology has emerged as a revolutionary force that holds the promise of transforming the existing wireless network landscape with its exceptional capabilities and innovative features [10]. 5G brings a new era to the field of communication, empowered by emerging technologies like massive multi-input multi-output (MIMO) [11], internet of things (IoT) [12], millimeter-wave (mm-Wave) [13], spectrum sharing in cognitive radio networks [14, 15] and more. These technologies serve as enablers for the unparalleled potential of 5G.

1.1.2 Massive MIMO

Massive MIMO technology offers numerous advantages for wireless communication, particularly in the 5G networks field [16]. By deploying a large number of antennas at both the transmitter and receiver, or only on one side, massive MIMO significantly enhances the performance and efficiency of wireless systems [17–19]. One key benefit is the substantial increase in spectral efficiency [20]. In addition, higher data rates and improved capacity of wireless networks are enabled [16, 21]. With the ability to serve multiple users simultaneously, massive MIMO provides spatial multiplexing gains, effectively utilizing the available spectrum resources and optimizing network throughput [22–26]. The technology also offers enhanced interference management capabilities by employing advanced signal processing techniques, such as beamforming and spatial nulling [27–30]. This enables better coexistence in dense deployment scenarios and mitigates interference, resulting in improved overall system performance. Moreover, massive MIMO systems demonstrate robustness against channel fading and small-scale variations, ensuring reliable and consistent connections [31]. Furthermore, massive MIMO enhances energy efficiency by utilizing advanced algorithms for optimized resource allocation and power control, leading to reduced power consumption. The deployment of massive MIMO in 5G networks unlocks the potential for massive connectivity, supporting a massive number of devices and enabling IoT applications. Overall, massive MIMO technology is a fundamental block of 5G networks, offering higher spectral efficiency, improved capacity, enhanced interference management, and energy efficiency.

1.1.3 Beamforming

Beamforming is an effective technique employed in wireless communication systems, including 5G technology, to enhance the performance and efficiency of signal transmission [32,33]. It involves the precise shaping and directing transmitted or received signals using an array of antennas. Beamforming allows for the focusing of signal energy in specific directions, enabling improved signal quality, extended coverage, and increased

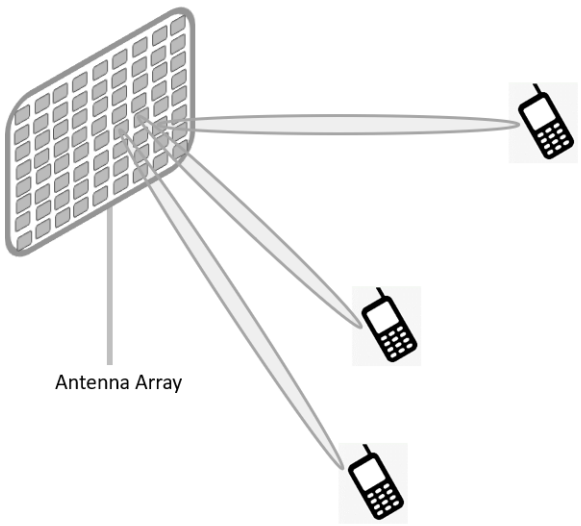

Figure 1.1: Massive MIMO with beamforming

capacity [34, 35]. In the context of 5G, massive MIMO beamforming techniques have gained significant attention. Massive MIMO beamforming utilizes a large number of antennas at both the transmitter and receiver, enabling the system to exploit spatial diversity and multiplex multiple users concurrently. By leveraging the high spatial resolution and channel capacity provided by massive MIMO, beamforming in 5G enhances the signal strength, mitigates interference, and increases spectral efficiency. This technique optimizes the transmission of data to multiple users simultaneously, leading to improved data rates, higher network capacity, and enhanced overall system performance [36]. The combination of beamforming and massive MIMO (Figure 1.1) in 5G technology offers substantial potential for meeting the increasing demands of high-speed and reliable wireless communication, supporting various applications such as high-definition video streaming and IoT deployments [37].

1.1.4 Spectrum Sharing

Spectrum sharing is a technique that allows multiple wireless communication systems to effectively utilize the limited available spectrum resources [38]. In the context of 5G, spectrum sharing is crucial for improving spectrum efficiency and accommodating

the growing demand for wireless services [39, 40]. A spectrum sharing network typically comprises two networks: the primary network (PN) and the secondary network (SN). The PN holds exclusive rights or licensed access to a specific portion of the radio frequency spectrum. In spectrum sharing scenarios, the SN coexists with the PN and opportunistically utilizes the spectrum resources of the PN under predefined conditions and constraints. Spectrum sharing techniques can be classified into three primary paradigms: underlay, overlay, and interweave [41]. Underlay spectrum sharing (USS) is highlighted in the existing literature as one of the paradigms, where secondary nodes (secondary transmitter(s) and secondary receiver(s)) are allowed to operate alongside primary nodes (primary transmitter(s) and primary receiver(s)) while ensuring that interference remains below a specified threshold [42, 43]. This constraint is crucial to maintain the quality of service (QoS) for the PN. In contrast, the overlay scheme enables collaboration between the SN and the PN, allowing simultaneous transmission by both networks. In this scheme, the interference generated by the SN can be compensated by utilizing a portion of the SN's power to retransmit PN signals [44, 45]. This requires the SN to possess knowledge of the primary users' (PUs) codebooks and messages [46, 47]. Another spectrum sharing paradigm mentioned is interweave spectrum sharing, where the SN opportunistically accesses the spectrum holes of the PN to avoid causing interference to the PN nodes. The SN operates only when the PN does not utilize the spectrum, ensuring interference-free communication for the PN [48, 49]. By incorporating spectrum sharing techniques, 5G networks can efficiently utilize spectrum resources, improve spectrum efficiency, and accommodate multiple networks and users. These techniques play a vital role in optimizing spectrum utilization, enhancing the overall capacity and performance of wireless networks, as well as satisfying the increasing demands of 5G applications [40, 50, 51].

1.1.5 TDD and FDD

Time-division duplexing (TDD) and frequency-division duplexing (FDD) are duplexing techniques widely used in wireless communication networks [52, 53]. In TDD, bidirec-

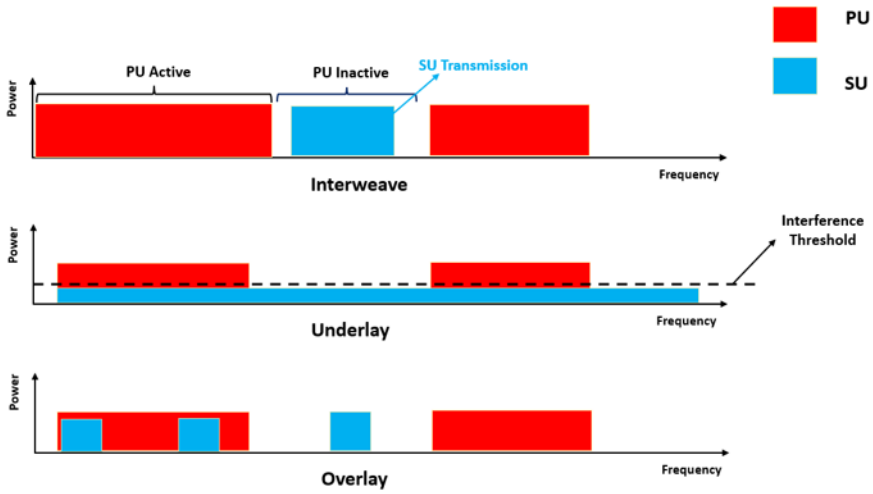

Figure 1.2: Spectrum sharing [1]

tional communication can be enabled over a shared frequency channel by dividing time into alternating time slots for uplink (UL) and downlink (DL) transmissions [54, 55]. In contrast, UL and DL transmissions are separated in FDD technique, using distinct frequency bands [56, 57]. Several advantages are achieved when TDD is utilized. Firstly, it allows for flexible allocation of UL and DL time slots, making it adaptable to varying traffic patterns. TDD systems can dynamically adjust the allocation ratio based on demand, optimizing resource utilization and enhancing system capacity [58, 59]. In massive MIMO systems, where traffic patterns can demonstrate substantial variations, TDD's adaptability is noticeable [60]. Secondly, employing TDD, which provides communication networks with the benefits of symmetrical channel characteristics, simplifies the implementation of techniques like beamforming and interference cancellation. TDD is extensively employed in wireless systems like Wi-Fi and certain 4G and 5G networks [61–63]. In contrast, utilizing FDD provides advantages through its clear separation of UL and DL transmissions. As different frequency bands are used in FDD for transmission and reception, a consistent QoS for both UL and DL can be guaranteed. Simultaneous transmission and reception are possible, reducing interference and enabling better coverage [62, 63]. FDD is widely used in established cellular networks

such as the global system for mobile communications (GSM) and long-term evolution (LTE) [63–65]. Each technique has certain limitations. Employing TDD may increase interference between UL and DL due to shared frequency resources, potentially affecting system performance [62, 66]. In communication networks, when FDD technique is utilized, dedicated frequency bands for UL and DL are required, which can lead to spectrum fragmentation and inefficient spectrum utilization [63]. The choice between TDD and FDD depends on specific application requirements, traffic characteristics, and the trade-off between flexibility and improved coverage.

1.1.6 Spectrum Sharing in Massive MIMO

Spectrum sharing in massive MIMO networks is a technique that enables efficient utilization of limited radio spectrum resources while catering to the increasing demands of wireless communication in the context of emerging technologies like 5G [67–69]. This technique facilitates the coexistence of multiple systems by allowing them to share the same frequency bands. One of the key benefits of spectrum sharing in massive MIMO networks is the significant improvement in spectral efficiency [51]. By efficiently allocating and sharing spectrum resources among different networks or users, spectrum utilization is optimized, leading to higher data rates, and improved overall system performance. The use of massive MIMO further enhances the benefits of spectrum sharing by leveraging spatial multiplexing and beamforming capabilities. The large number of antennas enables the system to exploit spatial diversity and multiplex multiple users concurrently, resulting in improved signal quality, enhanced coverage, and reduced interference [22, 70–72]. Moreover, spectrum sharing in massive MIMO networks promotes flexibility and scalability. It enables seamless integration of various technologies, services, and applications within the same frequency bands, facilitating the provision of diverse services to meet the varying needs of users. By effectively sharing spectrum resources, massive MIMO networks can accommodate the growing number of users and applications while ensuring efficient and reliable communication [68, 73, 74]. There are several studies in the literature that focus on the utilization of spectrum sharing in mas-

sive MIMO systems, where the PN shares the network information, i.e., the channel state information (CSI) of the PUs with the SN. We aim to minimize this information exchange. This goal is achieved by proposing a novel frame structure and designing a learning phase for the SN to listen to the PN and acquire as much information as possible about the PN during this phase. By employing this approach, the burden on the PN imposed by the SN is effectively mitigated. Two distinct frame structures for the training, uplink, and downlink alignment of the PN and SN are devised, and the system performance is subsequently compared.

1.2 Objectives and Methodologies

This section provides an overview of the objectives and research methodologies that will be pursued in the subsequent chapters of this dissertation.

1.2.1 C-TDD Approach in Multi-User Massive MIMO Networks with USS

Objective

- Chapter 3 of this dissertation focuses on the joint optimization of power allocation and beamforming in a single-cell wireless system comprising two networks, namely, the PN and SN. We employ the USS technique to enable the SN's opportunistic use of the PN's spectrum. This is done while respecting constraints to keep the interference below a certain threshold accepted by the PUs in both UL and DL and satisfying the SN's power constraints. The study considers conventional time-division duplexing (C-TDD) for PN and SN's UL and DL. The channels are assumed to be reciprocal and flat fading, considering both perfect and imperfect CSI. The primary goal is to maximize the total sum-rate of the SN in UL and DL while the individual rate requirements of the PN's users are guaranteed and SN's power constraints are satisfied. Furthermore, we aim to mitigate disruptions caused by the SN during collaboration and sharing the PN informa-

tion. We seek to find the optimal beamforming technique to reduce interference from the SN nodes on the PN nodes in both the UL and DL modes.

Methodology

- In Chapter 3, we consider a cognitive radio scheme where two massive MIMO networks, the PN and SN, are intended to operate in the same frequency spectrum. Our goal is maximizing the total sum-rate of the SN in UL and DL while the constraints of the PN and SN are satisfied. In our proposed wireless communication system, we assume that both networks are multi-user. The PN owns the licensed frequency spectrum, and the SN employs USS to access the PN's spectrum under specific conditions. The UL and DL modes for both PN and SN occur concurrently using C-TDD. A frame structure is designed, including phases of learning, training, UL, and DL for the SN. During the learning phase, SN is quiet, listening to the PN transmissions to gather PN's information. A spatial arrangement is established for PN and SN co-locations. The SN is located in the corner of the PN area, and the primary base station (PBS) and secondary base station (SBS) are located at the centers of the PN and SN, respectively. User terminals, the primary users (PUs) and secondary users (SUs), are randomly distributed within their designated regions. We assume that all channels are flat fading, reciprocal, and do not vary with time within their coherence time. While the PN does not take into account the presence of the SN in designing the PN parameters, the SN must recognize all PN nodes and control SN interference during UL and DL transmissions. Our optimization problem targets UL and DL sum-rate maximization of the SN while satisfying the SN's power and PUs' data rate constraints. This main optimization problem can be separated into UL and DL sub-problems, each includes the respective objective functions and associated constraints. In the UL state of the SN, some approximations are necessary to reformulate the constraints of optimization problem. Beamforming and power allocation coefficients are meticulously devised for both PN and SN, employing distinct beamforming

techniques in the UL and DL modes. Power allocation for the PUs and SUs is calculated using techniques like water-filling. Numerical analyses show the efficacy of our solutions, significantly amplifying spectral utilization in Scenario A. Further assessments illustrate the influence of SN presence on PN's UL and DL performance, and examine the implications of perfect and imperfect CSI, as well as the impact of our approximations.

1.2.2 R-TDD Approach in Multi-User Massive MIMO networks with USS

Objective

- Chapter 4 of this thesis builds upon the system model introduced in Chapter 3, where the focus remains on the joint optimization of power allocation and beamforming. However, in this chapter, the approach shifts to employing R-TDD to define the UL and DL alignment of both PN and SN. The primary objective is to obtain an optimized solution that addresses the joint design of beamformers and power allocation for user terminals to maximize the overall sum-rate of the SN in both UL and DL. This optimization problem is subject to crucial constraints, ensuring that the signal-to-interference-plus-noise ratios (SINRs) at the PUs maintain certain predefined thresholds while also satisfying the power constraints of the SN. We aim to leverage the knowledge of the subspace of two base stations in the SN to transmit in the spectrum holes of the PN and safeguard the PN from interference caused by the SN.

Methodology

- In Chapter 4 of our thesis, we address the challenge of maximizing the total sum-rate of the SN within our wireless communication system model. In contrast to chapter 3, our focus now shifts to the use of R-TDD to align the UL and DL modes of the PN and SN. Unlike C-TDD, where the PN's UL coincides with the SN's UL and vice versa, R-TDD synchronizes the PN's UL with the SN's DL and the

PN's DL with the SN's UL. As mentioned in Chapter 3, we assume that all channels are reciprocal, flat fading, and do not vary with time within their coherence time. While the design of PN parameters remains independent of the SN's presence, the SN must identify all PN nodes and regulate its impact on them during signal transmission. We address this challenge through an optimization problem, with the objective function aiming to maximize the SN's sum-rate in both UL and DL, while satisfying the SN's power constraints and ensuring the minimum acceptable individual rate for all PUs. Similar to chapter 3, this core optimization problem can be divided into separate UL and DL optimization sub-problems, each with its respective objective functions and constraints. Notably, in Scenario B, no approximation is required to solve the optimization problems. During the learning phase, the SN gathers PN information. Furthermore, we thoroughly design beamforming and power allocation coefficients for both the PN and SN, leveraging distinct beamforming techniques for UL and DL states in each network. Our numerical results demonstrate the effectiveness of our solutions, significantly enhancing spectral utilization in Scenario B. Additionally, we investigate the impact of varying SN parameters on the performances of both the PN and SN under various parameter settings.

1.3 Summary of Contributions

The principal contributions of this present dissertation are outlined below:

- One of the primary objectives of this study is to efficiently exploit the limited frequency resources in wireless communication systems. To achieve this goal, a USS scheme is employed and a communication frame is devised for the SN. This frame dictates that the SN nodes start communicating only after the PN's training phase to protect the PN's training performance. During the PN's training phase, referred to as the *learning phase* of the SN, all nodes in the SN remain silent and listen to the PN. This strategic approach enables the SN to estimate the CSI of the

PUs, thus significantly reducing the extent of cooperation required between the PN and the SN for channel estimation purposes.

- In this research, we study two distinct scenarios founded on the alignment of UL and DL modes between the PN and SN. Harnessing the adaptability and spectral efficiency inherent in TDD, the investigation employs conventional TDD (C-TDD) in Scenario A and reverse TDD (R-TDD) in Scenario B. Within both Scenarios A and B, a comprehensive approach is undertaken to jointly design the SBS's transmit and receive beamformers, as well as the SN's power allocation scheme for both UL and DL phases. To do so, two optimization problems are formulated, corresponding to Scenarios A and B. These problems aim to maximize the SN's sum-rates while considering the power constraints of the SN's nodes and guaranteeing the given data rates of the PUs. Solutions for these optimization problems are presented. Notably, the optimization problem corresponding to each scenario can be separated into two independent optimization problems: one dedicated to the SN's UL and the other dedicated to the SN's DL.

- In Scenario A, we adopt a accurate approach to address the SN's UL phase optimization problem. We employ the modified zero-forcing (MZF) beamforming strategy, as proposed in [75] to design the receive beamformers at the SBS. This MZF technique allows the SBS to fully protect itself from interference caused by the PUs, while also ensuring that each SU is shielded from interference caused by other SUs. Following this, we extend our approach to design the power allocation schemes for the SUs through a computationally efficient convex optimization problem. Shifting focus to the SN's DL phase within Scenario A, we once again apply the MZF beamforming methodology to design the SBS's transmit beamformers. This strategic choice empowers the SBS to provide comprehensive protection to the PUs. Notably, our devised scheme leads to a unique opportunity for the SN to operate efficiently in the spatial spectrum holes of the PN. Leveraging the effectiveness of the MZF, our solution for the SBS's power allocation strategy

ultimately converges to a water-filling type algorithm. This approach efficiently resolves the optimization problem while maintaining computational efficiency.

- Solving the optimization problem in Scenario B for the SN's UL phase requires an advanced approach. To ensure the comprehensive protection of the SBS from the interference caused by the PBS, we strategically design receive beamformers at the SBS. To achieve this, we propose a novel zero-forcing beamforming (ZF BF) method that effectively utilizes knowledge of the subspace of the SBS-PBS channel matrix, in addition to the SBS-SU channel matrix. Notably, our proposed zero-forcing (ZF) method does not require any DL training, significantly reducing training overhead for both the PN and SN. By adopting our proposed ZF approach, we determine the optimal power allocation scheme for the SUs through a convex optimization problem. In the SN's DL phase within Scenario B, we employ our newly proposed subspace-based ZF technique as the transmit beamformers of the SBS. This strategic choice empowers the SBS to entirely shield the PBS from the interference caused by the SBS. Based on these transmit beamformers, our study demonstrates that the optimum power allocation scheme for the SBS leads to a water-filling type algorithm, which offers an efficient and effective solution for the optimization problem.

- During the simulation section, it is shown that when the SN's coverage area is large (small), Scenario B outperforms (underperforms) Scenario A in terms of the total achievable sum-rate of the SN, for all tested values for the number of antennas at the SBS. In case of moderate SN's coverage areas, the performances of these two Scenarios are close to each other. Furthermore, our numerical experiments indicate that the SN's parameter variations have a minimal impact on the PN's sum-rate when our proposed scheme is implemented. Additionally, we illustrate that the impact of the imperfect CSI on our proposed technique is negligible, when we employ the channel estimation techniques proposed in [76]. Finally, we compare the performance of our proposed scheme with an existing work.

1.4 List of Publications

The research undertaken in this dissertation has resulted in the following publication [77].

1. R. Saif, Z. Pourgharehkhan, S. ShahbazPanahi, M. Bavand, and G. Boudreau, "Underlay Spectrum Sharing in Massive MIMO Systems", IEEE Transactions on Cognitive Communications and Networking, vol.9, no.3, pp.647-663, 2023.

1.5 Outline of Dissertation

The subsequent chapters of this dissertation are structured to provide a comprehensive understanding of our research objectives.

In Chapter 2, an extensive survey is conducted, exploring recent research discoveries relevant to our contexts concerning, massive MIMO and spectrum sharing techniques that cater to the requirements of 5G networks.

In chapter 3, we study the joint power allocation and beamforming challenge within a wireless communication system. This system consists of two multi-user networks, each equipped with a massive MIMO base station serving their respective users. One network (PN) has the frequency band ownership, while the other network (SN) seeks to access this frequency band through the USS mechanism under the C-TDD approach, denoted as Scenario A. We formulate an optimization problem with the aim to maximize total sum-rate of SN while satisfying the constraints associated with interference management and power allocation budgets. This leads to the derivation of optimal power allocation and beamforming coefficients for both networks.

In Chapter 4, the investigation extends to explore the implications of the R-TDD approach, designated as Scenario B, on the performance of the networks established within the system model presented in Chapter 3. A comprehensive evaluation of network performance in the UL and DL states is conducted, followed by an assessment of the impact of network-specific parameters on both networks' performances within the

context of both scenarios.

Chapter 5 summarizes everything, presenting a clear summary of the findings and suggesting directions for future research.

1.6 Notations

Boldface lowercase and uppercase letters are employed for column vectors and matrices. The transpose, Hermitian, conjugate, and pseudoinverse of matrix $\mathbf{X}$ are indicated as $\mathbf{X}^T$, $\mathbf{X}^H$, $\mathbf{X}^*$ and $\mathbf{X}^\dagger$, respectively. Notations $\mathbf{I}$ and $\mathbf{1}$ represent the identity matrix and a vector with all elements set to one, respectively. Lastly, $\|\mathbf{x}\|$ denotes the Euclidean norm of vector $\mathbf{x}$, and $\odot$ signifies the Hadamard product. The frame consists of N_f symbols, with N_t symbols allocated for training, N_up symbols for uplink, and N_dp symbols for downlink phases. The relationship $N_\mathrm{f} = N_\mathrm{t} + N_\mathrm{up} + N_\mathrm{dp}$ holds. The frame index is denoted by f, and the total frames in both scenarios are represented by F. We assume flat fading channels that are reciprocal and remain constant within their coherence time.

Chapter 2

Literature Review

2.1 Multi-User Networks

Wireless communication has undergone remarkable evolution, transitioning from its initial focus on point-to-point communication to addressing the growing demand for simultaneous multi-user connectivity [78–80]. The concept of multi-user networks, where multiple users can communicate and share resources concurrently, has significantly shaped the development of wireless communication systems. In the early years of wireless communication, systems were primarily designed for single-user scenarios. However, as the demand for multi-user networks and efficient connectivity grew, researchers and engineers began to explore the possibilities of enabling communication among multiple users within the same network infrastructure. This shift marked the emergence of multi-user networks and it is a crucial moment in the wireless communication landscape [81]. Initial attempts in multi-user networks aimed to accommodate more users simultaneously and improve spectral efficiency. Multi-user networks offer many advantages, leading their multiplication to modern wireless systems [82, 83]. The most notable advantage is increased capacity [84–86]. By enabling multiple users to share the available resources, multi-user networks effectively leverage the available spectrum, boosting the overall system capacity. This capacity enhancement is particularly crucial in meeting the growing demands of data-intensive applications and devices. Moreover, multi-user networks promote efficient resource utilization. By allowing con-

current communications, these networks reduce idle time and optimize the use of radio resources, resulting in improved spectral efficiency [85]. This efficiency directly leads to enhanced user experiences and enables service providers to serve larger user-base networks. While multi-user networks offer remarkable benefits, they also introduce complexities and challenges. One of the primary challenges is interference management. As multiple users communicate simultaneously, interference between users can degrade the quality of service [87]. Designing algorithms and protocols to mitigate interference and ensure fair resource allocation becomes critical in multi-user networks [88]. Over the years, the concept of multi-user networks has evolved, powered by advancements in technology, such as massive MIMO [89, 90] and cognitive radio [91, 92]. These technologies have enabled even more efficient resource allocation, interference mitigation, and improved overall network performance. Looking ahead, the emergence of 5G and beyond results in even more sophisticated multi-user network architectures to meet the demands of a hyper-connected world [93]. This journey of wireless communication from single-user to multi-user networks shows the strong commitment to enhance capacity, efficiency, and user experiences.

2.2 Spectrum Sharing Technique

Spectrum sharing is a promising solution in wireless communication, addressed the ever-increasing demand for spectrum resources [94]. The history of spectrum sharing traces back to the early days of wireless communication. The introduction of cellular networks marked a significant milestone in the evolution of spectrum sharing. The concept of cellular networks allowed for the reuse of frequencies across cells, effectively enabling spectrum sharing among multiple users. The implementation of frequency reuse patterns in cellular networks paved the way for more efficient spectrum utilization and greater capacity [95,96]. The late 1990s and early 2000s saw the emergence of cognitive radio [97], a revolutionary technology that introduced dynamic spectrum access [98,99]. Cognitive radio systems intelligently sense and utilize available spectrum bands oppor-

tunistically, dynamically allocating frequencies based on real-time spectrum availability. This technology enabled SN's nodes to access spectrum bands that were underutilized by PN's nodes [41, 94, 100–102], thereby optimizing spectrum utilization while minimizing interference [103]. In some networks, in return, the SN may pay a fee [104] and/or may help the primary network to improve the quality of service provided to the primary users [105]. Today, spectrum sharing has become a critical strategy in the face of spectrum scarcity and the increasing of wireless devices and applications. While spectrum sharing offers immense potential, it also poses challenges such as interference management, regulatory issues, and ensuring fair coexistence between different users. Researchers and industry stakeholders continue to explore advanced technologies, such as advanced modulation schemes, interference mitigation techniques, and cooperative spectrum sharing, to address these challenges and unlock the full potential of spectrum sharing [106–109].

2.3 Massive MIMO Technology

Massive MIMO is a revolutionary technology that has transformed the topography of wireless communication systems. It represents a paradigm shift from traditional antenna configurations to systems with an extraordinary number of antennas at both the transmitter and receiver [110]. The concept of massive MIMO in wireless communication emerged in the early 2000s through the foundational work of researchers like Gerard J. Foschini [21] and Thomas L. Marzetta [111, 112]. Their pioneering ideas centered around deploying a large number of antennas at base stations, paving the way for the revolutionary massive MIMO technology. Subsequent research advancements demonstrated the potential benefits of increased spectral efficiency [72, 110, 113–117], link reliability [118, 119], and energy efficiency [17] with massive antenna arrays. As technology evolved, practical implementations and testbeds were developed, leading to its incorporation into standards by organizations like the 3rd Generation Partnership Project (3GPP) for 4G and 5G networks [120]. In the 2010s, massive MIMO witnessed

its debut in commercial networks [121, 122]. Mobile network operators recognized its potential to address the explosive growth in data demand and the need for higher network capacity [114]. With the rollout of 5G networks, massive MIMO became a defining feature, offering significant improvements in spectral efficiency, coverage, and user experience [20]. Ongoing research continues to explore advanced beamforming techniques, interference management, and integration with emerging technologies, ensuring that massive MIMO remains at the forefront of wireless communication innovation, addressing the evolving demands of modern connectivity [123].

2.4 ZF beamforming

Zero-Forcing Beamforming (ZF BF) is a signal processing technique widely used in wireless communication systems, particularly in the context of multi-user MIMO networks [124, 125]. It aims to nullify the interference caused by signals transmitted from the users to unintended receivers. The fundamental idea behind ZF BF is to create nulls in the beamforming weights corresponding to interfering users, effectively canceling their contribution at the intended receivers. This technique has gained significant attention due to its ability to mitigate multi-user interference and improve spectral efficiency [125]. ZF BF offers substantial benefits in multi-user scenarios, where multiple users transmit simultaneously to their respective receivers. By minimizing interference, ZF BF enhances the overall signal quality and capacity of the network [126, 127]. However, it has limitations when channel conditions are challenging or channel estimation is inaccurate as it may amplify noise [125, 128]. Over the past few decades, research has focused on enhancing ZF BF's performance, including hybrid techniques that combine it with other methods like maximum ratio transmission (MRT) to mitigate its weaknesses [129]. While ZF BF has its advantages in simplifying beamforming and managing interference, further advancements are being explored to overcome its limitations and optimize its application in various wireless scenarios.

2.5 Spectrum Sharing in Massive MIMO Systems

As we explained in previous sections, both massive MIMO schemes and spectrum sharing approaches aim to improve the utilization of heavily under-utilized precious radio frequency spectrum. In this study, we focus on these techniques to address 5G requirements and performance objectives. We focus on a single-cell communication network configuration. This network comprises two significant components: a multi-user massive MIMO PN and a multi-user massive MIMO SN. The PUs and SUs in this network are assumed to be single-antenna. Our goal is to allow the SBS to communicate with the SUs by exploiting the *spatial spectrum holes* of the PN. By using a USS scheme in this massive MIMO networks, we can get advantages of both *spectral* and *spatial* dimensions. To accomplish this, we explore two distinct communication protocols: C-TDD, referred to as Scenario A, and R-TDD, denoted as Scenario B. These protocols enable us to align the UL and DL transmission modes between the PN and SN. For each of these scenarios, we formulate an optimization problem. Our main objective is to maximize the weighted sum-rates in both the UL and DL for the SN. However, it's crucial to emphasize that we must do this while guaranteeing the QoS constraints for the PN and power constraints for the SN. To do so, we devise joint power allocation and beamforming schemes at the SN for both scenarios.

Several studies have focused on exploiting the advantages of the massive MIMO techniques in the USS cognitive radio systems [75, 130–136].

In [75], the authors consider a multi-user massive MIMO SN and a multi-pair PN. Assuming imperfect CSI of the PUs and the SUs at the SBS, the authors address the problem of joint power allocation and maximization of the number of the SUs served by the SBS in the DL transmission. To this end, they propose a modified ZF (MZF) which allows the SBS to work in the null-space of the PUs' channels, thereby protecting the PUs.

The authors of [130] consider a system consisting of a multi-user massive MIMO PN and a single-user massive MIMO SN and study the DL transmission of the SN. In

such a system, for both cases of perfect and imperfect CSI, a lower bound for the average achievable rate of the SU is derived. It is shown that using a large number of antennas at the secondary base station (SBS) mitigates the harmful effect of the channel estimation errors on the SN's performance. However, when the number of antennas at the primary base station (PBS) and number of primary users (PUs) grow large with the same rate, the SN's performance is severely degraded.

The study in [131] considers the uplink (UL) transmission in a multi-cell massive MIMO system where each cell consists of a multi-user PN and a multi-user SN. The SN's UL achievable rate is obtained based on a relay-assisted method for the perfect/imperfect CSI of the SBS-Relay-SU and the PBS-PU channels. It is proven that for such massive MIMO scheme, the SN's performance is independent of the PN's interference. However, the SN's performance is significantly degraded when the CSI errors are high.

In [132], the DL communication of a system consisting of a multi-cell multi-user PN and a single-cell multi-user SN is investigated. Employing massive MIMO technology at both the PBS and the SBS, the authors solve the power allocation optimization problem at the SN by maximizing the DL sum-rate of the SN while satisfying each PU's QoS. It is illustrated that in this scheme, both PN and SN are required to share their users' CSI in addition to their positions. Also, using this method, the number of the SUs served by the SBS is limited to the number of inactive PUs, yielding the spectral efficiency reduction in the SN.

The study in [133] focuses on UL transmission of a system consisting of a PN and a SN, which are multi-cell multi-user massive MIMO networks and employ the conventional zero-forcing (ZF) method at the base stations. The optimal transmit power control coefficients for the SUs and PUs are derived through maximizing the UL achievable rates of the SUs. For the case when perfect CSI of the SBS-SU links and perfect CSI of PBS-PU links are available at the SBS, this scheme allows the PN and the SN to operate independently with unbounded number of the antennas at the PBS and the SBS.

However, this method suffers from a remarkable performance degradation for the case of the imperfect CSI.

The authors of [134] consider a multi-user massive MIMO SN which co-exists with a multi-user massive MIMO PN. They devise a DL power allocation in the SN using a clustering-based approach, which relies on a non-orthogonal pilot transmission. The DL achievable rates of the SUs heavily hinge on the accuracy of the CSI.

The authors of [135] consider a setup consisting of a peer-to-peer PN and a multi-cell multi-user massive MIMO SN equipped with two SBSs in each cell. For such a system, the authors maximize the number of the SUs served by the SBSs by proposing a DL scheduling strategy. This scheme may yield a high latency in the SN, thereby degrading the SN's spectral efficiency. Moreover, deploying two SBSs per cell increases the implementation cost of the network.

All aforementioned studies operate in TDD mode, as relying on channel reciprocity, TDD results in less training overhead, compared to FDD mode[1] [116, 137]. Nevertheless, utilizing TDD causes more interference in co-existing networks because of pilot contamination [136].

In [138], a new TDD-based scheme, referred to as R-TDD, is employed to manage the interference between the networks. In the R-TDD approach, the co-existing networks synchronously operate in opposite transmission directions. In other words, when one network is in UL, the other one is in DL and vice versa.

In [136], the authors compare the performances of the C-TDD and the R-TDD schemes in massive MIMO USS setups consisting of a multi-cell PN and a multi-cell SN. To do so, assuming imperfect CSI of the SUs (PUs) at the SBS (PBS), the authors derive the UL and the DL achievable rates of the PN and those of the SN, when both PBS and SBS employ the conventional ZF beamformer. They prove that by using the R-TDD protocol, the SN's and PN's performances are asymptotically independent. However, in this protocol, designing the PN's parameters, such as the lengths of the UL/DL intervals, depends on the SN's parameters.

[1]The scheme presented in [135] is applicable in both FDD and TDD systems.

It is important to acknowledge that these studies, [75, 130–136], have some unexplored aspects that need to be considered in future research within this field of study.

The authors of [75, 130], exclusively focus on the DL mode of their respective communication networks. Furthermore, in [75], the PN is equipped with single-antenna primary receivers and transmitters, which results in more interference to the SN nodes compared to the time that PN is equipped with a massive MIMO base station.

In [131], only the UL state of the network is examined. Additionally, the authors utilize a relay in the SN, which results in increased complexity and latency in the communication network.

In [132], only the DL mode of communication is studied. Moreover, a backhaul link is employed to share users' locations and CSI information. This necessitates the PBS providing the SBS with the PN's information, leading to disruption and performance degradation in the PN.

The authors of [133] exclusively focus on the UL state of communication and do not take the DL state into account. Furthermore, conventional ZF BF is employed at both PBS and SBS. It is worth noting that by utilizing pilot sharing schemes, interference between the networks increases, necessitating additional efforts to compensate for its effects.

In [134], only the DL mode is considered. Moreover, the non-orthogonal multiple access (NOMA) technique is employed, which implies that network performance is highly sensitive to channel conditions.

In [135], the authors only study the performance of the system in DL. They also utilize two SBS in each cell which increases the implementation cost.

In [136], the conventional ZF BF is employed at both the SBS and PBS. This means that the SBS does not have any further protection protocol to avoid interference with the PN nodes. Additionally, both the UL and DL modes of the SN relay on information provided by the PBS to the SBS. This increases the potential for disruption of the PBS and has a negative effect on PN performance.

In this dissertation, we consider two multi-user networks, both equipped with massive MIMO base stations, while the PUs and SUs are single-antenna terminals. We investigate two communication protocols: C-TDD (Scenario A) and R-TDD (Scenario B) protocols. Our study focuses on assessing the performance of both the PN and SN in both UL and DL states. Our optimization problems address joint power allocation and beamforming schemes at the SN for both scenarios. These problems aim to maximize the SN sum-rate in both UL and DL, while ensuring the satisfaction of PN and SN constraints. Instead of employing conventional ZF BF, we utilize the MZF and a newly proposed ZF BF technique to mitigate the interference caused by the SN nodes to the PN nodes. The PN parameters are designed without taking the SN presence into account. We introduce a *learning phase* for the SN, where the SN remains quiet and listen to the PN to gather as much information as possible about the PN. This approach is adopted to minimize disruption caused by the SBS to the PBS. Additionally, we investigate the impact of changing PN and SN parameters on the performance of both networks. This analysis provides insights into how adjustments in network parameters affect overall network performance.

It is noteworthy that our proposed work differs in several aspects from the aforementioned studies. We briefly summarize the key distinctions of each as follows. In contrast to [130–132, 134], where only UL or DL transmission is studied, we herein investigate the USS problem for both UL and DL phases. In addition, where only the SN's performance is studied in [130–132,134], we comprehensively investigate the performances of both PN and SN. Different from [130,131,134,136], our proposed solution mitigates the sensitivity the SN's and PN's performances on the channel estimations errors. Compared with [130–134, 136], in our proposed method, the PN will have less cooperation with the SN in order to fulfill the aim of the USS. Unlike the C-TDD and R-TDD schemes of [136], in our proposed Scenarios A and B, the SN remains silent during the PN's training phase and this is what differentiates our scheme from the those proposed in [136]. Also, we present a solution in which the PN's power allocation strat-

egy does not depend on that of the SN. Last but not least, while the schemes of [136] rely on the conventional ZF, we devise a ZF-type of beamformer which allows the SBS to work in the spatial spectrum holes of the PN.

To the best of the author's knowledge, the investigation of both primary and secondary network performances in UL and DL modes under both C-TDD and R-TDD approaches remains unexplored. This includes scenarios where the presence of the SN is not considered during the design of PN parameters. It is done with the aim of focusing on minimizing communication between primary and secondary base stations. Additionally, there is a lack of comprehensive exploration into the impact of each network's parameters changes on the performance of the other network and the overall system.

Chapter 3

Underlay Spectrum Sharing in a C-TDD Massive MIMO Network

In this chapter, our main focus is on addressing the joint power allocation and beamforming design challenges in the context of the C-TDD protocol, referred to as Scenario A. The primary objective is to ensure the QoS requirements of the PN while maximizing the total sum-rate of the SN in both the UL and DL. We formulate an optimization problem to achieve this, considering the minimum acceptable data rate of each PU in both UL and DL, while satisfying the power constraints of the SN. To tackle the main optimization problem effectively, we divide it into two separate optimization problems for UL and DL, each with its corresponding solutions. The remainder of this chapter is structured as follows: Section 3.1 and 3.2 present the system model and data models of the signals received by the SN's and PN's nodes in both UL and DL, respectively. In Section 3.3, we introduce the main optimization problem and detail the strategies used to address the UL and DL aspects separately. Subsequently, Section 3.4 delves into a comprehensive discussion of the numerical results obtained from our proposed approaches. These results clarify the effectiveness and performance of the power allocation and beamforming schemes in enhancing the overall system capacity and ensuring the desired QoS for both PN and SN in the C-TDD mode.

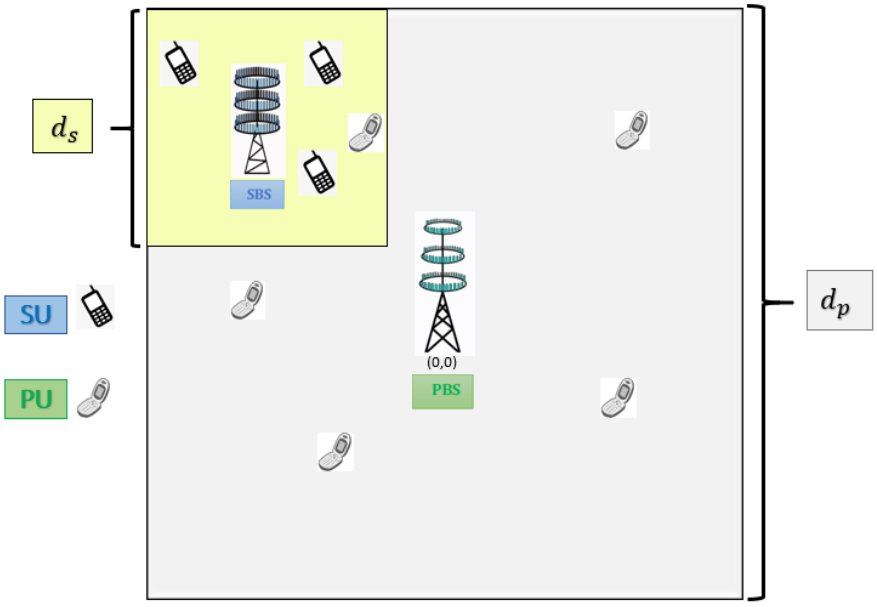

Figure 3.1: Geometry of the two networks.

3.1 System Model

As shown in Fig. 3.1, we consider a cognitive radio scheme where two massive MIMO networks are meant to operate in the same RF bandwidth. One of these two networks, referred to as the PN, owns the RF bandwidth. The other network, herein referred to as the SN, aims to use the RF bandwidth in an opportunistic manner with as minimal a disturbance as possible to the PN. The PN consists of a base station, equipped with M_{p} antennas, and N_{p} single-antenna users, which are referred to as the PUs. Similarly the SN consists of a base station, which is equipped with M_{s} antennas, and N_{s} single-antenna users, which are referred to as the SUs. Each base station employs transmit beamformer (pre-coder) and receive beamformer (combiner) in downlink and uplink, respectively, to communicate with their respective users. We refer to the base stations in the PN and SN as PBS and SBS, respectively. In the PN, the communication frame consists of three modes (phases), namely the training mode, the UL mode; and the DL mode. In this chapter, we study the performance of Scenario A, as shown in Fig. 3.2.

As can be seen in this figure when the PN is in training mode (signified as "T" interval), the SN remains quiet i.e., the SN is in here (signified as "L" interval). The reason is that during the PN training phase, the PBS is "naked" or unarmed meaning that the PBS is not equipped with a beamformer during training. Indeed, the goal in training is to estimate the PUs channels, at each antenna of the PBS, simultaneously using temporally orthogonal training symbols via matched filtering. These matched filters are nothing but the linear combiners constructed from the orthogonal vectors of the training symbols. We assume that the SN does not have the knowledge of which training symbol vectors have been used by the PN users, and hence, the SN must avoid training during the training phase of the PN. As a result, the training in the SN will have to coincide with UL mode in the PN. In Scenario A, the SN uplink follows the SN training and the SN downlink coincides with the PN downlink. In this chapter, our goal is to devise communication schemes (i.e., design beamformers and power allocations) for Scenario A and analyze the PN and SN performances in both UL and DL.

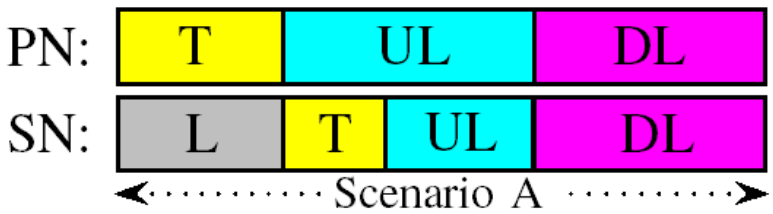

Figure 3.2: Scenario A in frame f.

3.2 Learning Phase

This section includes a brief explanation of the channel estimation method proposed in [76] for a multi-user massive MIMO system, which is utilized in the current research. The authors of [76] proposed a communication frame structure for the SN containing two phases, namely the learning phase and the spectrum sharing phase. During the learning phase, the SN is silent and listens to the PN to estimate the SBS-PUs' chan-

nels at the SBS. A least Squares estimator is employed to perform this estimation by utilizing the knowledge of the subspace spanned by the SBS-PUs' channel vectors. In the spectrum sharing phase, the SBS estimates the SBS-SUs' channels and then serves the SUs. Aiming to estimate the SUs' channels at the SBS, a time-multiplexed training phase, is designed. In this scheme, the training phase of the SN has an overlap with both the training and UL modes of the PN. Two different approaches are studied to estimate the SBS-SUs' channels at the SBS by utilizing the estimated SBS-PUs' channels and the data received at the SBS during the spectrum sharing interval.

3.3 Data Models of Scenario A

In this section, we formulate data models of the signals received by the SN's and PN's nodes in both UL and DL for Scenario A.

3.3.1 PN's UL data model

Let $\mathbf{r}_1(f,t) \in \mathbb{C}^{N_\mathrm{p}\times 1}$ represent the vector of the received signals after beamforming at the PBS during the PN's UL in frame f at time t, for $t = 1, 2, \ldots, N_{\mathrm{up}}$. We can write

$$\mathbf{r}_1(f,t) = \mathbf{W}_1^H \mathbf{H}_1\big(\mathbf{a}_1(t) \odot \mathbf{s}_1(f,t)\big) + \mathbf{W}_1^H \mathbf{H}_{12}\big(\mathbf{a}_2(t) \odot \mathbf{s}_2(f,t)\big) + \mathbf{W}_1^H \mathbf{n}_1(f,t). \tag{3.1}$$

Here, we define $\mathbf{H}_1 \triangleq [\mathbf{h}_{1,1} \;\; \mathbf{h}_{1,2} \;\; \cdots \;\; \mathbf{h}_{1,N_\mathrm{p}}] \in \mathbb{C}^{M_\mathrm{p}\times N_\mathrm{p}}$, and $\mathbf{H}_{12} \triangleq [\mathbf{h}_{12,1} \;\; \mathbf{h}_{12,2} \;\; \cdots \;\; \mathbf{h}_{12,N_\mathrm{s}}] \in \mathbb{C}^{M_\mathrm{p}\times N_\mathrm{s}}$, where $\mathbf{h}_{1,l} \in \mathbb{C}^{M_\mathrm{p}\times 1}$ is the channel vector between the PBS and the l-th PU, for $l = 1, 2, \ldots, N_\mathrm{p}$, and $\mathbf{h}_{12,k} \in \mathbb{C}^{M_\mathrm{p}\times 1}$ is the channel vector between the PBS and the k-th SU, for $k = 1, 2, \ldots, N_\mathrm{s}$. Also, we use $\mathbf{s}_1(f,t) \in \mathbb{C}^{N_\mathrm{p}\times 1}$ to represent the vector of the UL unit-power symbols transmitted by all PUs at time t in frame f, for $t = 1, 2, \ldots, N_{\mathrm{up}}$, whereas $\mathbf{s}_2(f,t) \in \mathbb{C}^{N_\mathrm{s}\times 1}$ stands for the vector[1] of the unit-power symbols transmitted by all SUs during training and UL of frame f, for $t = 1, 2, \ldots, N_{\mathrm{up}}$, whereas $\mathbf{s}_2(f,t) \in \mathbb{C}^{N_\mathrm{s}\times 1}$ stands for the vector of the unit-power symbols transmitted

[1]Note that as shown in Fig. 3.2, the length of the signal transmitted by SUs during training and UL is equal to the length of the signals transmitted by the PUs during uplink.

by all SUs during training and UL of frame f, for $t = 1, 2, \ldots, N_{\text{up}}$. We also define the matrix of PU's UL beamformers as $\mathbf{W}_1 \triangleq [\mathbf{w}_{1,1} \quad \mathbf{w}_{1,2} \quad \cdots \quad \mathbf{w}_{1,N_{\text{p}}}] \in \mathbb{C}^{M_{\text{p}} \times N_{\text{p}}}$ with $\mathbf{w}_{1,l} \in \mathbb{C}^{M_{\text{p}} \times 1}$ being the unit-norm beamforming weight vector used by the PBS to serve the l-th PU. The $N_{\text{p}} \times 1$ vector $\mathbf{a}_1(t)$ is defined as $\mathbf{a}_1(t) \triangleq [\sqrt{p_{1,1}} \quad \sqrt{p_{1,2}} \quad \cdots \quad \sqrt{p_{1,N_{\text{p}}}}]^T$, for $t = 1, 2, \ldots, N_{\text{up}}$, where $p_{1,l}$ stands for the transmit power of the l-th PU, for $l = 1, 2, \ldots, N_{\text{p}}$. Also, the $N_{\text{s}} \times 1$ vector $\mathbf{a}_2(t)$ is defined as

$$\mathbf{a}_2(t) \triangleq \begin{cases} \sqrt{\alpha}\mathbf{1}, & \text{for } t = 1, 2, \ldots N_{\text{t}} \\ \left[\sqrt{p_{2,1}} \quad \sqrt{p_{2,2}} \quad \cdots \quad \sqrt{p_{2,N_{\text{s}}}}\right]^T, & \text{for } t = N_{\text{t}}+1, N_{\text{t}}+2, \ldots, N_{\text{up}} \end{cases} \tag{3.2}$$

where α is the transmit power of the SUs during training and $p_{2,k}$ stands for the transmit power of the k-th SU, for $k = 1, 2, \ldots, N_{\text{s}}$. We use $\mathbf{n}_1(f,t) \in \mathbb{C}^{M_{\text{p}} \times 1}$ to represent the vector of measurement noise at the PBS at time t of frame f, for $t = 1, 2, \ldots, N_{\text{up}}$. The noise is assumed to be zero-mean and of variance σ^2. Based on (3.1), at time t, the SINR, from [139], at the PBS corresponding to the l-th PU, denoted as $\gamma_{1,l}(t)$, is given by

$$\gamma_{1,l}(t) = \frac{p_{1,l}|\mathbf{w}_{1,l}^H \mathbf{h}_{1,l}|^2}{\sum\limits_{\substack{l'=1 \\ l' \neq l}}^{N_{\text{p}}} p_{1,l'}|\mathbf{w}_{1,l}^H \mathbf{h}_{1,l'}|^2 + \sum\limits_{k=1}^{N_{\text{s}}} \varrho_k(t)|\mathbf{w}_{1,l}^H \mathbf{h}_{12,k}|^2 + \sigma^2 \|\mathbf{w}_{1,l}\|^2}, \text{ for } t = 1, 2, \ldots, N_{\text{up}}. \tag{3.3}$$

where we define

$$\varrho_k(t) \triangleq \begin{cases} \alpha, & \text{for } t = 1, 2, \ldots N_{\text{t}} \\ p_{2,k}, & \text{for } t = N_{\text{t}}+1, N_{\text{t}}+2, \ldots, N_{\text{up}}. \end{cases} \tag{3.4}$$

3.3.2 SN's UL data model

Let $\mathbf{r}_2(f,t) \in \mathbb{C}^{N_{\text{s}} \times 1}$ represent the vector of the UL received signals after beamforming at the SBS at time t within frame f, for $t = N_{\text{t}}+1, N_{\text{t}}+2, \ldots, N_{\text{up}}$. We can then write

$$\mathbf{r}_2(f,t) = \mathbf{W}_2^H \mathbf{H}_2\big(\mathbf{a}_2(t) \odot \mathbf{s}_2(f,t)\big) + \mathbf{W}_2^H \mathbf{H}_{21}\big(\mathbf{a}_1(t) \odot \mathbf{s}_1(f,t)\big) + \mathbf{W}_2^H \mathbf{n}_2(f,t). \tag{3.5}$$

Here, we define $\mathbf{H}_2 \triangleq [\mathbf{h}_{2,1} \;\; \mathbf{h}_{2,2} \;\; \cdots \;\; \mathbf{h}_{2,N_\mathrm{s}}] \in \mathbb{C}^{M_\mathrm{s} \times N_\mathrm{s}}$, $\mathbf{H}_{21} \triangleq [\mathbf{h}_{21,1} \;\; \mathbf{h}_{21,2} \;\; \cdots \;\; \mathbf{h}_{21,N_\mathrm{p}}] \in \mathbb{C}^{M_\mathrm{s} \times N_\mathrm{p}}$, $\mathbf{W}_2 \triangleq [\mathbf{w}_{2,1} \;\; \mathbf{w}_{2,2} \;\; \cdots \;\; \mathbf{w}_{2,N_\mathrm{s}}] \in \mathbb{C}^{M_\mathrm{s} \times N_\mathrm{s}}$, where $\mathbf{h}_{2,k} \in \mathbb{C}^{M_\mathrm{s} \times 1}$ is the channel vector between the SBS and the k-th SU, $\mathbf{h}_{21,l} \in \mathbb{C}^{M_\mathrm{s} \times 1}$ represents the channel vector between the SBS and the l-th PU, $\mathbf{w}_{2,k} \in \mathbb{C}^{M_\mathrm{s} \times 1}$ is the beamforming weight vector used by the SBS to serve the k-th SU, and $\mathbf{n}_2(f,t) \in \mathbb{C}^{M_\mathrm{s} \times 1}$ denotes the receiver noise vector at frame f and time t. Based on (3.5), at time t, the SINR at the SBS corresponding to the k-th SU, denoted as $\gamma_{2,k}(t)$, is given by

$$\gamma_{2,k}(t) = \frac{p_{2,k}|\mathbf{w}_{2,k}^H \mathbf{h}_{2,k}|^2}{\sum\limits_{\substack{k'=1 \\ k' \neq k}}^{N_\mathrm{s}} p_{2,k'}|\mathbf{w}_{2,k}^H \mathbf{h}_{2,k'}|^2 + \sum\limits_{l=1}^{N_\mathrm{p}} p_{1,l}|\mathbf{w}_{2,k}^H \mathbf{h}_{21,l}|^2 + \sigma^2 \|\mathbf{w}_{2,k}\|^2}, \text{ for } t = N_\mathrm{t}+1, \ldots, N_\mathrm{up}. \tag{3.6}$$

3.3.3 PN's DL data model

If $y_{1,l}(f,t)$ represents the signal received at the l-th PU in frame f at time t, we can then write

$$y_{1,l}(f,t) = \mathbf{h}_{1,l}^T \mathbf{W}_1^* \big(\tilde{\mathbf{a}}_1(t) \odot \mathbf{x}_1(f,t)\big) + \mathbf{h}_{21,l}^T \tilde{\mathbf{W}}_2^* \big(\tilde{\mathbf{a}}_2(t) \odot \mathbf{x}_2(f,t)\big) + \nu_{1,l}(f,t). \tag{3.7}$$

Here, $\mathbf{x}_1(f,t) \in \mathbb{C}^{N_\mathrm{p} \times 1}$ is the vector of the DL unit-power symbols transmitted by the PBS towards all PUs at time t in frame f, for $t = 1, 2, \ldots, N_\mathrm{dp}$; $\mathbf{x}_2(f,t) \in \mathbb{C}^{N_\mathrm{s} \times 1}$ is the vector of the DL unit-power symbols transmitted by the SBS towards all the SUs at time t in frame f, for $t = 1, 2, \ldots, N_\mathrm{dp}$; $\nu_{1,l}(f,t)$ is the complex noise component at the l-th PU in frame f and time t; $\tilde{\mathbf{W}}_2 \triangleq [\tilde{\mathbf{w}}_{2,1} \;\; \tilde{\mathbf{w}}_{2,2} \;\; \cdots \;\; \tilde{\mathbf{w}}_{2,N_\mathrm{s}}] \in \mathbb{C}^{M_\mathrm{s} \times N_\mathrm{s}}$ is the matrix of the DL beamformers of the SN; $\tilde{\mathbf{w}}_{2,k} \in \mathbb{C}^{M_\mathrm{s} \times 1}$ is the unit-norm beamforming vector used in the SBS during DL to precode data for the k-th SU, for $k = 1, 2, \ldots, N_\mathrm{s}$ and for $t = 1, 2, \ldots, N_\mathrm{dp}$; the transmit power adjusting vectors $\tilde{\mathbf{a}}_1(t)$ and $\tilde{\mathbf{a}}_2(t)$ are defined as $\tilde{\mathbf{a}}_1(t) \triangleq [\sqrt{\tilde{p}_{1,1}} \;\; \sqrt{\tilde{p}_{1,2}} \;\; \cdots \;\; \sqrt{\tilde{p}_{1,N_\mathrm{p}}}]^T$ and $\tilde{\mathbf{a}}_2(t) = [\sqrt{\tilde{p}_{2,1}} \;\; \sqrt{\tilde{p}_{2,2}} \;\; \cdots \;\; \sqrt{\tilde{p}_{2,N_\mathrm{s}}}]^T$, where $\tilde{p}_{1,l}$ and $\tilde{p}_{2,k}$ stand for the transmit powers allocated to signals intended for the l-th PU and the k-th SU, respectively, at the PBS and the SBS. Note that in the PN, the UL and DL beamformers are identical as the PN is not meant to be bothered by the presence

of the SN, while the SU's UL BF matrix, denoted as $\mathbf{W}_2$ in (3.5), is different from the transmit beamforming matrix, denoted as $\tilde{\mathbf{W}}_2$ in (3.7), used by the SBS in the DL. Such different UL and DL beamformers provide us with more degrees of freedom to control or suppress interference imposed by the SN on the PN. Based on (3.7), at time t, the SINR at the l-th PU in the DL, denoted as $\tilde{\gamma}_{1,l}(t)$, is given by

$$\tilde{\gamma}_{1,l}(t) = \frac{\tilde{p}_{1,l}|\mathbf{h}_{1,l}^H \mathbf{w}_{1,l}|^2}{\sum\limits_{l' \neq l} \tilde{p}_{1,l'}|\mathbf{h}_{1,l}^H \mathbf{w}_{1,l'}|^2 + \sum\limits_{k=1}^{N_\mathrm{s}} \tilde{p}_{2,k}|\mathbf{h}_{21,l}^H \tilde{\mathbf{w}}_{2,k}|^2 + \sigma^2}, \text{ for } t = 1, 2, \ldots, N_\mathrm{dp}\,. \quad (3.8)$$

3.3.4 SN's DL data model

Let $y_{2,k}(f,t)$ represent the signal received at the k-th SU in frame f at time t, for $t = 1, 2, \ldots, N_\mathrm{dp}$. We can then write

$$y_{2,k}(f,t) = \mathbf{h}_{2,k}^T \tilde{\mathbf{W}}_2^* \big(\tilde{\mathbf{a}}_2(t) \odot \mathbf{x}_2(f,t)\big) + \mathbf{h}_{12,k}^T \mathbf{W}_1^* \big(\tilde{\mathbf{a}}_1(t) \odot \mathbf{x}_1(f,t)\big) + \nu_{2,k}(f,t) \quad (3.9)$$

where $\nu_{2,k}(f,t)$ is the complex noise component at the k-th SU at time t of frame f. Based on (3.9), at time t, the SINR at the k-th SU in DL, denoted as $\tilde{\gamma}_{2,k}(t)$, is given by

$$\tilde{\gamma}_{2,k}(t) = \frac{\tilde{p}_{2,k}|\mathbf{h}_{2,k}^H \tilde{\mathbf{w}}_{2,k}|^2}{\sum\limits_{k' \neq k} \tilde{p}_{2,k'}|\mathbf{h}_{2,k}^H \tilde{\mathbf{w}}_{2,k'}|^2 + \sum\limits_{l=1}^{N_\mathrm{p}} \tilde{p}_{1,l}|\mathbf{h}_{12,k}^H \mathbf{w}_{1,l}|^2 + \sigma^2}, \text{ for } t = 1, 2, \ldots, N_\mathrm{dp}\,. \quad (3.10)$$

In the next section, the optimization problem of Scenario A for both UL and DL will be formulated.

3.4 Optimization Problems in Scenario A

Considering $\mathbf{W}_2, \tilde{\mathbf{W}}_2, \mathbf{p}_2, \tilde{\mathbf{p}}_2$ as the design parameters, we now aim to maximize the total achievable sum-rate of the SN in both UL and DL states subject to satisfying pre-defined constraints on transmitted power of the SN and minimum acceptable individual

rate for the PUs. Let us represent the UL achievable rate of the l-th PU as

$$R_{1,l}(\mathbf{W}_1, \mathbf{p}_1, \mathbf{p}_2) = \frac{1}{N_{\text{up}}} \sum_{t=1}^{N_{\text{up}}} \log_2 \left(1 + \gamma_{1,l}(t)\right) \tag{3.11}$$

where we define $\mathbf{p}_1 \triangleq [p_{1,1} \quad p_{1,2} \quad \cdots \quad p_{1,N_{\text{p}}}]^T$ and $\mathbf{p}_2 \triangleq [p_{2,1} \quad p_{2,2} \quad \cdots \quad p_{2,N_{\text{p}}}]^T$. Also, we represent the DL achievable rate of the l-th PU as $\tilde{R}_{1,l}(\mathbf{W}_1, \tilde{\mathbf{W}}_2, \tilde{\mathbf{p}}_1, \tilde{\mathbf{p}}_2) = \frac{1}{N_{\text{dp}}} \sum_{t=1}^{N_{\text{dp}}} \log_2 \left(1 + \tilde{\gamma}_{1,l}(t)\right)$, where we define $\tilde{\mathbf{p}}_1 \triangleq [\tilde{p}_{1,1} \quad \tilde{p}_{1,2} \quad \cdots \quad \tilde{p}_{1,N_{\text{p}}}]^T$ and $\tilde{\mathbf{p}}_2 \triangleq [\tilde{p}_{2,1} \quad \tilde{p}_{2,2} \quad \cdots \quad \tilde{p}_{2,N_{\text{p}}}]^T$. Moreover, the UL achievable sum-rate of the SN is given by

$$R_2(\mathbf{W}_2, \mathbf{p}_1, \mathbf{p}_2) = \sum_{k=1}^{N_{\text{s}}} R_{2,k}(\mathbf{W}_2, \mathbf{p}_1, \mathbf{p}_2), \tag{3.12}$$

where $R_{2,k}(\mathbf{W}_2, \mathbf{p}_1, \mathbf{p}_2) = \frac{1}{N_{\text{up}}} \sum_{t=N_{\text{t}}+1}^{N_{\text{up}}} \log_2 \left(1 + \gamma_{2,k}(t)\right)$ is the UL achievable rate of the k-th SU. Also, we express the DL achievable sum-rate of the SN as

$$\tilde{R}_2(\mathbf{W}_1, \tilde{\mathbf{W}}_2, \tilde{\mathbf{p}}_1, \tilde{\mathbf{p}}_2) = \sum_{k=1}^{N_{\text{s}}} \tilde{R}_{2,k}(\mathbf{W}_1, \tilde{\mathbf{W}}_2, \tilde{\mathbf{p}}_1, \tilde{\mathbf{p}}_2) \tag{3.13}$$

where $\tilde{R}_{2,k}(\mathbf{W}_1, \tilde{\mathbf{W}}_2, \tilde{\mathbf{p}}_1, \tilde{\mathbf{p}}_2) = \frac{1}{N_{\text{dp}}} \sum_{t=1}^{N_{\text{dp}}} \log_2 \left(1 + \tilde{\gamma}_{2,k}(t)\right)$ is the DL achievable rate of the k-th SU. We can write the main optimization problem of maximizing the weighted UL and DL achievable sum-rates of the SN as

$$\max_{\mathbf{W}_2, \tilde{\mathbf{W}}_2, \mathbf{p}_2, \tilde{\mathbf{p}}_2} \quad \beta R_2(\mathbf{W}_2, \mathbf{p}_1, \mathbf{p}_2) + \tilde{\beta} \tilde{R}_2(\mathbf{W}_1, \tilde{\mathbf{W}}_2, \tilde{\mathbf{p}}_1, \tilde{\mathbf{p}}_2) \tag{3.14a}$$

$$\text{s.t.} \quad \text{C}_1 : 0 \leq p_{2,k} \leq p_{2,\max}, \qquad \text{for } k = 1, 2, \ldots, N_{\text{s}} \tag{3.14b}$$

$$\text{C}_2 : R_{1,l}(\mathbf{W}_1, \mathbf{p}_1, \mathbf{p}_2) \geq r_{1,l}, \qquad \text{for } l = 1, 2, \ldots, N_{\text{p}} \tag{3.14c}$$

$$\text{C}_3 : \|\tilde{\mathbf{w}}_{2,k}\|^2 = 1, \qquad \text{for } k = 1, 2, \ldots, N_{\text{s}} \tag{3.14d}$$

$$\text{C}_4 : \mathbf{1}^T \tilde{\mathbf{p}}_2 \leq \tilde{P}_2 \tag{3.14e}$$

$$\text{C}_5 : \tilde{R}_{1,l}(\mathbf{W}_1, \tilde{\mathbf{W}}_2, \tilde{\mathbf{p}}_1, \tilde{\mathbf{p}}_2) \geq \tilde{r}_{1,l}, \qquad \text{for } l = 1, 2, \ldots, N_{\text{p}} \tag{3.14f}$$

$$\text{C}_6 : \tilde{p}_{2,k} \geq 0\,, \qquad \text{for } k = 1, 2, \ldots, N_{\text{s}}. \tag{3.14g}$$

where $\tilde{P}_2$ is the total maximum transmit power of the SBS during DL, β and $\tilde{\beta}$ are two positive constant coefficients and can be chosen depending on whether SN's UL or DL has more priority, and $p_{2,\max}$ is the maximum transmit power budget of each SU. Moreover, $r_{1,l}$ is the achievable rate that the PBS requires the SBS to guarantee for the l-th PU in the UL and $\tilde{r}_{1,l}$ is the minimum acceptable DL rate of the l-th PU. The values of $\{r_{1,l}\}_{l=1}^{N_{\mathrm{P}}}$ and $\{\tilde{r}_{1,l}\}_{l=1}^{N_{\mathrm{P}}}$ are provided by the PBS to the SBS. Note that in (3.14) the UL (and DL) beamforming matrix of the PN, denoted as $\mathbf{W}_1$, the UL power adjusting matrix $\mathbf{p}_1$, and the DL power adjusting matrix $\tilde{\mathbf{p}}_1$ are not design parameters, they nevertheless affect the performance of the SN. We assume that these parameters are set by the PN without taking the presence of the SN into account, thereby ensuring that the presence of the SN will have as minimal an effect as possible on the frame structure and the system design of the PN. As such, $\mathbf{W}_1$ is chosen based on ZF approach with *normalized columns*, that is

$$\mathbf{W}_1 = \mathbf{H}_1(\mathbf{H}_1^H\mathbf{H}_1)^{-1}\mathbf{D}_1 \tag{3.15}$$

where we define $\mathbf{D}_1 = \mathrm{diag}\left(\{\mu_l\}_{l=1}^{N_{\mathrm{P}}}\right)$ with μ_l being the inverse of the ℓ_2 norm of the l-th column of $\mathbf{H}_1(\mathbf{H}_1^H\mathbf{H}_1)^{-1}$. With this ZF choice for $\mathbf{W}_1$, provided that $\mathbf{H}_1$ contains negligible estimation error, the PUs will not cause interference to each other at the PBS, and thus, we can choose $\mathbf{p}_1 = p_{1,\max}\mathbf{1}$, where $p_{1,\max}$ is the maximum transmit power budget of each PU. With this choice of $\mathbf{p}_1$, in the absence of the SN, the l-th PU will have an UL data rate of $r_{1,l}^{\max} \triangleq \log_2\left(1 + \frac{\mu_l^2 p_{1,\max}}{\sigma^2}\right)$. In the presence of the SN, however the PN will have to sacrifice a small portion of $\{r_{1,l}\}_{l=1}^{N_{\mathrm{P}}}$ in order to accommodate the SUs. Also, the DL power adjusting matrix of the PBS is calculated using the water-filling algorithm as $\tilde{p}_{1,l} = \max\{0, \psi - \varphi_l^{-1}\}$ where we define $\varphi_l \triangleq \frac{|\mathbf{h}_{1,l}^H\mathbf{w}_{1,l}|^2}{\sigma^2} = \frac{\mu_l^2}{\sigma^2}$ and ψ is determined from $\sum_{l=1}^{N_{\mathrm{P}}}\max\{0, \psi - \varphi_l^{-1}\} = \tilde{P}_1$, with $\tilde{P}_1$ being the maximum DL transmit power of the PBS. With these choices for $\mathbf{W}_1$, $\mathbf{p}_1$, and $\tilde{\mathbf{p}}_1$, one can see from (3.14) that the parameters determining the sum-rates of both networks in DL and UL

are different, and therefore, we can separate[2] the optimization problems of UL and DL sum-rates into two optimization problems given in (3.16) and (3.17), respectively.

$$\max_{\mathbf{W}_2,\mathbf{p}_2} \quad R_2(\mathbf{W}_2,\mathbf{p}_1,\mathbf{p}_2) \tag{3.16a}$$

$$\text{s.t.} \quad \mathrm{C}_1 : 0 \le p_{2,k} \le p_{2,\max}, \qquad \text{for } k = 1,2,\ldots,N_\mathrm{s} \tag{3.16b}$$

$$\mathrm{C}_2 : R_{1,l}(\mathbf{W}_1,\mathbf{p}_1,\mathbf{p}_2) \ge r_{1,l}, \qquad \text{for } l = 1,2,\ldots,N_\mathrm{p} \tag{3.16c}$$

and

$$\max_{\tilde{\mathbf{W}}_2,\tilde{\mathbf{p}}_2} \quad \tilde{R}_2(\mathbf{W}_1,\tilde{\mathbf{W}}_2,\tilde{\mathbf{p}}_1,\tilde{\mathbf{p}}_2) \tag{3.17a}$$

$$\text{s.t.} \quad \mathrm{C}_3 : \|\tilde{\mathbf{w}}_{2,k}\|^2 = 1, \qquad \text{for } k = 1,2,\ldots,N_\mathrm{s} \tag{3.17b}$$

$$\mathrm{C}_4 : \mathbf{1}^T\tilde{\mathbf{p}}_2 \le \tilde{P}_2, \tag{3.17c}$$

$$\mathrm{C}_5 : \tilde{R}_{1,l}(\mathbf{W}_1,\tilde{\mathbf{W}}_2,\tilde{\mathbf{p}}_1,\tilde{\mathbf{p}}_2) \ge \tilde{r}_{1,1}, \qquad \text{for } l = 1,2,\ldots,N_\mathrm{p} \tag{3.17d}$$

$$\mathrm{C}_6 : \tilde{p}_{2,k} \ge 0\,, \qquad \text{for } k = 1,2,\ldots,N_\mathrm{s}. \tag{3.17e}$$

In the next two subsections, the UL and DL optimization problems are simplified and solved.

3.4.1 SN Optimization Problem in UL

We now aim to solve (3.16). Using the ZF BF in (3.15) for $\mathbf{W}_1$, we can simplify $\gamma_{1,l}(t)$, given in (3.3), as

$$\gamma_{1,l}(t) = \frac{\mu_l^2 p_{1,\max}}{\sum_{k=1}^{N_\mathrm{s}} \varrho_k(t)|\mathbf{w}_{1,l}^H\mathbf{h}_{12,k}|^2 + \sigma^2\|\mathbf{w}_{1,l}\|^2} = \frac{\mu_l^2 p_{1,\max}}{\sum_{k=1}^{N_\mathrm{s}} \varrho_k(t)|\mathbf{w}_{1,l}^H\mathbf{h}_{12,k}|^2 + \sigma^2}. \tag{3.18}$$

Using (3.18), we can then write (3.11) as

$$R_{1,l}(\mathbf{W}_1,\mathbf{p}_1,\mathbf{p}_2) = \frac{1}{N_\mathrm{up}}\left(\sum_{t=1}^{N_\mathrm{t}} \log_2\,(1+\gamma_{1,l}(t)) + \sum_{t=N_\mathrm{t}+1}^{N_\mathrm{up}} \log_2\,(1+\gamma_{1,l}(t))\right)$$

[2]This implies the values of β and $\tilde{\beta}$ will not affect the forthcoming solutions and can be chosen equal to 1.

$$= \frac{N_{\rm t}}{N_{\rm up}} \log_2 \left(1 + \frac{\mu_l^2 p_{1,\max}}{\alpha \sum_{k=1}^{N_{\rm s}} |\mathbf{w}_{1,l}^H \mathbf{h}_{12,k}|^2 + \sigma^2}\right)$$
$$+ \frac{(N_{\rm up} - N_{\rm t})}{N_{\rm up}} \log_2 \left(1 + \frac{\mu_l^2 p_{1,\max}}{\sum_{k=1}^{N_{\rm s}} p_{2,k} |\mathbf{w}_{1,l}^H \mathbf{h}_{12,k}|^2 + \sigma^2}\right) \quad (3.19)$$

We can now use (3.19) to write Constraints C_2 equivalently as

$$\sum_{k=1}^{N_{\rm s}} p_{2,k} |\mathbf{w}_{1,l}^H \mathbf{h}_{12,k}|^2 \leq \zeta_{1,l}, \text{ for } l = 1, 2, \ldots, N_{\rm p} \quad (3.20)$$

where we define

$$\zeta_{1,l} \triangleq \frac{\mu_l^2 p_{1,\max}}{2^{\frac{N_{\rm up} r_{1,l} - \pi_l}{N_{\rm up} - N_{\rm t}}} - 1} - \sigma^2, \qquad \text{and} \qquad \pi_l \triangleq N_{\rm t} \log_2 \left(1 + \frac{\mu_l^2 p_{1,\max}}{\alpha \|\mathbf{w}_{1,l}^H \mathbf{H}_{12}\|^2 + \sigma^2}\right) \quad (3.21)$$

We now deal with the objective function in (3.16). As $\gamma_{2,k}(t)$ dose not change for $t = N_{\rm t} + 1, N_{\rm t} + 2, \ldots, N_{\rm up}$, we drop the index t in the rest of this section for the sake of convenience and use (3.12) to write the optimization problem (3.16) as

$$\max_{\mathbf{p}_2, \mathbf{W}_2} \quad \frac{N_{\rm up} - N_{\rm t}}{N_{\rm up}} \sum_{k=1}^{N_{\rm s}} \log_2(1 + \gamma_{2,k}) \qquad \text{s.t.} \quad (\mathrm{C}_1 \text{ and } \mathrm{C}_2)\,. \quad (3.22)$$

It is worth mentioning that if the minimum data rates $\{r_{1,l}\}_{l=1}^{N_{\rm up}}$ are too large, parameters $\{\zeta_{1,l}\}_{l=1}^{N_{\rm up}}$ may become negative for given values of $p_{1,\max}$, $N_{\rm up}$, $N_{\rm t}$, and α (which is the SU's training power), $\{\mu_l\}_{l=1}^{N_{\rm up}}$ (which depends on the PU's channel realization). In such a case, problem (3.22) becomes infeasible, meaning that the SUs may not be accommodated. To overcome this matter, one solution could be to reduce the value of the SU's training power α. Note that to solve (3.22), we need to enforce C_2 as in (3.20), and this requires the SBS to have the knowledge of the coefficients $|\mathbf{w}_{1,l}^H \mathbf{h}_{12,k}|^2$, for $k = 1, 2, \ldots, N_{\rm s}$, and $l = 1, 2, \ldots, N_{\rm p}$, or, equivalently, the UL receive beamforming matrix of the PBS (i.e., $\mathbf{W}_1$) along with the channel matrix $\mathbf{H}_{12}$. Such a requirement may not be practical[3] as it requires the PBS to provide these parameters to the SBS. To

[3] Although not practical, this assumption can be used as a performance benchmark of the proposed schemes.

tackle this issue, we modify constraints C_2 and use the following *approximation*:

$$|\mathbf{w}_{1,l}^H \mathbf{h}_{12,k}|^2 \approx \frac{\sum_{l=1}^{N_\mathrm{p}} \tilde{p}_{1,l} |\mathbf{w}_{1,l}^H \mathbf{h}_{12,k}|^2}{\sum_{l=1}^{N_\mathrm{p}} \tilde{p}_{1,l}} = \frac{\vartheta_k}{\tilde{P}_1} \tag{3.23}$$

where the numerator $\vartheta_k \triangleq \sum_{l=1}^{N_\mathrm{p}} \tilde{p}_{1,l} |\mathbf{w}_{1,l}^H \mathbf{h}_{12,k}|^2$ is the power of the interference observed by the k-th SU during the DL transmission of the PN. Indeed, the k-th SU can measure this power in the *learning phase* (when the SN "listens" to the PN with the aim to acquire as much information as possible about the PN) and report that back to the SBS . As such, assuming $\xi_k \triangleq \frac{\sum_{l=1}^{N_\mathrm{p}} \tilde{p}_{1,l} |\mathbf{w}_{1,l}^H \mathbf{h}_{12,k}|^2}{\tilde{P}_1}$ is known, for $k = 1, 2, \ldots, N_\mathrm{s}$, we replace the linear constraints in C_2 with the following set of linear constraints:

$$\sum_{k=1}^{N_\mathrm{s}} p_{2,k} \xi_k \leq \hat{\zeta}_{1,l}, \text{ for } l = 1, 2, \ldots, N_\mathrm{p}, \qquad \text{or} \qquad \sum_{k=1}^{N_\mathrm{s}} p_{2,k} \xi_k \leq \min_{1 \leq l \leq N_\mathrm{p}} \hat{\zeta}_{1,l}, \tag{3.24}$$

where

$$\hat{\zeta}_{1,l} \triangleq \frac{\mu_l^2 p_{1,\max}}{2^{\frac{N_\mathrm{up} r_{1,l} - \hat{\pi}_l}{N_\mathrm{up} - N_\mathrm{t}}} - 1} - \sigma^2, \quad \text{and} \quad \hat{\pi}_l \triangleq N_\mathrm{t} \log_2 \left(1 + \frac{\mu_l^2 p_{1,\max}}{\alpha \sum_{k=1}^{N_\mathrm{s}} \xi_k + \sigma^2}\right), \tag{3.25}$$

are, respectively, the approximated values of $\zeta_{1,l}$ and π_l, obtained by replacing $\|\mathbf{w}_{1,l}^H \mathbf{H}_{12}\|^2$ in (3.21) with its approximation: that is $\|\mathbf{w}_{1,l}^H \mathbf{H}_{12}\|^2 = \sum_{k=1}^{N_\mathrm{s}} |\mathbf{w}_{1,l}^H \mathbf{h}_{12,k}|^2 \approx \sum_{k=1}^{N_\mathrm{s}} \xi_k$. As can be seen from (3.25), parameter $\hat{\zeta}_{1,l}$ depends on $\mu_l^2 p_{1,\max}$, $r_{1,l}$, and $\hat{\pi}_l$, while parameter $\hat{\pi}_l$ in-turn depends on $\mu_l^2 p_{1,\max}$. Hence, parameters $\mu_l^2 p_{1,\max}$ and $r_{1,l}$ should be provided to the SBS by the PBS. One should however note that constraint (3.24) is merely an approximation for Constraints C_2, and thus, using constraint (3.24) instead of C_2 may not always lead to a solution that is feasible for problem (3.22). Indeed, our numerical experiments show that for a rather large majority of channel realizations, using constraint (3.24) instead of C_2 leads to a solution that is infeasible for problem (3.22). To tackle this issue, one may tighten constraint C_2' by replacing $\min_{1 \leq l \leq N_\mathrm{p}} \hat{\zeta}_{1,l}$ in (3.26) with a smaller value with the hope to decrease the probability of the corresponding solution being infeasible for (3.22). That is, we propose to replace C_2 with the following constraint:

$$\mathrm{C}_2' : \quad \sum_{k=1}^{N_\mathrm{s}} p_{2,k} \xi_k \leq \eta \min_{1 \leq l \leq N_\mathrm{p}} \hat{\zeta}_{1,l}, \tag{3.26}$$

where the parameter $\eta \in (0,1)$ is used to control the tightness of constraint C_2'. We now turn our attention to the objective function in (3.16). As $\gamma_{2,k}(t)$ dose not change for $t = N_\mathrm{t}+1, N_\mathrm{t}+2, \ldots, N_\mathrm{up}$, we drop the index t in the rest of this section for the sake of convenience and use (3.12) to write the optimization problem (3.16) as

$$\max_{\mathbf{p}_2, \mathbf{W}_2} \quad \tfrac{N_\mathrm{up}-N_\mathrm{t}}{N_\mathrm{up}} \textstyle\sum_{k=1}^{N_\mathrm{s}} \log_2(1+\gamma_{2,k}), \qquad \text{s.t.} \quad (\mathrm{C}_1 \text{ and } \mathrm{C}_2'). \tag{3.27}$$

For fixed $\mathbf{p}_2$, the maximization over $\mathbf{W}_2$ amounts to maximizing $\gamma_{2,k}$ in (3.6), and therefore, results in an MVDR-type of solution [140], that is, the optimal value of $\mathbf{w}_{2,k}$ is given by[4] $\mathbf{w}_{2,k} = \mathbf{A}_k^{-1}\mathbf{h}_{2,k}$ where we define $\mathbf{A}_k \triangleq \sum_{k' \neq k} p_{2,k'}\mathbf{h}_{2,k'}\mathbf{h}_{2,k'}^H + p_{1,\max}\sum_{l=1}^{N_\mathrm{p}} \mathbf{h}_{21,l}\mathbf{h}_{21,l}^H + \sigma^2\mathbf{I}$. The corresponding value of $\gamma_{2,k}$ is then given by $\gamma_{2,k} = p_{2,k}\mathbf{h}_{2,k}^H\mathbf{A}_k^{-1}\mathbf{h}_{2,k}$ In light of $\gamma_{2,k}$, the optimization problem (3.27) does not appear to be amenable to computationally affordable solution. Nevertheless, one way to tackle this problem is to resort to interior point methods which result in a local maximum, at least. In the absence of proven convexity, no claim can be made with respect to the global optimality of such a solution. Alternatively, we propose to use ZF BF, instead of the MVDR solution. That is, we propose to use the ZF BF matrix given as

$$\mathbf{W}_2 = \mathbf{H}(\mathbf{H}^H\mathbf{H})^{-1}\mathbf{J} \tag{3.28}$$

where $\mathbf{H} \triangleq [\mathbf{H}_{21} \quad \mathbf{H}_2] \in \mathbb{C}^{M_\mathrm{s}\times(N_\mathrm{p}+N_\mathrm{s})}$ and $\mathbf{J}$ is an $(N_\mathrm{p}+N_\mathrm{s}) \times N_\mathrm{s}$ selection matrix which, upon multiplication by a matrix from right, extracts the last N_s columns of that matrix. It is noteworthy that to guarantee that the ZF solution to (3.28) exists, we need to ensure that $M_\mathrm{s} \geq N_\mathrm{p} + N_\mathrm{s}$ holds true (i.e., enough degrees of freedom must exist). In other words, the number of antennas at the SBS must be greater than the sum of the numbers of SUs and PUs. With $\mathbf{W}_2$ given in (3.28), we can simplify (3.6) as $\gamma_{2,k} = \frac{p_{2,k}}{\sigma^2\|\mathbf{w}_{2,k}\|^2}$. Now, we deduce that the optimization problem (3.27) is now a convex problem [141] with linear constraints in $\mathbf{p}_2$. Thus this problem can be solved using any convex problem solver.

[4]Note that as long as SINR is concerned, the optimal value of $\mathbf{w}_{2,k}$ is unique up to a complex scaler. Here, we choose the scaler equal to 1.

3.4.2 SN Optimization Problem in DL

We now aim to tackle the DL optimization problem (3.17). To do so, we note that Constraints C_5 aim to control interference caused by the SBS to the PUs. To satisfy this constraint, it appears that the knowledge of $\tilde{\mathbf{p}}_1$, $\mathbf{W}_1$, and $\mathbf{H}_1$ is required at the SBS. Being known at the PBS, these parameters may not be assumed known at the SBS in practice. To tackle this issue, we replace constraints C_5 by a tighter constraint on $\tilde{\mathbf{W}}_2$ as

$$\mathrm{C}_5' : \mathbf{H}_{21}^T \tilde{\mathbf{W}}_2^* = 0\,, \tag{3.29}$$

thereby ZF the interference caused to the PUs. Using C_5' along with (3.15), we simplify (3.8) as

$$\tilde{\gamma}_{1,l}(t) = \frac{\tilde{p}_{1,l}|\mathbf{h}_{1,l}^H \mathbf{w}_{1,l}|^2}{\sigma^2} = \frac{\tilde{p}_{1,l}\mu_l^2}{\sigma^2}, \quad \text{for } t = 1, 2, \ldots, N_{\mathrm{dp}} \tag{3.30}$$

which implies that the downlink transmission of the SN does not affect the downlink transmission of the PN. Hence, using C_5' ensures that C_5 is guaranteed. Also to ensure that the signal intended for any SU causes no interference to other SUs, we add the following ZF constraint on $\tilde{\mathbf{W}}_2$:

$$\mathrm{C}_5'' : \mathbf{H}_2^T \tilde{\mathbf{W}}_2^* = \mathbf{D}^*, \tag{3.31}$$

where $\mathbf{D}$ is a complex diagonal matrix. Based on (3.31), we can simplify (3.10) as

$$\tilde{\gamma}_{2,k} = \frac{\tilde{p}_{2,k}|\mathbf{D}_{k,k}|^2}{\vartheta_k + \sigma^2}. \tag{3.32}$$

where the term $\vartheta_k \triangleq \sum_{l=1}^{N_{\mathrm{p}}} \tilde{p}_{1,l}|\mathbf{h}_{12,k}^H \mathbf{w}_{1,l}|^2$ is the power of the interference observed by the k-th SU during the DL transmission of the PN and can be measured as described earlier. Indeed, ϑ_k can be measured in the learning phase, where the SN listens to the PN with the aim to acquire as much information as possible about the PN. In such a learning phase, the k-th SU measures ϑ_k and reports that to the SBS. Based on this discussion, we now aim to solve the following optimization problem:

$$\max_{\tilde{\mathbf{W}}_2, \tilde{\mathbf{p}}_2, \mathbf{D}} \quad \sum_{k=1}^{N_{\mathrm{s}}} \log_2\left(1 + \frac{\tilde{p}_{2,k}|\mathbf{D}_{k,k}|^2}{\vartheta_k + \sigma^2}\right) \tag{3.33a}$$

$$\text{s.t.} \quad \mathrm{C}_3 : \|\tilde{\mathbf{w}}_{2,k}\|^2 = 1, \qquad \text{for } k = 1, 2, \ldots, N_\mathrm{s} \tag{3.33b}$$

$$\mathrm{C}_4 : \mathbf{1}^T \tilde{\mathbf{p}}_2 \leq \tilde{P}_2 \tag{3.33c}$$

$$\mathrm{C}_5' : \tilde{\mathbf{W}}_2^H \mathbf{H}_{21} = 0 \tag{3.33d}$$

$$\mathrm{C}_5'' : \tilde{\mathbf{W}}_2^H \mathbf{H}_2 = \mathbf{D}^*, \tag{3.33e}$$

$$\mathrm{C}_6 : \tilde{p}_{2,k} \geq 0, \qquad \text{for } k = 1, 2, \ldots, N_\mathrm{s} \tag{3.33f}$$

$$\mathrm{C}_7 : \mathbf{D}_{i,j} = 0, \qquad \text{for } i, j = 1, 2, \ldots, N_\mathrm{s} \;\&\; i \neq j \tag{3.33g}$$

Let us define the $M_\mathrm{s} \times (M_\mathrm{s} - N_\mathrm{p})$ matrix $\mathbf{\Psi}$ whose columns are orthogonal and span the null space of $\mathbf{H}_{21}$, that is, we have $\mathbf{\Psi}^H \mathbf{\Psi} = \mathbf{I}_{M_\mathrm{s} - N_\mathrm{p}}$ and $\mathbf{H}_{21}^H \mathbf{\Psi} = \underline{0}_{N_\mathrm{p} \times (M_\mathrm{s} - N_\mathrm{p})}$. In other words, the orthogonal columns of $\mathbf{\Psi}$ span the null space of $\mathbf{H}_{21}$. In light of C_5', we must ensure that $\tilde{\mathbf{W}}_2 = \mathbf{\Psi}\mathbf{\Omega}$ holds true, for some $(M_\mathrm{s} - N_\mathrm{p}) \times N_\mathrm{s}$ matrix $\mathbf{\Omega}$. To satisfy C_5'', it is required to have $\mathbf{H}_2^H \mathbf{\Psi}\mathbf{\Omega} = \mathbf{D}$, which in turn requires $N_\mathrm{s} \leq (M_\mathrm{s} - N_\mathrm{p})$. With these requirements, we obtain $\mathbf{\Omega} = (\mathbf{H}_2^H \mathbf{\Psi})^\dagger \mathbf{D}$. Therefore, we can write $\tilde{\mathbf{W}}_2 = \breve{\mathbf{W}}\mathbf{D}$ where we define $\breve{\mathbf{W}} \triangleq \mathbf{\Psi}(\mathbf{H}_2^H \mathbf{\Psi})^\dagger = [\breve{\mathbf{w}}_1 \;\; \breve{\mathbf{w}}_2 \;\; \cdots \;\; \breve{\mathbf{w}}_{N_\mathrm{s}}] \in \mathbb{C}^{M_\mathrm{s} \times N_\mathrm{s}}$ with $\breve{\mathbf{w}}_k \in \mathbb{C}^{M_\mathrm{s} \times 1}$. Now, in order to ensure C_3 is satisfied, we must choose $\mathbf{D}_{k,k} = 1/\|\breve{\mathbf{w}}_{2,k}\|$, for $k = 1, 2, \ldots, N_\mathrm{s}$. Thus, we can rewrite (3.33) as

$$\max_{\tilde{\mathbf{p}}_2} \quad \sum_{k=1}^{N_\mathrm{s}} \log_2 \left(1 + \frac{\tilde{p}_{2,k}}{\|\breve{\mathbf{w}}_{2,k}\|^2 (\vartheta_k + \sigma^2)}\right) \tag{3.34a}$$

$$\text{s.t.} \quad \mathrm{C}_4 : \mathbf{1}^T \tilde{\mathbf{p}}_2 \leq \tilde{P}_2, \tag{3.34b}$$

$$\mathrm{C}_6 : \tilde{p}_{2,k} \geq 0, \qquad \text{for } k = 1, 2, \ldots, N_\mathrm{s}\,. \tag{3.34c}$$

The solution to (3.34) can be obtained using the well-known water-filling algorithm as

$$\tilde{p}_{2,k} = \max\{0, \psi_2 - \|\breve{\mathbf{w}}_{2,k}\|^2 (\vartheta_k + \sigma^2)\} \tag{3.35}$$

where ψ_2 is determined, using a bisection method, as the solution to the following equation: $\sum_{k=1}^{N_\mathrm{s}} \max\{0, \psi_2 - \|\breve{\mathbf{w}}_{2,k}\|^2 (\vartheta_k + \sigma^2)\} = \tilde{P}_2$.

To Summarize, we designed beamforming and power allocation schemes to be used in the SBS for the communication scheme in Scenario A. As we showed in this section, developing beamforming and power allocation schemes for Scenario A requires approx-

imations to some of the constraints. Moreover, Scenario A may suffer from problem infeasibility.

3.5 Simulation Results

Throughout our derivations, we assumed perfect CSI at the PBS, at the SBS, and at the SUs. In our first set of simulation examples, we compare the performance of our proposed solution for the two cases of perfect and estimated CSI. For the case of estimated CSI, we use the channel estimation technique proposed in [76]. This technique has been adopted for the communication scheme considered in this paper using the following parameters: $N_{\mathrm{t}} = 12$, $N_{\mathrm{up}} = 200$, and $N_{\mathrm{dp}} = 200$. Also, we assume $\alpha_1 = 0.8$, $F_{\mathrm{p}} = 1$, $F_{\mathrm{s}} = 1$ and $\check{F}_{\mathrm{s}} = 1$ [76]. The training powers of the SUs are all equal to $\alpha = \tilde{P}_2/N_{\mathrm{s}}$, while the maximum UL transmit powers of the PUs and SUs are set to be $p_{1,\max} = \tilde{P}_1/N_{\mathrm{p}}$ and $p_{2,\max} = \tilde{P}_2/N_{\mathrm{s}}$, respectively.

The relative physical locations of the two networks are shown in Fig. 3.1. As can be seen from this figure, the PN coverage area is a $d_{\mathrm{p}} \times d_{\mathrm{p}}$ square area, centered around the PBS, which is located at $(0, 0)$. The coverage area of the SN is a $d_{\mathrm{s}} \times d_{\mathrm{s}}$ square area centered around the SBS, which is located at $((-d_{\mathrm{p}} + d_{\mathrm{s}})/2, (d_{\mathrm{p}} - d_{\mathrm{s}})/2)$. We choose $d_{\mathrm{p}} = 1000$ meters. The channel between any two nodes located d meters apart are modeled as zero-mean complex Gaussian random variables with variance $a(d/d_0)^{-3.5}$, with $a = -137$ dB and $d_0 = 1000$ meters. The noise power is $\sigma^2 = -104$ dBm [142]. In all simulations, we assume $M_{\mathrm{p}} = 32$, $d_{\mathrm{p}} = 1000$ m and choose $\eta = 0.5$.

3.5.1 The effect of approximation error

In our first set of numerical examples, we evaluate the accuracy of the approximation in (3.23). As mentioned earlier, in the UL state of Scenario A, the SBS may not have the knowledge of the PBS's UL beamforming matrix $\mathbf{W}_1$ and the channel matrix $\mathbf{H}_{12}$. As such, we approximated the coefficients $|\mathbf{w}_{1,l}^H \mathbf{h}_{12,k}|^2$, for all k and l, as in (3.23). We now study the accuracy of our approximation in (3.23) for different values of the system

parameters using numerical examples. In each simulation run, we choose $r_{1,l} = \rho r_{1,l}^{\max}$ and $\tilde{r}_{1,l} = \rho \tilde{r}_{1,l}^{\max}$, for $l = 1, \ldots, N_{\rm p}$, $\rho = 0.9$. Assuming $M_{\rm s} = 20$, $N_{\rm p} = 4$, $N_{\rm s} = 4$, $\tilde{P}_2 = 20$ dBm, we plot the UL average per-user achievable rate (APAR) of the SN and that of the PN in Scenario A versus the total power of the PN in DL for three different solutions:

i. the solution to (3.22) while assuming perfect global CSI is available at all nodes. This solution provides an upper bound and is herein referred to as "clairvoyant" solution.

ii. the solution to (3.27) while assuming perfect global CSI is available at all nodes,

iii. the solution to (3.27), while assuming the estimated CSI (obtained by using the technique proposed in [76]) is available at all nodes.

Figs. 3.3(a) and 3.3(b) show the APAR for all the aforementioned solutions versus the total power $\tilde{P}_1$ of the PN in downlink for the SN and the PN, respectively, for $d_{\rm s} = 500$ m, while Figs. 3.4(a) and 3.4(b) illustrate the same performance curves for $d_{\rm s} = 800$ m. As can be seen from these figures, the performance of the proposed scheme with estimated CSI is very close to the case when perfect CSI is used. Figs. 3.3(a) and 3.4(a) also show that solving (3.27) (which relies on the approximation in (3.23)) yields about 0.3 to 0.7 bps/Hz/user lower APAR for the SN compared to the clairvoyant solution. Figs. 3.3(b) and 3.4(b) show that solving (3.27) (which relies on the approximation in (3.23)) results in a slightly better performance for the PN. This shows that for those channel realizations, where the solution to (3.27) is feasible for (3.22), C_2' is tighter compared to C_2. This causes the solution to (3.27) to have a lower UL APAR efficiency for the SN, and at the same time, causing slightly less interference to the PN, compared to the clairvoyant solution to (3.22). We need to stress that all curves in Figs. 3.3 and 3.4 are averaged over those channel realizations where the solution to (3.27) is feasible for (3.22). The plots in Figs. 3.5 and 3.6 show the probabilities of the solution to (3.27) being infeasible for (3.22), for different values of $d_{\rm s}$, for different numbers of PUs, and

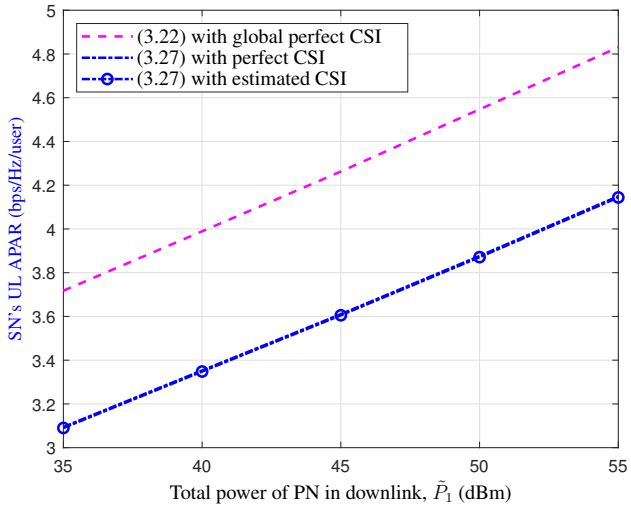

(a) $d_{\mathrm{s}} = 500$ m.

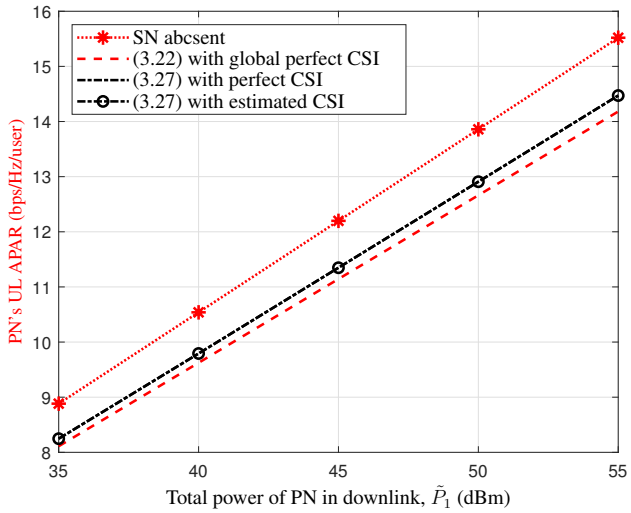

(b) $d_{\mathrm{s}} = 500$ m.

Figure 3.3: Scenario A: SN's and PN's APARs in the UL versus total power of the PN for perfect and estimated CSI, with $M_{\mathrm{p}} = 32$, $M_{\mathrm{s}} = 20$, $N_{\mathrm{p}} = 4$, $N_{\mathrm{s}} = 4$, $d_{\mathrm{p}} = 1000$ m, $\tilde{P}_2 = 20$ dBm, $\eta = 0.5$, $\rho = 0.9$, $N_{\mathrm{t}} = 12$, $N_{\mathrm{up}} = 200$, $N_{\mathrm{dp}} = 200$.

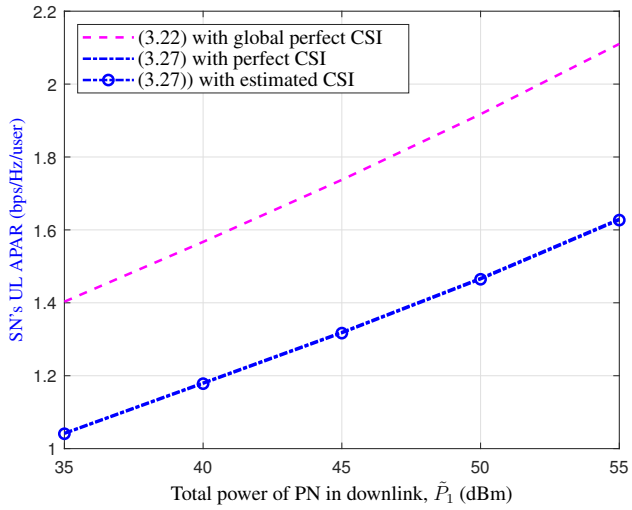

(a) $d_{\mathrm{s}} = 800$ m.

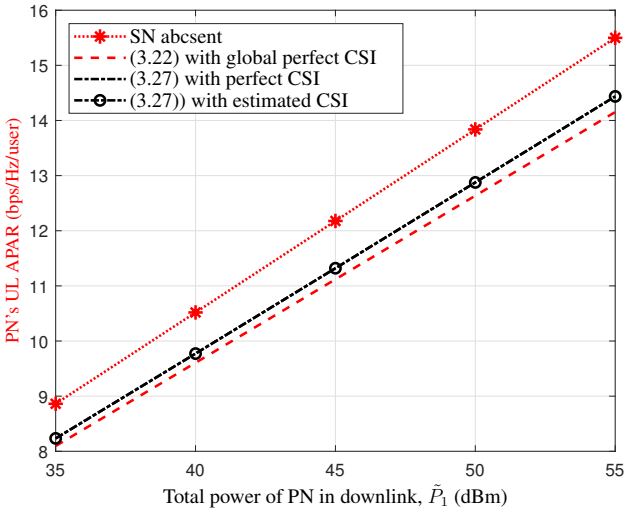

(b) $d_{\mathrm{s}} = 800$ m.

Figure 3.4: Scenario A: SN's and PN's APARs in the UL versus total power of the PN for perfect and estimated CSI, with $M_{\mathrm{p}} = 32$, $M_{\mathrm{s}} = 20$, $N_{\mathrm{p}} = 4$, $N_{\mathrm{s}} = 4$, $d_{\mathrm{p}} = 1000$ m, $\tilde{P}_2 = 20$ dBm, $\eta = 0.5$, $\rho = 0.9$, $N_{\mathrm{t}} = 12$, $N_{\mathrm{up}} = 200$, $N_{\mathrm{dp}} = 200$.

for different required rates of the PUs. As mentioned in subsection (3.4.1), it is essential to introduce a new parameter, denoted as η, to address the potential infeasibility that may arise due to the approximation used for constraints C_2. By utilizing this parameter, the tightness of C_2' can be regulated by varying the values of $\eta \in (0, 1)$, thereby reducing the probability of the solution being infeasible for (3.22). For the sake of convenience, these probabilities are referred to as "Probability of infeasibility". As this figure shows, with the choice of $\eta = 0.5$, for a rather large majority of channel realizations, solving (3.27) yields a feasible solution for (3.22).

3.5.2 The effect of PN and SN parameters

In this set of numerical examples, we examine the effect of some parameters on the performance of both networks in Scenarios A, when the corresponding solutions rely on the estimated CSI obtained using the method of [76]. Figs. 3.7, 3.8 and 3.9 illustrate the UL, DL, and UL+DL APAR versus $\tilde{P}_1$ for both networks in Scenarios A, for $M_{\mathrm{s}} = 20$, $N_{\mathrm{p}} = 4$, $N_{\mathrm{s}} = 4$, $\tilde{P}_2 = 20$ dBm, $d_{\mathrm{s}} = 500$ m, and $\rho = 0.9$. As can be seen from Fig. 3.7(a), by increasing $\tilde{P}_1$, the SN's UL APAR is increased. This is due to the fact that $r_{1,l}^{\max}$ are increased by increasing $\tilde{P}_1$, and thus, as we choose $r_{1,l} = \rho r_{1,l}^{\max}$, the SN's UL APAR is improved in this scenario. In other words, increasing $r_{1,l}^{\max}$ allows the SN to impose more interference on the PN, and thus, provides the SN with more spectral usage opportunities, resulting in the SN's UL APAR improvement. We note that in the UL state of the SN, the SUs cause interference to the PBS in Scenario A. Fig. 3.7(b) shows that increasing $\tilde{P}_1$ degrades in the DL state of the SN, as the PN causes more interference to the SUs with increase in $\tilde{P}_1$. Fig. 3.8(a) and Fig. 3.8(b) show that the performance of the PN degrades in the presence of the SN compared to the case when the SN is absent, as we expected. We note that in the UL state of the SN in Scenario A, the SUs cause interference on the PBS and cannot protect the PBS as they are single-antenna units. In Scenario A when the SN is in DL (Fig. 3.8(b)), the SBS can protect the PUs in the PN's DL. Furthermore, we observe that in the absence of the SN, the performance of the PN's DL is approximately the same when the SN is present in Scenario A. It is worth

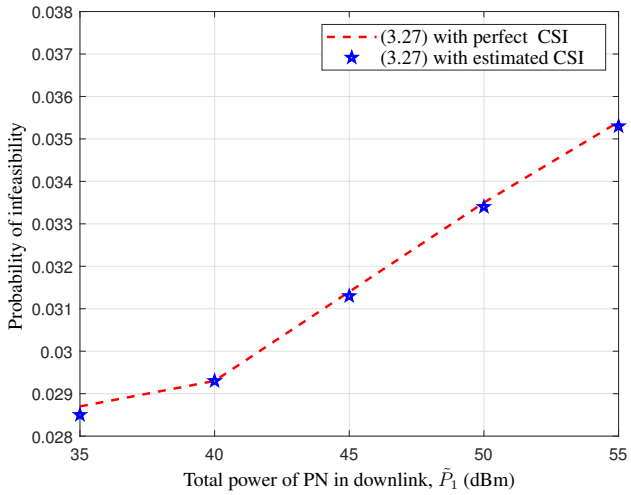

(a) $d_{\mathrm{s}} = 500$ m.

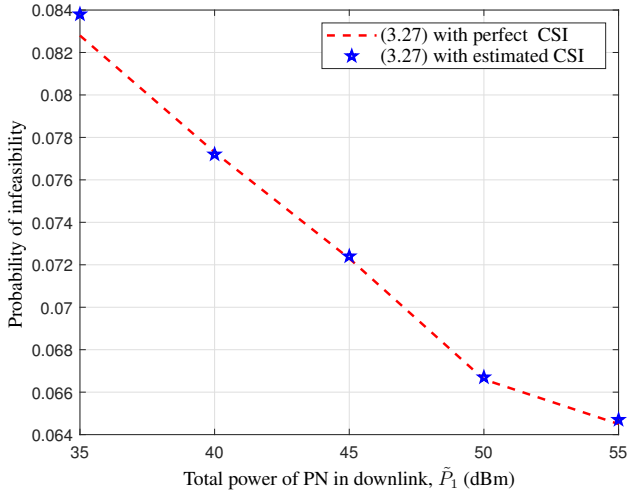

(b) $d_{\mathrm{s}} = 800$ m.

Figure 3.5: Probability that the solution to (3.27) is infeasible for (3.22), when $\eta = 0.5$, versus the total power of PN for perfect and estimated CSI, with $M_{\mathrm{p}} = 32$, $M_{\mathrm{s}} = 20$, $N_{\mathrm{p}} = N_{\mathrm{s}} = 4$, $d_{\mathrm{p}} = 1000$ m, $\rho = 0.9$, $\tilde{P}_2 = 20$ dBm, $N_{\mathrm{t}} = 12$, $N_{\mathrm{up}} = 200$, $N_{\mathrm{dp}} = 200$.

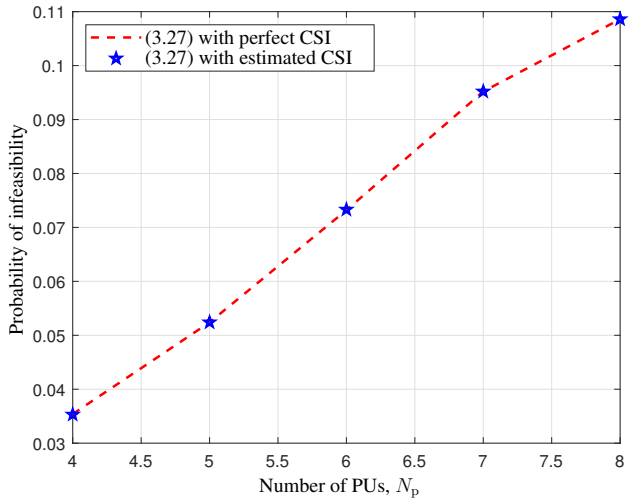

(a) $d_{\mathrm{s}} = 500$ m.

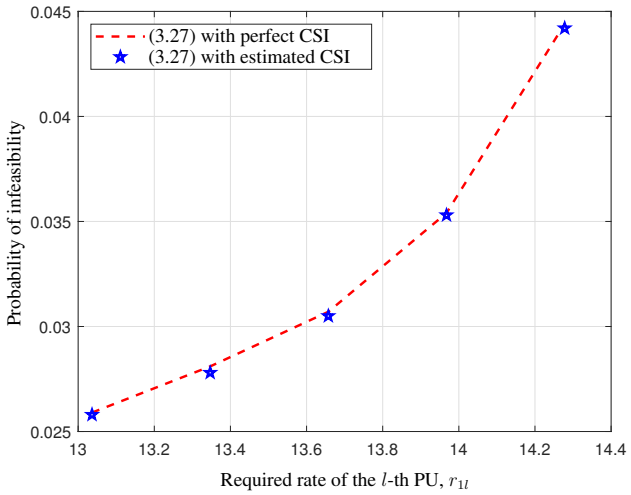

(b) $d_{\mathrm{s}} = 800$ m.

Figure 3.6: Probability that the solution to (3.27) is infeasible for (3.22), when $\eta = 0.5$, for perfect and estimated CSI, with $M_{\mathrm{p}} = 32$, $M_{\mathrm{s}} = 20$, $N_{\mathrm{p}} = N_{\mathrm{s}} = 4$, $d_{\mathrm{p}} = 1000$ m, $\rho = 0.9$, $\tilde{P}_2 = 20$ dBm, $N_{\mathrm{t}} = 12$, $N_{\mathrm{up}} = 200$, $N_{\mathrm{dp}} = 200$.

emphasizing that when the PN is in DL, the SN can protect the PUs in Scenario A, and also, the SN's training phase does not overlap with the PN's DL.

Fig. 3.9(a) reveals the UL+DL APAR for the SN and PN for this set of parameters. As we expected, the PN total APAR in the presence of the SN, is a slightly lower than UL+DL APAR for the PN when the SN is absent. Fig. 3.9(b) shows that the APAR of the whole network (PN+SN) is higher than that of the PN network without SN. Indeed, as can be seen here, the overall APAR of the network is improved by using the proposed USS approach.

Figs. 3.10 and 3.11 examine the effect of $d_{\rm s}$ on the APARs of both networks. Assuming $M_{\rm s} = 20$, $N_{\rm p} = 4$, $N_{\rm s} = 4$, $\tilde{P}_1 = 25$ dBm, $\tilde{P}_2 = 20$ dBm and $\rho = 0.9$, we depict the UL, DL, and UL+DL APAR versus $d_{\rm s}$ for the PN and the SN in Scenarios A. As can be seen from Figs. 3.10(a) and 3.10(b), by increasing $d_{\rm s}$, the UL and DL APARs of the SN for Scenario A are decreased. This result can be explained by the fact that as $d_{\rm s}$ is increased, the average distance between the SUs and the SBS is increased, and hence, the average quality of the channels between the SUs and the SBS is degraded. Also, by increasing $d_{\rm s}$, the average distances between the SN's and the PN's nodes are decreased, and as a consequence, the average quality of the channels between them is improved, leading to more interference caused by the PN to the SN. Figs. 3.11(a) and 3.11(b) show that the PN's UL and DL APARs in Scenarios A change slightly by increasing $d_{\rm s}$. Fig. 3.11(c) reveals the UL+DL APAR of the SN and PN in Scenario A. It follows from this figure that increasing (decreasing) $d_{\rm s}$ does not have any significant effect on the PN performance while by increasing that, the SN performance remarkably degrades. In Fig. 3.12, we study the performance of Scenario A in terms of the SN's and PN's APARs, when $M_{\rm s}$ is changed. In this figure, we assume $N_{\rm p} = 4$, $N_{\rm s} = 4$, $d_{\rm s} = 500$ m, $\tilde{P}_1 = 25$ dBm, $\tilde{P}_2 = 20$ dBm and $\rho = 0.9$. As expected, we can see from Figs. 3.12(a) and 3.12(b) that by increasing $M_{\rm s}$, the SN's performance in both the UL and the DL is improved as the beamforming performance is enhanced. Figs. 3.13(a) and 3.13(b) show that changing $M_{\rm s}$ has a negligible effect on the PN's APARs in the

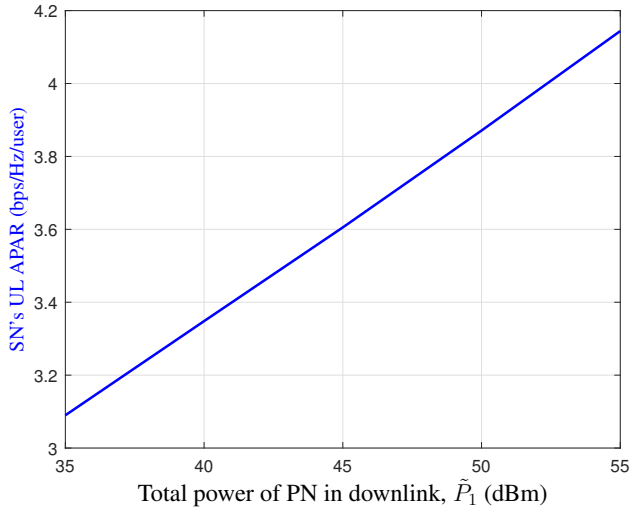

(a) SN in uplink.

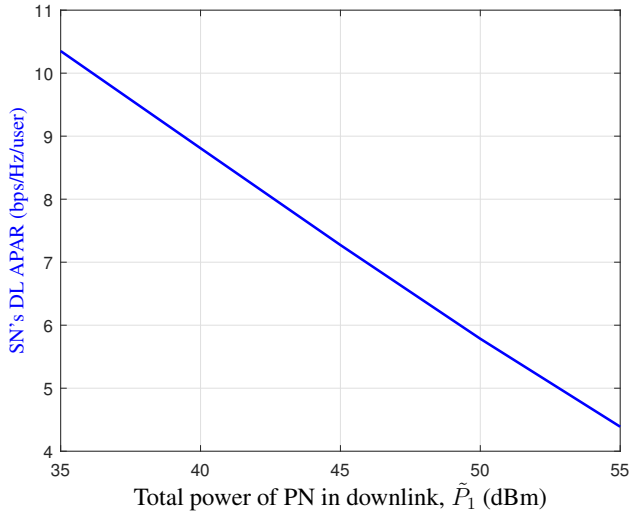

(b) SN in downlink.

Figure 3.7: SN's APARs in both scenarios versus total power of the PN for estimated CSI, with $M_{\mathrm{p}} = 32$, $M_{\mathrm{s}} = 20$, $N_{\mathrm{p}} = 4$, $N_{\mathrm{s}} = 4$, $d_{\mathrm{p}} = 1000$ m, $d_{\mathrm{s}} = 500$ m, $\tilde{P}_2 = 20$ dBm, $\eta = 0.5$, $\rho = 0.9$, $N_{\mathrm{t}} = 12$, $N_{\mathrm{up}} = 200$, $N_{\mathrm{dp}} = 200$.

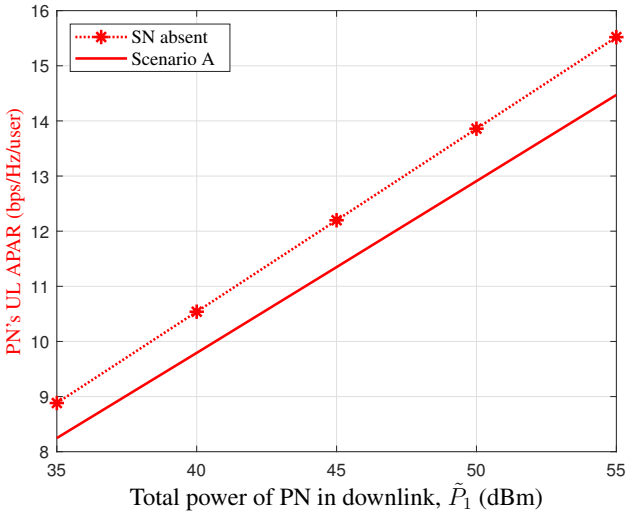

(a) PN in uplink.

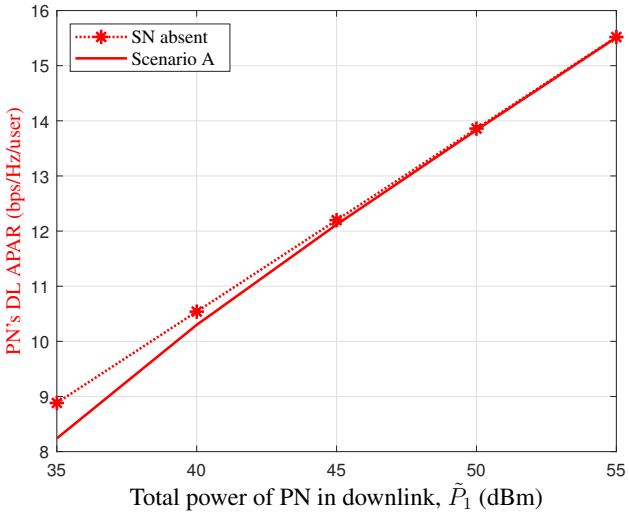

(b) PN in downlink.

Figure 3.8: PN's APARs in both scenarios versus total power of the PN for estimated CSI, with $M_{\mathrm{p}} = 32$, $M_{\mathrm{s}} = 20$, $N_{\mathrm{p}} = 4$, $N_{\mathrm{s}} = 4$, $d_{\mathrm{p}} = 1000$ m, $d_{\mathrm{s}} = 500$ m, $\tilde{P}_2 = 20$ dBm, $\eta = 0.5$, $\rho = 0.9$, $N_{\mathrm{t}} = 12$, $N_{\mathrm{up}} = 200$, $N_{\mathrm{dp}} = 200$.

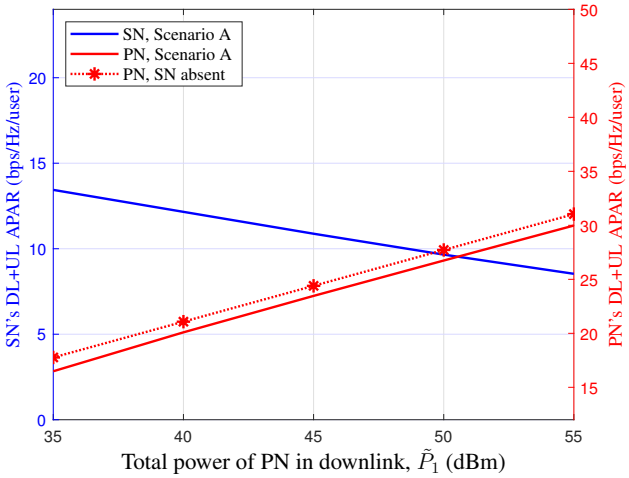

(a) DL+UL APARs of SN and PN.

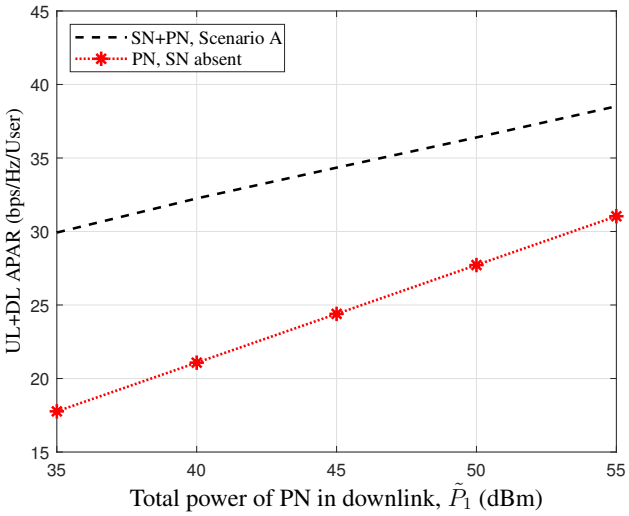

(b) DL+UL APARs of SN+PN and PN.

Figure 3.9: SN's and PN's APARs in both scenarios versus total power of the PN for estimated CSI, with $M_{\mathrm{p}} = 32$, $M_{\mathrm{s}} = 20$, $N_{\mathrm{p}} = 4$, $N_{\mathrm{s}} = 4$, $d_{\mathrm{p}} = 1000$ m, $d_{\mathrm{s}} = 500$ m, $\tilde{P}_2 = 20$ dBm, $\eta = 0.5$, $\rho = 0.9$, $N_{\mathrm{t}} = 12$, $N_{\mathrm{up}} = 200$, $N_{\mathrm{dp}} = 200$.

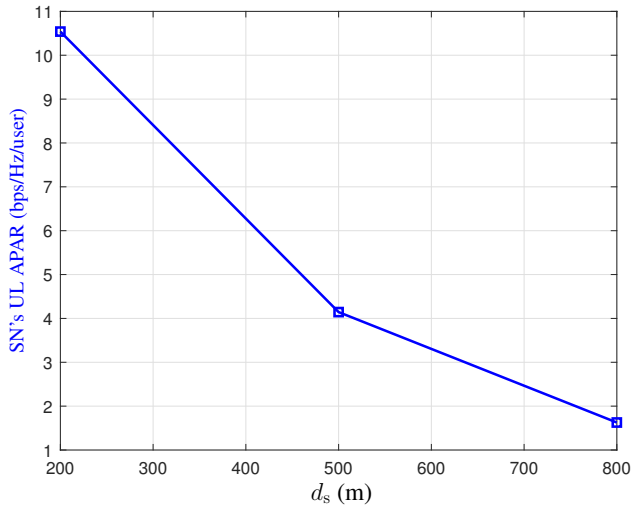

(a) SN in uplink.

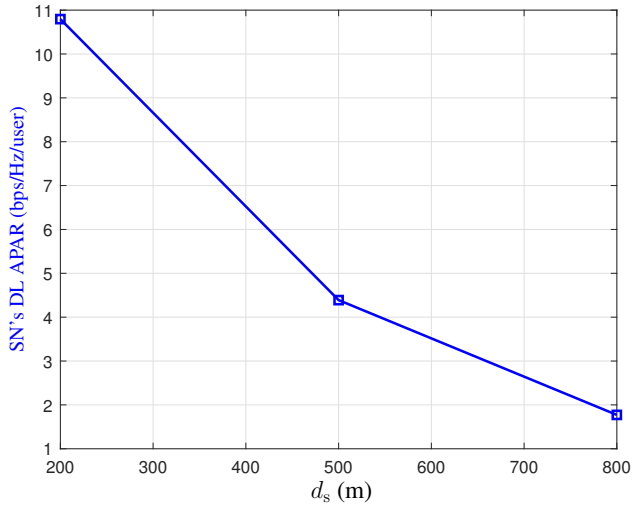

(b) SN in downlink.

Figure 3.10: SN's APARs in both scenarios versus d_{s} for estimated CSI, with $M_{\mathrm{p}} = 32$, $M_{\mathrm{s}} = 20$, $N_{\mathrm{p}} = 4$, $N_{\mathrm{s}} = 4$, $d_{\mathrm{p}} = 1000$ m, $\tilde{P}_1 = 25$ dBW, $\tilde{P}_2 = 20$ dBW, $\eta = 0.5$, $\rho = 0.9$, $N_{\mathrm{t}} = 12$, $N_{\mathrm{up}} = 200$, $N_{\mathrm{dp}} = 200$.

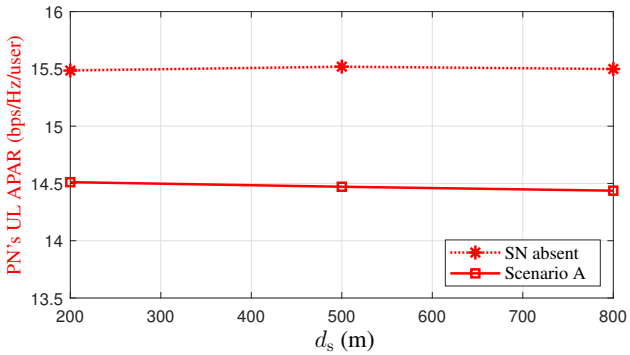

(a) PN in uplink.

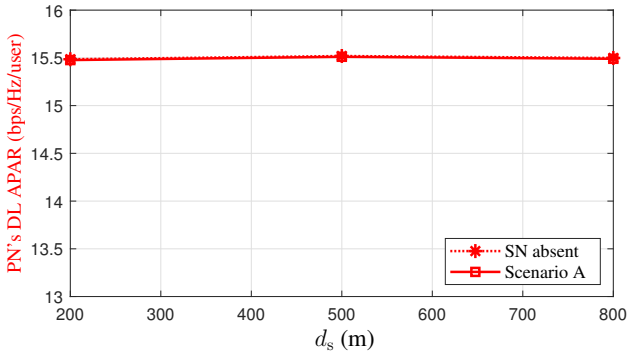

(b) PN in downlink.

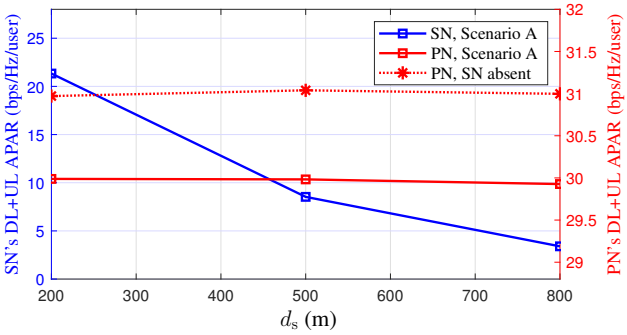

(c) DL+UL APARs of SN and PN.

Figure 3.11: SN's and PN's APARs in both scenarios versus d_s for estimated CSI, with $M_p = 32$, $M_s = 20$, $N_p = 4$, $N_s = 4$, $d_p = 1000$ m, $\tilde{P}_1 = 25$ dBW, $\tilde{P}_2 = 20$ dBW, $\eta = 0.5$, $\rho = 0.9$, $N_t = 12$, $N_{up} = 200$, $N_{dp} = 200$.

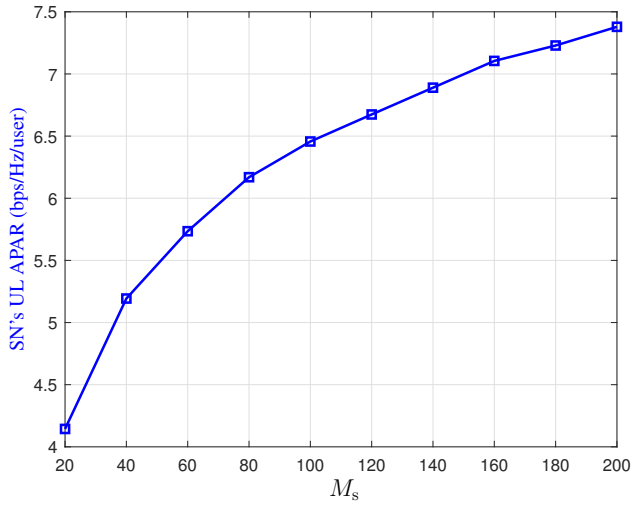

(a) SN in uplink.

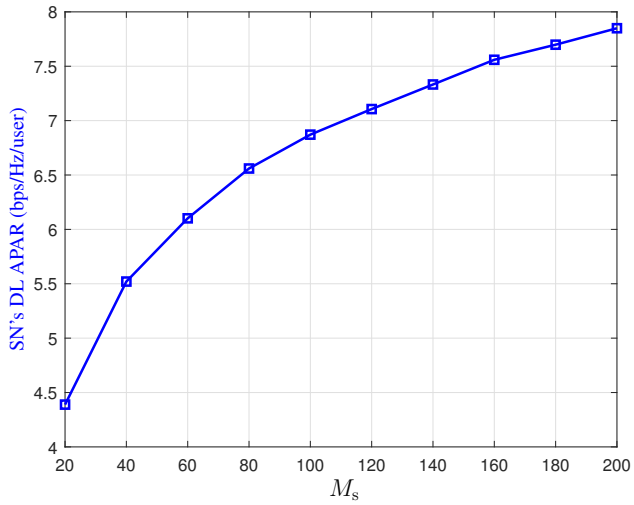

(b) SN in downlink.

Figure 3.12: SN's APARs in both scenarios versus M_{s} for estimated CSI, with $M_{\mathrm{p}} = 32$, $N_{\mathrm{p}} = 4$, $N_{\mathrm{s}} = 4$, $d_{\mathrm{p}} = 1000$ m, $d_{\mathrm{s}} = 500$ m, $\tilde{P}_1 = 25$ dBm, $\tilde{P}_2 = 20$ dBm, $\eta = 0.5$, $\rho = 0.9$, $N_{\mathrm{t}} = 12$, $N_{\mathrm{up}} = 200$, $N_{\mathrm{dp}} = 200$.

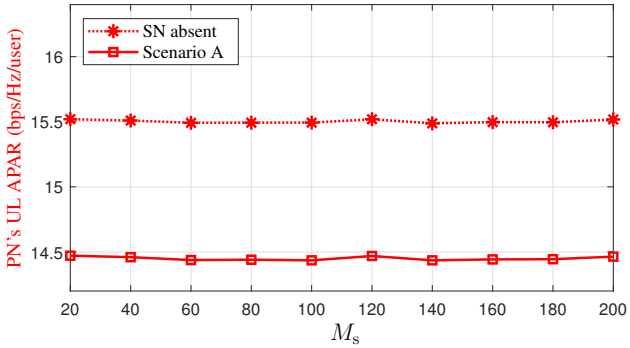

(a) PN in uplink.

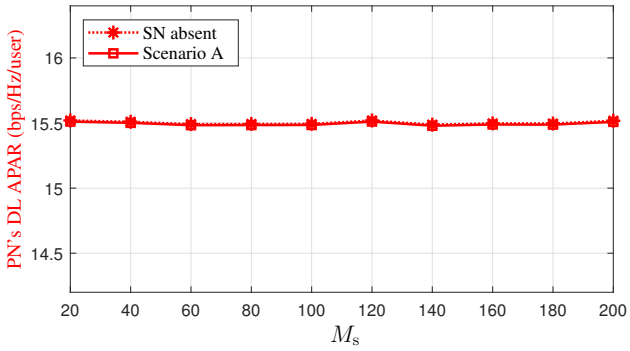

(b) PN in downlink.

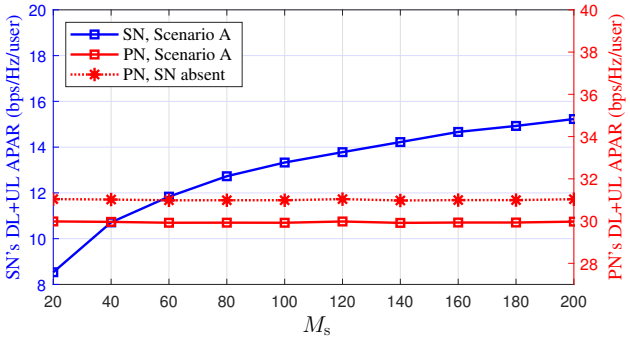

(c) DL+UL APARs of SN and PN.

Figure 3.13: SN's and PN's APARs in both scenarios versus M_{s} for estimated CSI, with $M_{\mathrm{p}} = 32$, $N_{\mathrm{p}} = 4$, $N_{\mathrm{s}} = 4$, $d_{\mathrm{p}} = 1000$ m, $d_{\mathrm{s}} = 500$ m, $\tilde{P}_1 = 25$ dBm, $\tilde{P}_2 = 20$ dBm, $\eta = 0.5$, $\rho = 0.9$, $N_{\mathrm{t}} = 12$, $N_{\mathrm{up}} = 200$, $N_{\mathrm{dp}} = 200$.

UL and the DL. It is worth emphasizing that in the SN's UL, the SN has to guarantee a minimum data rate for each PU. Thus, increasing the number of SBS's antennas does not change the PN performance considerably. Additionally, in the DL state of the SN, the SN works in the spatial spectrum holes of the PN, and hence, increasing M_{s} cannot affect the PN's performance noticeably. It should be added that the UL state of the PN coincides with the training and UL modes of the SN. Thus, the interference causes by the SN on PN during the training mode leads to more degradation of APAR of the PN in UL (Fig. 3.13(a)) compare to DL (Fig. 3.13(b)). For the considered set of parameters with all values of M_{s}, Fig. 3.13(c) indicates the UL+DL APAR for the SN and PN.

Chapter 4

Underlay Spectrum Sharing in a R-TDD Massive MIMO Network

This chapter is dedicated to addressing the joint challenges of power allocation and beamforming design within the context of the R-TDD protocol, referred to as Scenario B. In R-TDD, the PN operates in UL while the SN is in training and DL phases, and vice versa. Our primary goal is to ensure the QoS requirements of the PN while maximizing the total achievable sum-rate of the SN in both the UL and DL.

To achieve this, we formulate an optimization problem that takes into account the minimum acceptable data rate of each PU in both UL and DL, while satisfying the power constraints of the SN. Effectively, we divide the main optimization problem into two separate problems, one for UL and another for DL, each with its corresponding solutions. This chapter's structure is as follows: In Section 4.1 and 4.2, we introduce the system model and data models that describe the signals received by the SN and PN nodes in both UL and DL states, respectively. In Section 4.3, we introduce the main optimization problem and detail the strategies employed to address the UL and DL aspects independently. Subsequently, Section 4.4 and 4.5 provide some remarkable notes and an in-depth discussion of the numerical results obtained from our proposed approaches, respectively. We conduct a comparative analysis of the performances of the PN and SN in UL and DL for both Scenario A and Scenario B. Furthermore, we investigate how the APAR of the SN and PN in UL+DL scenarios may be affected by

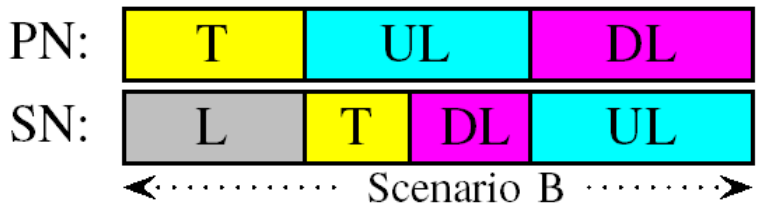

Figure 4.1: Scenario B in frame f.

variations in the PN or SN parameters. The obtained results provide valuable insights into the efficiency of the power allocation and beamforming schemes, which contribute to enhancing the overall system capacity and ensuring the desired QoS for both the PN and SN in the R-TDD mode. Lastly, we compare our proposed approach to an exit research [136].

4.1 System Model

In Scenario B, as previously mentioned, we adopt a cognitive radio scheme where two massive MIMO networks operate within the same RF bandwidth. In this setting, the PN is allocated the RF bandwidth, while the SN opportunistically utilizes the available spectrum with minimal interference to the PN's operations. The PN is composed of a base station equipped with M_{p} antennas, serving N_{p} single-antenna users. Similarly, the SN consists of a base station with M_{s} antennas, catering to N_{s} single-antenna users. The geometric configuration of the two networks remains the same as assumed in Scenario A (Fig. 3.1). However, the operational framework in Scenario B significantly differs, employing R-TDD (Fig. 4.1).

4.2 Data Models of Scenario B

Within this section, we establish data models for both UL and DL modes specific to Scenario B. To maintain simplicity and consistency, we repurpose some of the notations employed in the preceding section.

4.2.1 PN's DL data model

In Scenario B, when the SN is in UL, the PN is in DL. Let $y_{1,l}(f,t)$ represent the signal received at the l-th PU at time t of frame f, for $t = 1, 2, \ldots, N_{\rm dp}$. We can then write

$$y_{1,l}(f,t) = \mathbf{h}_{1,l}^T \mathbf{W}_1^* \big(\tilde{\mathbf{a}}_1(t) \odot \mathbf{x}_1(f,t)\big) + \mathbf{g}_l^T \big(\mathbf{a}_2(t) \odot \mathbf{s}_2(f,t)\big) + \nu_{1,l}(f,t). \tag{4.1}$$

Here, $\mathbf{g}_l \triangleq [g_{l1} \quad g_{l2} \quad \cdots \quad g_{lN_{\rm s}}]^T \in \mathbb{C}^{N_{\rm s}\times 1}$ is the channel vector between the l-th PU and all SUs, where g_{lk} is the channel gain between the l-th PU and the k-th SU. Also, $\mathbf{x}_1(f,t) \in \mathbb{C}^{N_{\rm p}\times 1}$ is the vector of the DL unit-power symbols transmitted by the PBS towards all PUs at time t of frame f, for $t = 1, 2, \ldots, N_{\rm dp}$; whereas $\mathbf{s}_2(f,t) \in \mathbb{C}^{N_{\rm s}\times 1}$ stands for the vector of the unit-power symbols transmitted by all SUs during the UL of frame f, for $t = 1, 2, \ldots, N_{\rm up}$. The power adjusting vectors $\tilde{\mathbf{a}}_1(t)$ and $\mathbf{a}_2(t)$ are defined as $\tilde{\mathbf{a}}_1(t) \triangleq [\sqrt{\tilde{p}_{1,1}} \quad \sqrt{\tilde{p}_{1,2}} \quad \cdots \quad \sqrt{\tilde{p}_{1,N_{\rm p}}}]^T$ and $\mathbf{a}_2(t) = [\sqrt{p_{2,1}} \quad \sqrt{p_{2,2}} \quad \cdots \quad \sqrt{p_{2,N_{\rm s}}}]^T$, where $\tilde{p}_{1,l}$ is the power allocated to the l-th PU by the PBS, and $p_{2,k}$ stands for the transmit power of the k-th SU; $\nu_{1,l}(f,t)$ is the measurement noise component at the l-th PU at time t in frame f. It should be mentioned that in Scenario B, we have $N_{\rm dp} = N_{\rm us}$ (see Fig. 3.2). From (4.1), the DL SINR at the l-th PU, denoted as $\tilde{\gamma}_{1,l}(t)$, is now given by

$$\tilde{\gamma}_{1,l}(t) = \frac{\tilde{p}_{1,l}|\mathbf{w}_{1,l}^H \mathbf{h}_{1,l}|^2}{\sum\limits_{l'\neq l} \tilde{p}_{1,l'}|\mathbf{w}_{1,l'}^H \mathbf{h}_{1,l}|^2 + \sum\limits_{k=1}^{N_{\rm s}} p_{2,k}|g_{lk}|^2 + \sigma^2}, \quad \text{for } t = 1, 2, \ldots, N_{\rm dp}. \tag{4.2}$$

4.2.2 SN's UL data model

We now use $\mathbf{r}_2(f,t) \in \mathbb{C}^{N_{\rm s}\times 1}$ to represent the vector of the UL received signals after beamforming at the SBS at time t within frame f, for $t = 1, 2, \ldots, N_{\rm dp}$. We can then write

$$\mathbf{r}_2(f,t) = \mathbf{W}_2^H \mathbf{H}_2 \big(\mathbf{a}_2(t) \odot \mathbf{s}_2(f,t)\big) + \mathbf{W}_2^H \mathbf{Q}_{12} \mathbf{W}_1^* \big(\tilde{\mathbf{a}}_1(t) \odot \mathbf{x}_1(f,t)\big) + \mathbf{W}_2^H \mathbf{n}_2(f,t) \tag{4.3}$$

where $\mathbf{Q}_{12} \in \mathbb{C}^{M_{\rm s}\times M_{\rm p}}$ represents the MIMO channel between the SBS and the PBS; $\mathbf{n}_2(f,t) \in \mathbb{C}^{M_{\rm s}\times 1}$ denotes the receiver noise vector at time t of frame f. Based on (4.3),

at time t, the SINR at the SBS corresponding to the k-th SU, denoted as $\gamma_{2,k}(t)$, is given by

$$\gamma_{2,k}(t) = \frac{p_{2,k}|\mathbf{w}_{2,k}^H \mathbf{h}_{2,k}|^2}{\sum_{k' \neq k} p_{2,k'}|\mathbf{w}_{2,k}^H \mathbf{h}_{2,k'}|^2 + \|\mathbf{w}_{2,k}^H \mathbf{Q}_{12} \mathbf{W}_1^* \mathrm{diag}(\tilde{\mathbf{a}}_1(t))\|^2 + \sigma^2 \|\mathbf{w}_{2,k}\|^2}, \quad \text{for } t = 1, 2, \ldots, N_{\mathrm{dp}}. \tag{4.4}$$

4.2.3 PN's UL data model

In Scenario B, when the SN is in training and DL, the PN is in UL. Let $\mathbf{r}_1(f,t) \in \mathbb{C}^{N_{\mathrm{p}} \times 1}$ represent the vector of the received signals after beamforming at the PBS during the PN's uplink at time t of frame f, for $t = 1, 2, \ldots, N_{\mathrm{up}}$. We can then write

$$\mathbf{r}_1(f,t) = \mathbf{W}_1^H \mathbf{H}_1\big(\mathbf{a}_1(t) \odot \mathbf{s}_1(f,t)\big) + \mathbf{W}_1^H \mathbf{z}_2(f,t) + \mathbf{W}_1^H \mathbf{n}_1(f,t). \tag{4.5}$$

where we use $\mathbf{s}_1(f,t) \in \mathbb{C}^{N_{\mathrm{p}} \times 1}$ to represent the vector of the UL unit-power symbols transmitted by all PUs at time t in frame f, for $t = 1, 2, \ldots, N_{\mathrm{up}}$; the power adjusting vector $\mathbf{a}_1(t)$ is defined as $\mathbf{a}_1(t) \triangleq [\sqrt{p_{1,1}} \quad \sqrt{p_{1,2}} \quad \cdots \quad \sqrt{p_{1,N_{\mathrm{p}}}}]^T = p_{1,\max}\mathbf{1}$, with $p_{1,l} = p_{1,\max}$ being the transmit power of the l-th PU. Also, $\mathbf{z}_2(f,t) \in \mathbb{C}^{M_{\mathrm{p}} \times 1}$ stands for the vector[1] of the unit-power symbols transmitted by all SUs during training at frame f, for $t = 1, 2, \ldots, N_{\mathrm{t}}$, concatenated by the vector of the unit-power symbols transmitted by the SBS during DL at frame f, for $t = N_{\mathrm{t}}+1, N_{\mathrm{t}}+2, \ldots, N_{\mathrm{up}}$. That is, we can write

$$\mathbf{z}_2(f,t) = \begin{cases} \mathbf{H}_{12}\big(\tilde{\mathbf{a}}_2(t) \odot \mathbf{t}_2(f,t)\big), & \text{for } t = 1, 2, \ldots, N_{\mathrm{t}} \\ \mathbf{Q}_{12}^T \tilde{\mathbf{W}}_2^*\big(\tilde{\mathbf{a}}_2(t) \odot \mathbf{x}_2(f,t)\big), & \text{for } t = N_{\mathrm{t}}+1, N_{\mathrm{t}}+2, \ldots, N_{\mathrm{up}} \end{cases} \tag{4.6}$$

where $\mathbf{t}_2(f,t) \in \mathbb{C}^{N_{\mathrm{s}} \times 1}$ is the vector of unit-power symbols transmitted by all SUs during training at frame f, for $t = 1, 2, \ldots, N_{\mathrm{t}}$ whereas $\mathbf{x}_2(f,t) \in \mathbb{C}^{N_{\mathrm{s}} \times 1}$ is the vector of the DL unit-power symbols transmitted by the SBS towards all the SUs at time t of frame f, for $t = N_{\mathrm{t}}+1, N_{\mathrm{t}}+2, \ldots, N_{\mathrm{up}}$. The $N_{\mathrm{s}} \times 1$ vector $\tilde{\mathbf{a}}_2(t)$ is defined as

$$\tilde{\mathbf{a}}_2(t) \triangleq \begin{cases} \sqrt{\alpha}\mathbf{1}, & \text{for } t = 1, 2, \ldots N_{\mathrm{t}} \\ \big[\sqrt{\tilde{p}_{2,1}} \quad \sqrt{\tilde{p}_{2,2}} \quad \cdots \quad \sqrt{\tilde{p}_{2,N_{\mathrm{s}}}}\big]^T, & \text{for } t = N_{\mathrm{t}}+1, N_{\mathrm{t}}+2, \ldots, N_{\mathrm{up}} \end{cases} \tag{4.7}$$

[1]Note that as shown in Fig. 3.2, the sum of the length of the vector of the symbols transmitted by SUs during training and that of the vector of the symbol transmitted by the SBS during DL is equal to the length of the symbol vector transmitted by the PUs during uplink.

where α is the transmit power of the SUs during training and $\tilde{p}_{2,k}$ stands for the transmit power of the SBS allocated to the k-th SU, for $k = 1, 2, \ldots, N_{\mathrm{s}}$. Based on (4.5), at time t, the SINR at the PBS corresponding to the l-th PU, denoted as $\gamma_{1,l}(t)$, is given by

$$\gamma_{1,l}(t) = \frac{p_{1,\max}|\mathbf{w}_{1,l}^H \mathbf{h}_{1,l}|^2}{\sum_{l' \neq l} p_{1,\max}|\mathbf{w}_{1,l}^H \mathbf{h}_{1,l'}|^2 + \varrho_l(t) + \sigma^2 \|\mathbf{w}_{1,l}\|^2}, \text{ for } t = 1, 2, \ldots, N_{\mathrm{up}} \tag{4.8}$$

where we define

$$\varrho_l(t) \triangleq \begin{cases} \alpha \|\mathbf{w}_{1,l}^H \mathbf{H}_{12}\|^2, & \text{for } t = 1, 2, \ldots N_{\mathrm{t}} \\ \|\mathbf{w}_{1,l}^H \mathbf{Q}_{12}^T \tilde{\mathbf{W}}_2^* \operatorname{diag}(\tilde{\mathbf{a}}_2(t))\|^2, & \text{for } t = N_{\mathrm{t}}+1, N_{\mathrm{t}}+2, \ldots, N_{\mathrm{up}}. \end{cases} \tag{4.9}$$

4.2.4 SN's DL data model

Let $y_{2,k}(f,t)$ represent the signal received at the k-th SU at time t of frame f, for $t = N_{\mathrm{t}}+1, N_{\mathrm{t}}+2, \ldots, N_{\mathrm{up}}$. We can then write

$$y_{2,k}(f,t) = \mathbf{h}_{2,k}^T \tilde{\mathbf{W}}_2^* \big(\tilde{\mathbf{a}}_2(t) \odot \mathbf{x}_2(f,t)\big) + \breve{\mathbf{g}}_k^T \big(\mathbf{a}_1(t) \odot \mathbf{s}_1(f,t)\big) + \nu_{2,k}(f,t). \tag{4.10}$$

where $\breve{\mathbf{g}}_k \triangleq [\breve{g}_{k1} \;\; \breve{g}_{k2} \;\; \cdots \;\; \breve{g}_{kN_{\mathrm{p}}}]^T \in \mathbb{C}^{N_{\mathrm{p}} \times 1}$ is the channel vector between the k-th SU and all PUs and $\breve{g}_{kl}$ is the channel gain between the k-th SU and the l-th PU; $\nu_{2,k}(f,t)$ is the measurement noise component at the k-th SU at time t of frame f. Based on (4.10), at time t, the SINR at the k-th SU in DL, denoted as $\tilde{\gamma}_{2,k}(t)$, is given by

$$\tilde{\gamma}_{2,k}(t) = \frac{\tilde{p}_{2,k}|\mathbf{h}_{2,k}^H \tilde{\mathbf{w}}_{2,k}|^2}{\sum_{k' \neq k} \tilde{p}_{2,k'}|\mathbf{h}_{2,k}^H \tilde{\mathbf{w}}_{2,k'}|^2 + \sum_{l=1}^{N_{\mathrm{p}}} p_{1,\max}|\breve{g}_{kl}|^2 + \sigma^2}, \text{ for } t = N_{\mathrm{t}}+1, N_{\mathrm{t}}+2, \ldots, N_{\mathrm{up}}. \tag{4.11}$$

In the next section, we present the solutions to the optimization problems of Scenario B in UL and DL.

4.3 Optimization Problems in Scenario B

We now aim to maximize the total sum-rate of the SN in both UL and DL states subject to satisfying predefined constraints on transmitted power of the SN and minimum

acceptable individual rate for the PUs. Let us the UL achievable rate of the l-th PU as

$$R_{1,l}(\mathbf{W}_1, \tilde{\mathbf{W}}_2, \mathbf{p}_1, \tilde{\mathbf{p}}_2) = \frac{1}{N_{\text{up}}} \sum_{t=1}^{N_{\text{up}}} \log_2 \left(1 + \gamma_{1,l}(t)\right) \tag{4.12}$$

Also, we represent the DL achievable rate of the l-th PU as

$$\tilde{R}_{1,l}(\mathbf{W}_1, \tilde{\mathbf{p}}_1, \mathbf{p}_2) = \frac{1}{N_{\text{dp}}} \sum_{t=1}^{N_{\text{dp}}} \log_2 \left(1 + \tilde{\gamma}_{1,l}(t)\right) \tag{4.13}$$

is the DL achievable rate of the l-th PU. Moreover, the total UL sum-rate of the SN is given by

$$R_2(\mathbf{W}_1, \mathbf{W}_2, \tilde{\mathbf{p}}_1, \mathbf{p}_2) = \sum_{k=1}^{N_{\text{s}}} R_{2,k}(\mathbf{W}_1, \mathbf{W}_2, \tilde{\mathbf{p}}_1, \mathbf{p}_2), \tag{4.14}$$

where

$$R_{2,k}(\mathbf{W}_1, \mathbf{W}_2, \tilde{\mathbf{p}}_1, \mathbf{p}_2) = \frac{1}{N_{\text{dp}}} \sum_{t=1}^{N_{\text{dp}}} \log_2 \left(1 + \gamma_{2,k}(t)\right) \tag{4.15}$$

is the UL achievable rate of the k-th SU. Also, we express the total DL sum-rate of the SN as $\tilde{R}_2(\tilde{\mathbf{W}}_2, \mathbf{p}_1, \tilde{\mathbf{p}}_2) = \sum_{k=1}^{N_{\text{s}}} \tilde{R}_{2,k}(\tilde{\mathbf{W}}_2, \mathbf{p}_1, \tilde{\mathbf{p}}_2)$, where $\tilde{R}_{2,k}(\tilde{\mathbf{W}}_2, \mathbf{p}_1, \tilde{\mathbf{p}}_2) = \frac{1}{N_{\text{up}}} \sum_{t=N_{\text{t}}+1}^{N_{\text{up}}} \log_2 \left(1 + \tilde{\gamma}_{2,k}(t)\right)$ is the DL achievable rate of the k-th SU. We can now write the optimization problem of maximizing the weighted UL and DL sum-rates of the SN as

$$\max_{\mathbf{W}_2, \tilde{\mathbf{W}}_2, \mathbf{p}_2, \tilde{\mathbf{p}}_2} \quad \beta R_2(\mathbf{W}_1, \mathbf{W}_2, \tilde{\mathbf{p}}_1, \mathbf{p}_2) + \tilde{\beta} \tilde{R}_2(\tilde{\mathbf{W}}_2, \mathbf{p}_1, \tilde{\mathbf{p}}_2) \tag{4.16a}$$

$$\text{s.t.} \quad \mathcal{C}_1 : 0 \leq p_{2,k} \leq p_{2,\max}, \qquad \text{for } k = 1, 2, \ldots, N_{\text{s}} \tag{4.16b}$$

$$\mathcal{C}_2 : R_{1,l}(\mathbf{W}_1, \tilde{\mathbf{W}}_2, \mathbf{p}_1, \tilde{\mathbf{p}}_2) \geq r_{1,l}, \qquad \text{for } l = 1, 2, \ldots, N_{\text{p}} \tag{4.16c}$$

$$\mathcal{C}_3 : \|\tilde{\mathbf{w}}_{2,k}\|^2 = 1, \qquad \text{for } k = 1, 2, \ldots, N_{\text{s}} \tag{4.16d}$$

$$\mathcal{C}_4 : \mathbf{1}^T \tilde{\mathbf{p}}_2 \leq \tilde{P}_2 \tag{4.16e}$$

$$\mathcal{C}_5 : \tilde{R}_{1,l}(\mathbf{W}_1, \tilde{\mathbf{p}}_1, \mathbf{p}_2) \geq \tilde{r}_{1,l}, \qquad \text{for } l = 1, 2, \ldots, N_{\text{p}} \tag{4.16f}$$

$$\mathcal{C}_6 : \tilde{p}_{2,k} \geq 0\,, \qquad \text{for } k = 1, 2, \ldots, N_{\text{s}}. \tag{4.16g}$$

Based on our assumption that $\mathbf{W}_1$, $\mathbf{p}_1$ and $\tilde{\mathbf{p}}_1$ are set by the PN without taking the presence of the SN into account, these parameters are obtained similar to Scenario A. As it can be seen in (4.16), the parameters determining the sum-rates of both networks in DL and UL are different and thus, we can separate the optimization problems of UL and DL sum-rates as

$$\max_{\mathbf{W}_2,\mathbf{p}_2} \quad R_2(\mathbf{W}_1, \mathbf{W}_2, \tilde{\mathbf{p}}_1, \mathbf{p}_2) \tag{4.17a}$$

$$\text{s.t.} \quad \mathcal{C}_1 : 0 \leq p_{2,k} \leq p_{2,\max}, \qquad \text{for } k = 1, 2, \ldots, N_\text{s} \tag{4.17b}$$

$$\mathcal{C}_5 : \tilde{R}_{1,l}(\mathbf{W}_1, \tilde{\mathbf{p}}_1, \mathbf{p}_2) \geq \tilde{r}_{1,l},, \qquad \text{for } l = 1, 2, \ldots, N_\text{p} \tag{4.17c}$$

and

$$\max_{\tilde{\mathbf{W}}_2,\tilde{\mathbf{p}}_2} \quad \tilde{R}_2(\tilde{\mathbf{W}}_2, \mathbf{p}_1, \tilde{\mathbf{p}}_2) \tag{4.18a}$$

$$\text{s.t.} \quad \mathcal{C}_2 : R_{1,l}(\mathbf{W}_1, \tilde{\mathbf{W}}_2, \mathbf{p}_1, \tilde{\mathbf{p}}_2) \geq r_{1,l}, \qquad \text{for } l = 1, 2, \ldots, N_\text{p} \tag{4.18b}$$

$$\mathcal{C}_3 : \|\tilde{\mathbf{w}}_{2,k}\|^2 = 1, \qquad \text{for } k = 1, 2, \ldots, N_\text{s} \tag{4.18c}$$

$$\mathcal{C}_4 : \mathbf{1}^T \tilde{\mathbf{p}}_2 \leq \tilde{P}_2 \tag{4.18d}$$

$$\mathcal{C}_6 : \tilde{p}_{2,k} \geq 0\,, \qquad \text{for } k = 1, 2, \ldots, N_\text{s}. \tag{4.18e}$$

In the next two subsections, we aim to solve the above two problems.

4.3.1 SN Optimization Problem in UL

Note that obtaining the optimal value of $\mathbf{W}_2$ amounts to maximizing $\gamma_{2,k}(t)$, for $t = 1, 2, \ldots, N_\text{dp}$, as given in (4.4). However such an optimal value, which is indeed the MVDR solution, requires the knowledge of $\mathbf{Q}_{12}\mathbf{W}_1^*$ at the SBS and this knowledge may not be available at the SBS[2]. To tackle this issue, we note that the second term in the denominator of (4.4) is the power of interference caused by the PBS at the SBS during the UL reception of the k-th SU. We propose to cancel this interference by designing the SBS's beamforming matrix such that $\mathbf{W}_2^H \mathbf{Q}_{12}\mathbf{W}_1^* = \mathbf{0}$. As the knowledge of $\mathbf{Q}_{12}\mathbf{W}_1^*$

[2]The MIMO channel $\mathbf{Q}_{12}$ can not be estimated at the SBS as the PBS is not meant to transmit any training symbols, neither may the beamforming matrix $\mathbf{W}_1$ be known at the SBS.

may not be available at the SBS, we propose to ensure that $\mathbf{W}_2^H \boldsymbol{\Upsilon} = \mathbf{0}$, where $\boldsymbol{\Upsilon}$ is an $M_\mathrm{s} \times N_\mathrm{p}$ matrix whose columns span the column space of the *effective* MIMO channel $\mathbf{Q}_{12}\mathbf{W}_1^*$ corresponding to the SBS-PBS links[3]. While $\mathbf{Q}_{12}$ and $\mathbf{W}_1$ may not be known at the SBS, one can estimate $\boldsymbol{\Upsilon}$ during the learning phase, when the PN is in DL. Indeed, during the learning phase[4], the SBS can collect signal vectors when the PN is in DL mode and construct the sample covariance matrix of the received data. The N_p orthogonal eigenvectors of the so-obtained sample covariance matrix corresponding to the N_p largest eigenvalues can be used as the N_p columns of $\boldsymbol{\Upsilon}$. Let us define the $M_\mathrm{s} \times (M_\mathrm{s} - N_\mathrm{p})$ matrix $\boldsymbol{\Gamma}$ such that its columns span the orthogonal column space (left null space) of $\boldsymbol{\Upsilon}$, then the constraint $\mathbf{W}_2^H \boldsymbol{\Upsilon} = \underline{0}$ implies that $\mathbf{W}_2 = \boldsymbol{\Gamma}\boldsymbol{\Lambda}$ must hold true, for some $(M_\mathrm{s} - N_\mathrm{p}) \times N_\mathrm{s}$ matrix $\boldsymbol{\Lambda}$. One simple way to determine $\mathbf{W}_2$ is to ensure that the UL signals of different SUs do not interfere with each other. To do so, we can add the constraint $\mathbf{W}_2{}^H\mathbf{H_2} = \mathbf{I}$, which is equivalent to the constraint $\mathbf{H}_2^H\boldsymbol{\Gamma}\boldsymbol{\Lambda} = \mathbf{I}$. If $M_\mathrm{s} \geq N_\mathrm{s} + N_\mathrm{p}$, we obtain $\boldsymbol{\Lambda} = (\boldsymbol{\Gamma}^H\mathbf{H}_2)(\mathbf{H}_2^H\boldsymbol{\Gamma}\boldsymbol{\Gamma}^\mathbf{H}\mathbf{H_2})^{-\mathbf{1}}$. As a result, by choosing $\mathbf{W}_2 = \boldsymbol{\Gamma}(\boldsymbol{\Gamma}^\mathbf{H}\mathbf{H_2})(\mathbf{H_2^H}\boldsymbol{\Gamma}\boldsymbol{\Gamma}^\mathbf{H}\mathbf{H_2})^{-\mathbf{1}}$, the first two terms in the denominator of (4.4) vanish, and hence, we can write

$$\gamma_{2,k}(t) = \frac{p_{2,k}}{\sigma^2 \|\mathbf{w}_{2,k}\|^2}, \quad \text{for } t = 1, 2, \ldots, N_\mathrm{dp}. \tag{4.19}$$

Now, we turn our attention to the objective function of (4.17). Using the ZF BF in (3.15) for $\mathbf{W}_1$, we can simplify $\tilde{\gamma}_{1,l}(t)$, given in (4.2) as $\tilde{\gamma}_{1,l}(t) = \dfrac{\tilde{p}_{1,l}\mu_l^2}{\sum_{k=1}^{N_\mathrm{s}} p_{2,k}|g_{lk}|^2 + \sigma^2}$, for $t =$

[3]As such, our proposed scheme does not require the knowledge of the MIMO channel $\mathbf{Q}_{12}$ corresponding to the SBS-PBS links using pilot signals, thereby saving communication resources.

[4]Note that the learning phase comprises of several SN's communication frames, where all nodes in the SN remain quiet and listen to the PN. Indeed, what have been shown in Fig. 3.2, are only portions of the learning phase that overlap with the training phase of the PN. The other portion of the learning phase, not shown in Fig. 3.2, comprises of several complete PN's frames, where all nodes in the SN remain quiet and use the signals received from the PN nodes to estimate $\boldsymbol{\Upsilon}$ as well as to estimate the channel vectors corresponding to the SBS-PU and SBS-SU links. For the estimation of the these channel vectors, we refer reader to [76].

$1, 2, \ldots, N_{\rm dp}$. We can then write (4.13) as

$$\tilde{R}_{1,l}(\mathbf{W}_1, \tilde{\mathbf{p}}_1, \mathbf{p}_2) = \frac{1}{N_{\rm dp}} \sum_{t=1}^{N_{\rm dp}} \log_2 \left(1 + \tilde{\gamma}_{1,l}(t)\right) = \log_2 \left(1 + \frac{\mu_l^2 \tilde{p}_{1,l}}{\sum_{k=1}^{N_{\rm s}} p_{2,k} |g_{lk}|^2 + \sigma^2}\right) \tag{4.20}$$

We can now use (4.20) to write Constraints $\mathcal{C}_5$ equivalently as

$$\sum_{k=1}^{N_{\rm s}} p_{2,k} |g_{lk}|^2 \leq \zeta_{1,l}, \text{ for } l = 1, 2, \ldots, N_{\rm p} \tag{4.21}$$

where we define $\zeta_{1,l} \triangleq \frac{\mu_l^2 \tilde{p}_{1,l}}{2^{\tilde{r}_{1,l}} - 1} - \sigma^2$. To enforce (4.21), the SBS requires the knowledge of the parameters $\{\zeta_{1,l}\}_{l=1}^{N_{\rm p}}$. These parameters depend on $\{\mu_l^2 \tilde{p}_{1,l}\}_{l=1}^{N_{\rm p}}$ and $\{\tilde{r}_{1,l}\}_{l=1}^{N_{\rm p}}$. Hence, the PBS is required to provide these parameters to the SBS. Note that as we assume that the PBS uses the water-filling for DL, some of the PUs might not be served by the PBS, i.e., they receive zero power. In such case, those users need not be protected by the SBS. Hence, without loss of generality we assume that all $N_{\rm p}$ PUs receive power in DL, that $\tilde{p}_{1,l} > 0$ and $\tilde{r}_{1,l} > 0$. Note that to enforce $\mathcal{C}_5$ as in (4.21), the SBS requires the knowledge of the coefficients $|g_{lk}|^2$, for $k = 1, 2, \ldots, N_{\rm s}$, and $l = 1, 2, \ldots, N_{\rm p}$, which is the channel gain between the l-th PU and k-th SU. Each SU can use the training symbols transmitted by different PUs during the PN phase to estimate these channel gains and provide the SBS with the channel gain estimates over a control channel. Using $\mathbf{W_2} = \mathbf{\Gamma}(\mathbf{\Gamma^H H_2})(\mathbf{H_2^H \Gamma \Gamma^H H_2})^{-1}$ along with (4.14), (4.15), (4.19), and (4.21), the optimization problem (4.17) is simplified as

$$\max_{\mathbf{p}_2} \quad \sum_{k=1}^{N_{\rm s}} \log_2 (1 + \frac{p_{2,k}}{\sigma^2 \|\mathbf{w}_{2,k}\|^2}) \tag{4.22a}$$

$$\text{s.t.} \quad \mathcal{C}_1 : 0 \leq p_{2,k} \leq p_{2,\max}, \qquad \text{for } k = 1, 2, \ldots, N_{\rm s} \tag{4.22b}$$

$$\mathcal{C}_5 : \sum_{k=1}^{N_{\rm s}} p_{2,k} |g_{lk}|^2 \leq \zeta_{1,l}, \qquad \text{for } l = 1, 2, \ldots N_{\rm p}. \tag{4.22c}$$

The cost function of optimization problem (4.22) is convex, while the constraints are linear. Hence, this problem can be solved using interior point methods.

4.3.2 SN Optimization Problem in DL

We now aim to tackle the optimization problem (4.18). To simplify Constraint $\mathcal{C}_2$, we can use (4.8), (4.9), and (4.12) to write this constraint, for $l = 1, 2, \ldots, N_{\mathrm{p}}$, as

$$\sum_{t=1}^{N_{\mathrm{t}}} \log_2 \left(1 + \frac{p_{1,\max}\mu_l^2}{\alpha \sum_{k=1}^{N_{\mathrm{s}}} |\mathbf{h}_{12,k}^H \mathbf{w}_{1,l}|^2 + \sigma^2}\right) +$$

$$\sum_{t=N_{\mathrm{t}}+1}^{N_{\mathrm{up}}} \log_2 \left(1 + \frac{p_{1,\max}\mu_l^2}{\|\mathbf{w}_{1,l}^H \mathbf{Q}_{12}^T \tilde{\mathbf{W}}_2^* \operatorname{diag}(\tilde{\mathbf{a}}_2(t))\|^2 + \sigma^2}\right) \geq N_{\mathrm{up}} r_{1,l}. \tag{4.23}$$

In order to guarantee (4.23), the SBS requires, among other parameters, the knowledge of$\{\mathbf{w}_{1,l}\mathbf{Q}_{12}\}_{l=1}^{N_{\mathrm{p}}}$. Such knowledge, however, may not be available to the SBS. To tackle this issue, we use a tighter constraint on $\tilde{\mathbf{W}}_2$ as $\tilde{\mathbf{W}}_2^H \boldsymbol{\Upsilon} = \underline{0}$. Doing so ensures that $\tilde{\mathbf{W}}_2$ has no role in guaranteeing (4.23). Furthermore, to ensure that the signal intended for any SU causes no interference to other SUs, we resort to the ZF constraint on $\tilde{\mathbf{W}}_2$, written as $\tilde{\mathbf{W}}_2^H \mathbf{H}_2 = \mathbf{D}$, where $\mathbf{D}$ is a complex diagonal matrix used to satisfy Constraint $\mathcal{C}_3$. As the columns of $\boldsymbol{\Gamma}$ span the orthogonal column space (left null space) of $\boldsymbol{\Upsilon}$, then the constraint $\tilde{\mathbf{W}}_2^H \boldsymbol{\Upsilon} = \mathbf{0}$ implies that $\tilde{\mathbf{W}}_2 = \boldsymbol{\Gamma}\tilde{\boldsymbol{\Lambda}}$ must hold true, for some $(M_{\mathrm{s}} - N_{\mathrm{p}}) \times N_{\mathrm{s}}$ matrix $\tilde{\boldsymbol{\Lambda}}$. If $M_{\mathrm{s}} \geq N_{\mathrm{s}} + N_{\mathrm{p}}$, we obtain $\tilde{\boldsymbol{\Lambda}} = (\boldsymbol{\Gamma}^H \mathbf{H}_2)(\mathbf{H}_2^H \boldsymbol{\Gamma}\boldsymbol{\Gamma}^{\mathbf{H}} \mathbf{H_2})^{-1}\mathbf{D}$. Therefore, we can show that

$$\tilde{\mathbf{W}}_2 = \boldsymbol{\Gamma}(\boldsymbol{\Gamma}^H \mathbf{H}_2)(\mathbf{H}_2^H \boldsymbol{\Gamma}\boldsymbol{\Gamma}^{\mathbf{H}} \mathbf{H_2})^{-1}\mathbf{D}, \tag{4.24}$$

where the k-th diagonal element of $\mathbf{D}$ can be defined as the inverse of the ℓ_2-norm of the k-th column of $\boldsymbol{\Gamma}(\boldsymbol{\Gamma}^{\mathbf{H}} \mathbf{H_2})(\mathbf{H_2^H}\boldsymbol{\Gamma}\boldsymbol{\Gamma}^{\mathbf{H}} \mathbf{H_2})^{-1}$. Note also that in (4.23), the term $|\mathbf{h}_{12,k}^H \mathbf{w}_{1,l}|^2$ is not known at the SBS. To address this issue, we replace this term with the approximation given by (3.23). Given $\tilde{\mathbf{W}}_2$ in (4.24), the optimization problem (4.18) is simplified as

$$\max_{\tilde{\mathbf{p}}_2} \quad \frac{N_{\mathrm{up}} - N_{\mathrm{t}}}{N_{\mathrm{up}}} \sum_{k=1}^{N_{\mathrm{s}}} \log_2 \Big[1 + \frac{\tilde{p}_{2,k}\mathbf{D}_{k,k}^2}{\sum_{l=1}^{N_{\mathrm{p}}} p_{1,\max}|\breve{g}_{kl}|^2 + \sigma^2}\Big] \tag{4.25a}$$

$$\text{s.t.} \quad \mathcal{C}_4 : \mathbf{1}^T \tilde{\mathbf{p}}_2 \leq \tilde{P}_2, \tag{4.25b}$$

$$\mathcal{C}_6 : \tilde{p}_{2,k} \geq 0\,, \qquad \text{for } k = 1, 2, \ldots, N_{\mathrm{s}}. \tag{4.25c}$$

The solution to (4.25) can be obtained using the well-known water-filling algorithm as

$$\tilde{p}_{2,k} = \max\{0, \psi_2 - \mathbf{D}_{k,k}^{-2}(\sum_{l=1}^{N_{\mathrm{p}}} p_{1,\max}|\breve{g}_{kl}|^2 + \sigma^2)\} \tag{4.26}$$

where ψ_2 is determined, using a bisection method, as the solution to the following equation: $\sum_{k=1}^{N_{\mathrm{s}}} \max\{0, \psi_2 - \mathbf{D}_{k,k}^{-2}(\sum_{l=1}^{N_{\mathrm{p}}} p_{1,\max}|\breve{g}_{kl}|^2 + \sigma^2)\} = \tilde{P}_2$.

4.4 Remarks

The following remarks are in order.

Remark 1: Note that the proposed solutions require a good time alignment. In this work we assumed such a time alignment has been achieved. Devising such time synchronization does not fit in the scope of this work. We believe available time synchronization techniques can be used to ensure the two networks are time-aligned within acceptable tolerance.

Remark 2: Note that the solution proposed for Scenario A requires that the PBS provide a few parameters, namely $\{\mu_l^2 p_{1,\max}\}_{l=1}^{N_{\mathrm{p}}}$, $\{r_{1,l}\}_{l=1}^{N_{\mathrm{p}}}$ and $\{\tilde{r}_{1,l}\}_{l=1}^{N_{\mathrm{p}}}$ to the SBS. In Scenario B, the PBS is required to provide the parameters $\{\mu_l^2 \tilde{p}_{1,l}\}_{l=1}^{N_{\mathrm{p}}}$, $\{\tilde{r}_{1,l}\}_{l=1}^{N_{\mathrm{p}}}$, and $p_{1,\max}$ to the SBS. As such, in each scenario, there is only a minimal information exchange between the two networks. Upon receiving these parameters from the PBS, the SBS can then find the solution to corresponding optimization problem for each scenario, thereby obtaining the respective beamformers and the power allocation scheme.

4.5 Simulation Results

4.5.1 The impact of varying PN and SN parameters on the performances of both scenarios

In this part of our dissertation, we investigate the influence of various parameters on the performances of the PN and SN in both scenarios A and B. The corresponding solutions

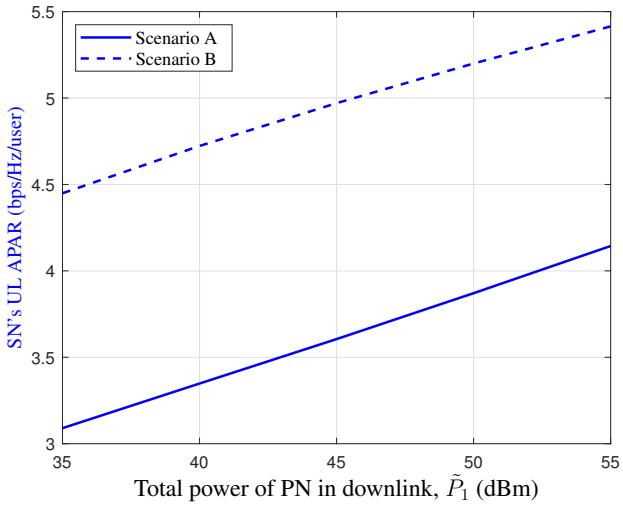

(a) SN in uplink.

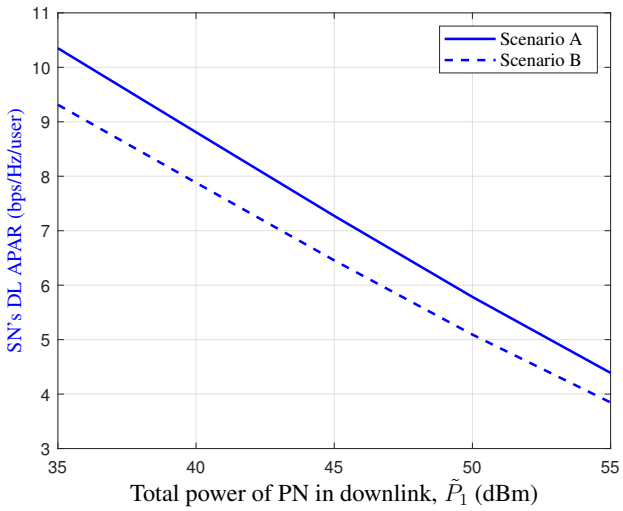

(b) SN in downlink.

Figure 4.2: SN's APARs in both scenarios versus total power of the PN for estimated CSI, with $M_{\mathrm{p}} = 32$, $M_{\mathrm{s}} = 20$, $N_{\mathrm{p}} = 4$, $N_{\mathrm{s}} = 4$, $d_{\mathrm{p}} = 1000$ m, $d_{\mathrm{s}} = 500$ m, $\tilde{P}_2 = 20$ dBm, $\eta = 0.5$, $\rho = 0.9$, $N_{\mathrm{t}} = 12$, $N_{\mathrm{up}} = 200$, $N_{\mathrm{dp}} = 200$.

are based on the estimated CSI obtained using the method proposed in [76]. Fig. 4.2 presents the achieved APAR in the UL, DL, and combined UL+DL versus $\tilde{P}_1$ for both networks under certain conditions: $M_{\mathrm{s}} = 20$, $N_{\mathrm{p}} = 4$, $N_{\mathrm{s}} = 4$, $\tilde{P}_2 = 20$ dBm, $d_{\mathrm{s}} = 500$ m, and $\rho = 0.9$. As depicted in Fig. 4.2(a), increasing the transmit power, $\tilde{P}_1$, enhances the SN's UL APAR in both scenarios. This improvement, same as what we explained in chapter 3, is attributed to the increase in the maximum achievable rates ($r_{1,l}^{\max}$ and $\tilde{r}_{1,l}^{\max}$). As $\tilde{P}_1$ rises, allowing the SN to exploit more spectral usage by imposing more interference on the PN. Consequently, the SN's UL APAR is augmented. Moreover, Scenario B outperforms Scenario A by approximately 1.3 (bps/Hz/user) in terms of the SN's UL APAR. This is attributed to the fact that in Scenario B, the SBS receives less interference from the PBS, which is equipped with beamforming, compared to Scenario A, where the single-antenna PUs cannot employ beamforming techniques and cause more interference on the SBS in this state. On the other hand, Fig. 4.2(b), illustrates that increasing $\tilde{P}_1$ degrades the performance of both scenarios in the DL state of the SN, as the PN causes more interference to the Secondary Users (SUs) with the increase in $\tilde{P}_1$. In this phase, Scenario A exhibits better performance compared to Scenario B. This difference arises because in Scenario A, the SUs experience less interference from the PBS, which employs beamforming, while in Scenario B, the single-antenna PUs cannot control interference and have an omni-directional transmission pattern. According to Fig. 4.3(a), in the PN's UL state, Scenario B demonstrates approximately 0.4 (bps/Hz/user) higher performance in terms of the PN's UL APAR compared to Scenario A. It should be noted that in Scenario B, the SBS utilizes a beamformer, allowing it to safeguard the PBS. Conversely, in Scenario A, the SUs lack the ability to protect the PBS since they are equipped with single-antenna units. Furthermore, it is evident from the graph that even though the SBS safeguards the PBS in Scenario B, the presence of the SN leads to a degradation in the PN's performance compared to the scenario without the SN. This can be attributed to the fact that the pilots transmitted by the SUs disrupt the signals received by the PBS from the PUs during the SN's training phase, which aligns with the

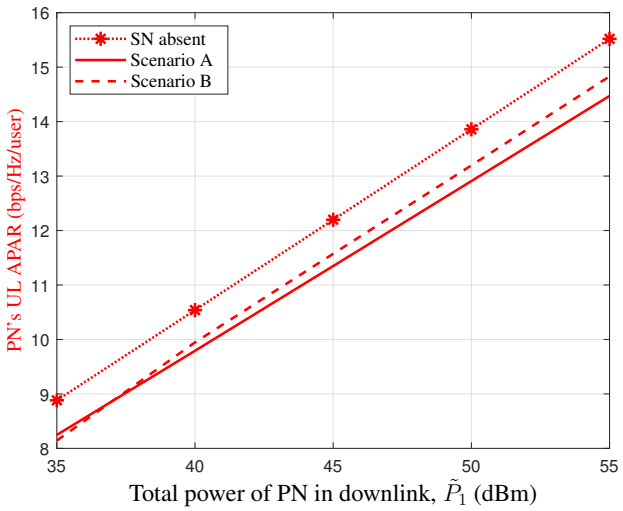

(a) PN in uplink.

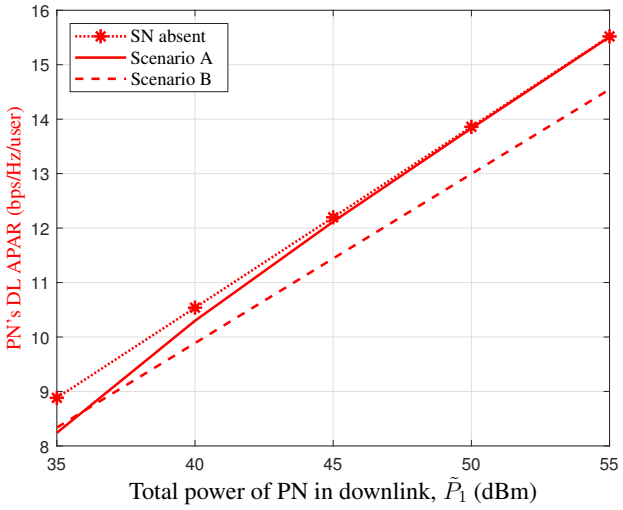

(b) PN in downlink.

Figure 4.3: PN's APARs in both scenarios versus total power of the PN for estimated CSI, with $M_{\mathrm{p}} = 32$, $M_{\mathrm{s}} = 20$, $N_{\mathrm{p}} = 4$, $N_{\mathrm{s}} = 4$, $d_{\mathrm{p}} = 1000$ m, $d_{\mathrm{s}} = 500$ m, $\tilde{P}_2 = 20$ dBm, $\eta = 0.5$, $\rho = 0.9$, $N_{\mathrm{t}} = 12$, $N_{\mathrm{up}} = 200$, $N_{\mathrm{dp}} = 200$.

UL interval of the PN (refer to Figs. 3.2 and 4.1). Despite the protection provided to the PBS during the SN's DL, this interference remains, impacting the overall performance of the PN in Scenario B. Fig. 4.3(b) illustrates that during the PN's DL phase, Scenario A enhances the PN's APAR by approximately 1 (bps/Hz/user) compared to Scenario B. In Scenario A, the SBS can safeguard the PUs during the PN's DL phase, while the SUs lack the capability to provide such protection in Scenario B. Moreover, we notice that the PN's DL performance remains nearly unchanged when the SN is absent compared to its presence in Scenario A. Importantly, in Scenario A, the SN can protect the PUs during the PN's DL phase, and the SN's training phase does not coincide with the PN's DL. As depicted in Fig. 4.4(a) for these simulation parameters, Scenario B exhibits a higher UL+DL APAR for the SN compared to Scenario A, while showing a slightly lower UL+DL APAR for the PN. As illustrated in Fig. 4.4(b), the APAR of the entire network (PN+SN) surpasses that of the PN network alone, without the presence of SN. This observation indicates that the adoption of the proposed USS approach leads to an enhancement in the overall APAR of the network.

In Fig. 4.5, we explore the impact of d_{s} on the APARs of both networks. Considering $M_{\mathrm{s}} = 20$, $N_{\mathrm{p}} = 4$, $N_{\mathrm{s}} = 4$, $\tilde{P}_1 = 25$ dBm, $\tilde{P}_2 = 20$ dBm and $\rho = 0.9$, we plot the UL, DL, and UL+DL APARs against d_{s} for both the PN and the SN in Scenario A and Scenario B. As illustrated in Figs. 4.5(a) and 4.5(a), the UL and DL APARs of the SN in both scenarios show a decrease as d_{s} increases. As we explain this situation in chapter 3, this observation can be attributed to the impact of increased d_{s} on the average distances between the SUs and the SBS. As d_{s} rises, the average distance between the SUs and the SBS increases, which results in a degradation of the average channel quality between them. Conversely, as d_{s} increases, the average distances between the SN's and the PN's nodes decrease, leading to an improvement in the average channel quality between them. Consequently, this situation results in more interference caused by the PN to the SN. As seen in Fig. 4.5(a), the increasing trend in d_{s} leads to a notable widening of the gap between the UL APAR of the SN in scenarios A and B. This outcome

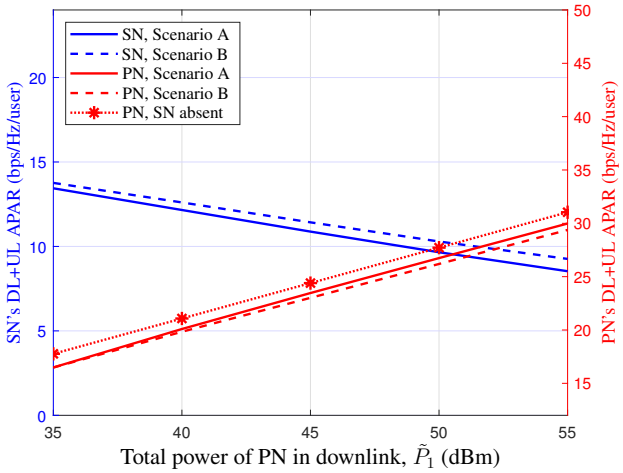

(a) DL+UL APARs of SN and PN.

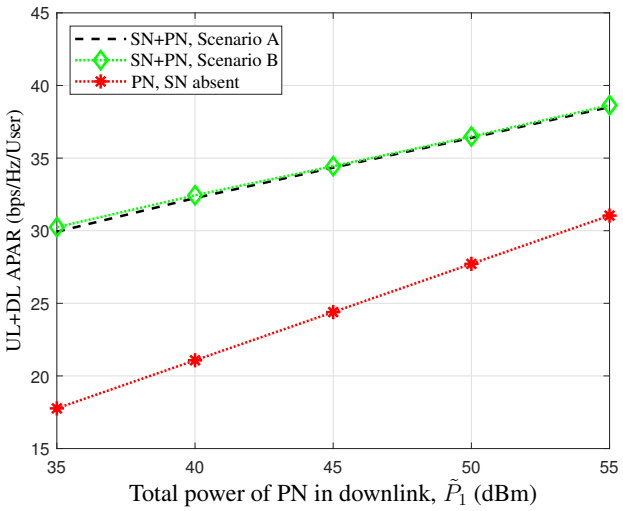

(b) DL+UL APARs of SN+PN and PN.

Figure 4.4: SN's and PN's APARs in both scenarios versus total power of the PN for estimated CSI, with $M_{\mathrm{p}} = 32$, $M_{\mathrm{s}} = 20$, $N_{\mathrm{p}} = 4$, $N_{\mathrm{s}} = 4$, $d_{\mathrm{p}} = 1000$ m, $d_{\mathrm{s}} = 500$ m, $\tilde{P}_2 = 20$ dBm, $\eta = 0.5$, $\rho = 0.9$, $N_{\mathrm{t}} = 12$, $N_{\mathrm{up}} = 200$, $N_{\mathrm{dp}} = 200$.

can be attributed to the differences in interference levels between the two scenarios. In Scenario B, the SBS encounters interference from the PBS, which is equipped with a beamformer. Consequently, the SBS faces reduced interference levels compared to Scenario A, where the SBS needs to guard against interference from single-antenna PUs transmitting omni-directionally. Based on Fig. 4.5(b), it is evident that in the SN's DL phase, Scenario A outperforms Scenario B for smaller to moderately sized SN's coverage areas. This is due to the fact that the SUs experience less interference caused by the PBS equipped with a beamformer in Scenario A, whereas in Scenario B, the single-antenna PUs cause more interference to the SUs. In relatively large SN's areas, Scenario B outperforms Scenario A, indicating that the power transmitted by the PBS (which is higher than the average power transmitted by the PUs) has a more significant impact than the use of beamforming by the PBS. Figs. 4.6(a) and 4.6(b) demonstrate that the PN's UL and DL APARs in scenarios A and B exhibit minimal variations when d_{s} is increased. Indeed, the marginal change in the PN's UL and DL APARs as d_{s} increases can be attributed to the SN's obligation to protect the PN. As a result, increasing the SN's parameters has limited impact on the PN's performance. Analysis of Fig. 4.7(a) shows that under the considered parameters, Scenario A yields higher UL+DL APAR for the SN in small SN coverage areas, whereas for large SN coverage areas, Scenario B exhibits superior performance over Scenario A. Furthermore, it is evident from this figure that Scenario B consistently results in a greater reduction in the PN's UL+DL APAR for all assumed values of d_{s}, compared to Scenario A. This observation can be explained by the substantial difference between Scenarios A and B in the PN's DL (as indicated in Fig. 4.6(b)), which is greater compared to the difference observed in the PN's UL (as shown in Fig. 4.6(a)). As shown in Fig. 4.7(b), the APAR of the PN+SN is markedly higher than the APAR of the PN in the absence of the SN, affirming the effective enhancement in utilizing the underutilized PN frequency band through the implementation of USS. Additionally, in line with our expectations (as seen in Figs. 4.6(a) and 4.6(b)), the performance of the PN remains unaffected by variations in d_{s}. Figs. 4.8,

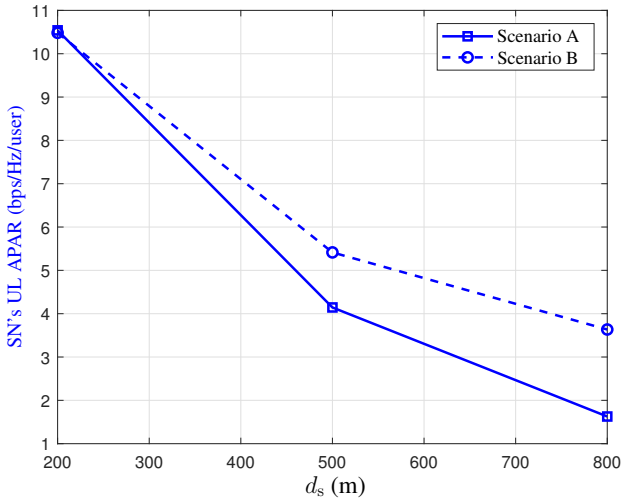

(a) SN in uplink.

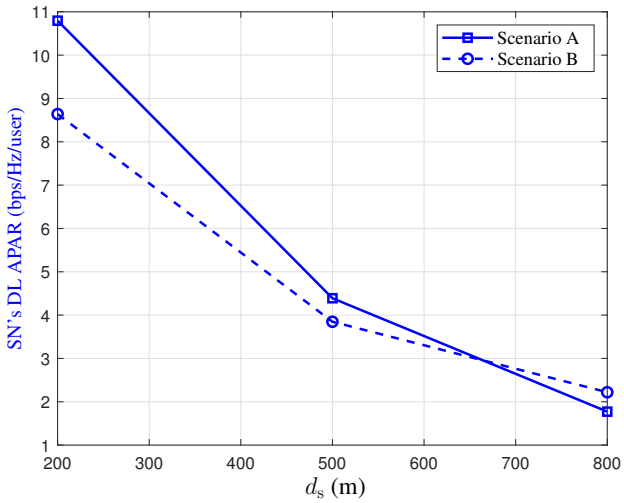

(b) SN in downlink.

Figure 4.5: SN's APARs in both scenarios versus d_s for estimated CSI, with $M_p = 32$, $M_s = 20$, $N_p = 4$, $N_s = 4$, $d_p = 1000$ m, $\tilde{P}_1 = 25$ dBm, $\tilde{P}_2 = 20$ dBm, $\eta = 0.5$, $\rho = 0.9$, $N_t = 12$, $N_{up} = 200$, $N_{dp} = 200$.

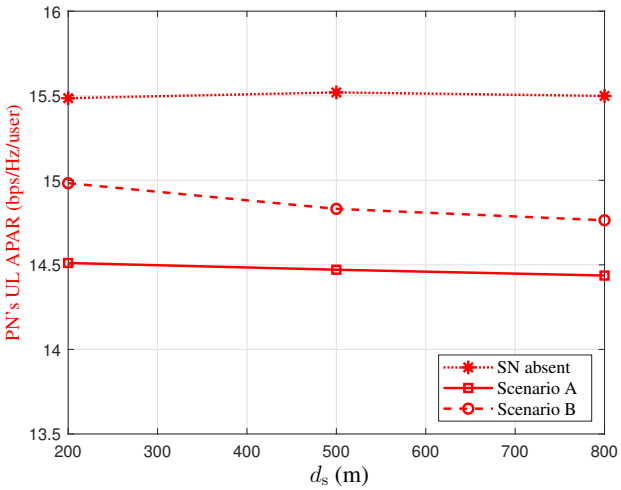

(a) PN in uplink.

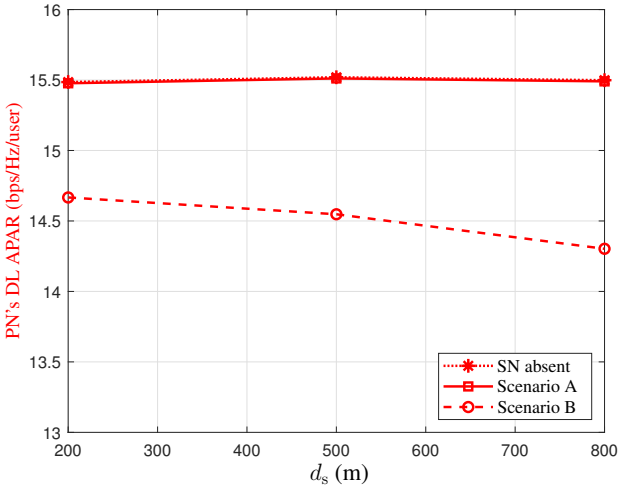

(b) PN in downlink.

Figure 4.6: PN's APARs in both scenarios versus d_s for estimated CSI, with $M_p = 32$, $M_s = 20$, $N_p = 4$, $N_s = 4$, $d_p = 1000$ m, $\tilde{P}_1 = 25$ dBm, $\tilde{P}_2 = 20$ dBm, $\eta = 0.5$, $\rho = 0.9$, $N_t = 12$, $N_{up} = 200$, $N_{dp} = 200$.

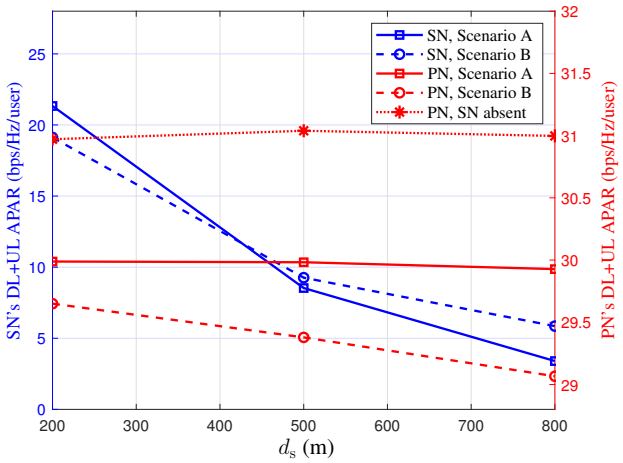

(a) DL+UL APARs of SN and PN.

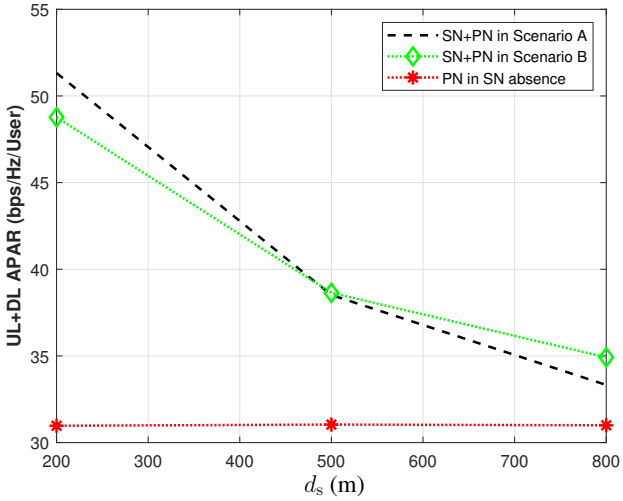

(b) DL+UL APARs of SN+PN and PN.

Figure 4.7: SN's and PN's APARs in both scenarios versus d_s for estimated CSI, with $M_p = 32$, $M_s = 20$, $N_p = 4$, $N_s = 4$, $d_p = 1000$ m, $\tilde{P}_1 = 25$ dBm, $\tilde{P}_2 = 20$ dBm, $\eta = 0.5$, $\rho = 0.9$, $N_t = 12$, $N_{up} = 200$, $N_{dp} = 200$.

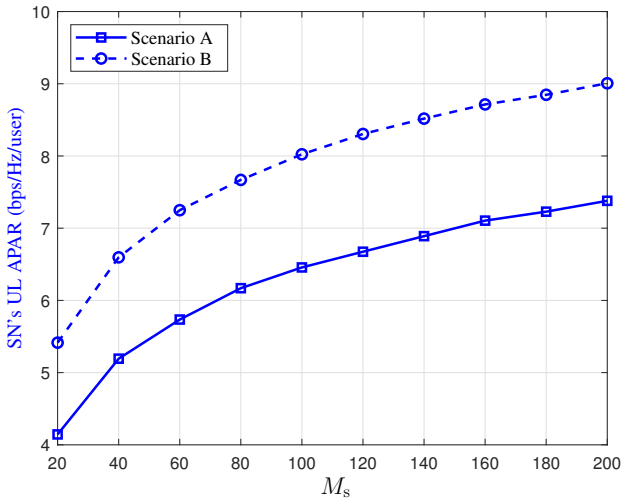

(a) SN in uplink.

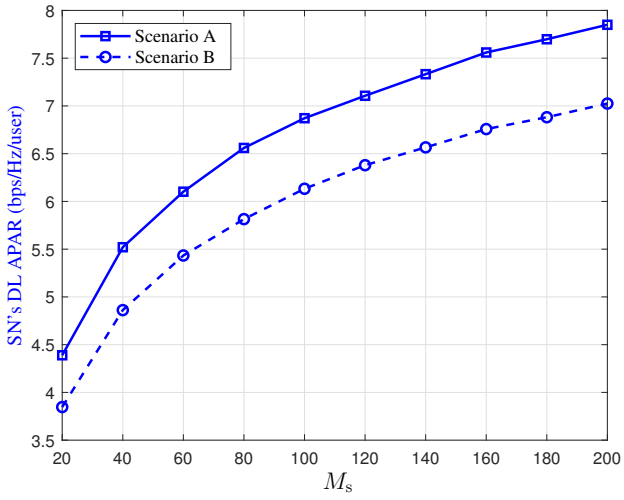

(b) SN in downlink.

Figure 4.8: SN's APARs in both scenarios versus M_{s} for estimated CSI, with $M_{\mathrm{p}} = 32$, $N_{\mathrm{p}} = 4$, $N_{\mathrm{s}} = 4$, $d_{\mathrm{p}} = 1000$ m, $d_{\mathrm{s}} = 500$ m, $\tilde{P}_1 = 25$ dBm, $\tilde{P}_2 = 20$ dBm, $\eta = 0.5$, $\rho = 0.9$, $N_{\mathrm{t}} = 12$, $N_{\mathrm{up}} = 200$, $N_{\mathrm{dp}} = 200$.

4.9 and 4.10 present a comparison of the performance between Scenarios A and B in relation to the APARs of the SN and PN, with varying M_{s}. The parameters assumed for this analysis are $N_{\mathrm{p}} = 4$, $N_{\mathrm{s}} = 4$, $d_{\mathrm{s}} = 500$ m, $\tilde{P}_1 = 25$ dBm, $\tilde{P}_2 = 20$ dBm and $\rho = 0.9$. As anticipated, Figs. 4.8(a) and 4.8(b) demonstrate that an increase in the number of antennas (M_{s}) enhances the performance of both the UL and DL phases of the SN in Scenario A and Scenario B. It can be explained by considering the fact that, increasing the number of SBS's antennas, leads to the implementation of a more effective beamformer. Notably, Scenario B exhibits superior performance in the SN's UL, while Scenario A performs better in the DL. This difference can be attributed to the SBS in Scenario B experiencing reduced interference from the PBS, which is equipped with a beamformer, in contrast to Scenario A, where the SBS faces interference from single-antenna PUs without beamforming capabilities. As illustrated in Figs. 4.9(a) and 4.9(b), varying the number of SBS's antennas (M_{s}) has a minimal impact on the APARs of the PN in both the UL and DL scenarios. This observation is due to specific operational constraints in the SN's UL and DL phases. In the SN's UL, the system must ensure the minimum data rate for each PU. Consequently, increasing the number of SBS's antennas does not significantly alter the PN's performance. Similarly, in the DL state of the SN, it operates in the spatial spectrum holes of the PN, and therefore, variations in M_{s} do not remarkably affect the PN's performance. Fig. 4.10(a) demonstrates that across all values of M_{s} for the considered parameter set, Scenario B outperforms Scenario A in terms of the UL+DL APAR for the SN and results in a higher value. On the other hand, Scenario A leads to a greater UL+DL APAR for the PN. This observation can be explained by the larger gap between the two scenarios in the PN's DL (as depicted in Fig. 4.9(b)) compared to the gap in the PN's UL (as shown in Fig. 4.9(a)). In addition, Fig. 4.10(b), as previously demonstrated, confirms that the utilization of USS significantly improves the overall network performance (PN+SN) for both scenarios when compared to the absence of the SN.

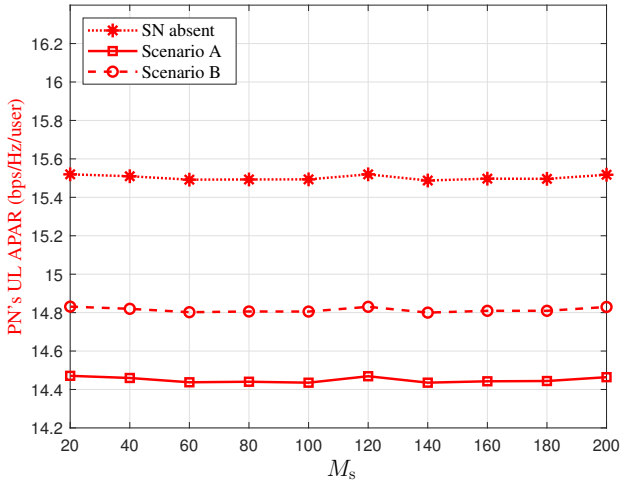

(a) PN in uplink.

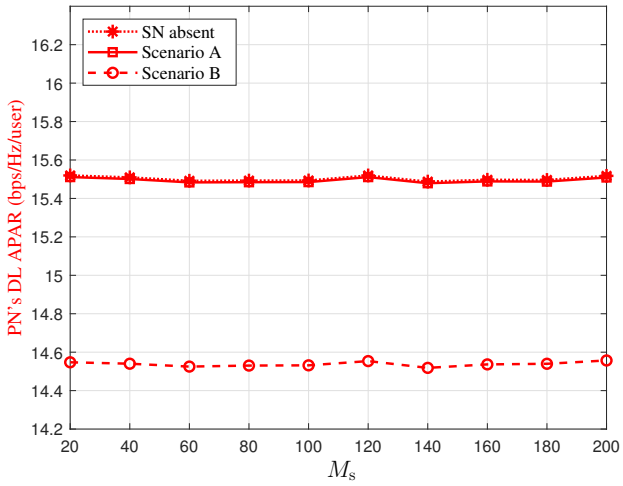

(b) PN in downlink.

Figure 4.9: PN's APARs in both scenarios versus M_{s} for estimated CSI, with $M_{\mathrm{p}} = 32$, $N_{\mathrm{p}} = 4$, $N_{\mathrm{s}} = 4$, $d_{\mathrm{p}} = 1000$ m, $d_{\mathrm{s}} = 500$ m, $\tilde{P}_1 = 25$ dBm, $\tilde{P}_2 = 20$ dBm, $\eta = 0.5$, $\rho = 0.9$, $N_{\mathrm{t}} = 12$, $N_{\mathrm{up}} = 200$, $N_{\mathrm{dp}} = 200$.

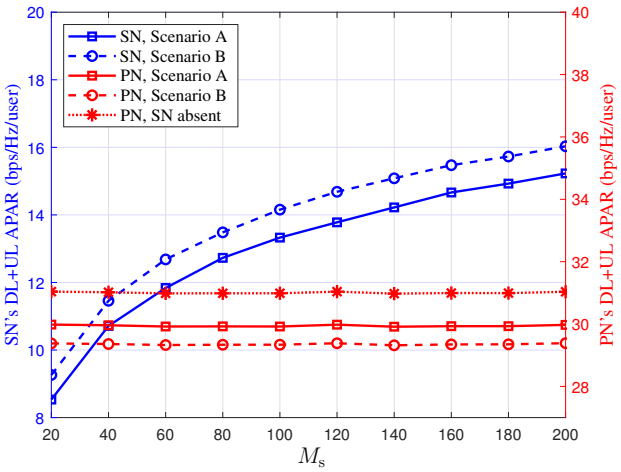

(a) DL+UL APARs of SN and PN.

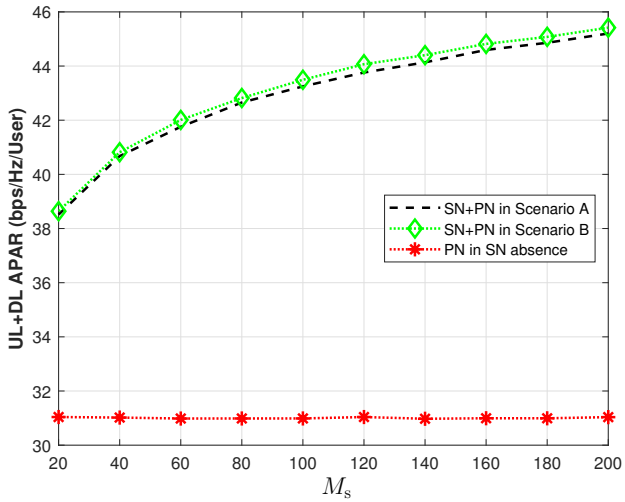

(b) DL+UL APARs of SN+PN and PN.

Figure 4.10: SN's and PN's APARs in both scenarios versus M_{s} for estimated CSI, with $M_{\mathrm{p}} = 32$, $N_{\mathrm{p}} = 4$, $N_{\mathrm{s}} = 4$, $d_{\mathrm{p}} = 1000$ m, $d_{\mathrm{s}} = 500$ m, $\tilde{P}_1 = 25$ dBm, $\tilde{P}_2 = 20$ dBm, $\eta = 0.5$, $\rho = 0.9$, $N_{\mathrm{t}} = 12$, $N_{\mathrm{up}} = 200$, $N_{\mathrm{dp}} = 200$.

4.6 Comparison and Discussion

In Section 4.5, we conduct a comparative analysis of both Scenario A and Scenario B. In this section, we now try to compare our findings to those presented in the literature, [136], and subsequently, we analyse forthcoming simulation results (Fig. 4.11). It is crucial to note that our initial assumptions significantly differ from those of [136]. Consequently, our comparison primarily focuses on the aspect of beamforming strategies. To clarify, in [136], the training phases of both the PN and SN occur concurrently, employing a pilot sharing technique for training. Conversely, in our proposed framework, the SN is restricted from transmitting during the PN training interval. We introduce a learning phase for the SN, during which it listens and gathers information about the PN, with the aim of minimizing PN disruption. Additionally, in [136], the SN and PN share all information jointly, whereas in our system, to mitigate disruption to the PN, the SN employs a learning phase to gather PN information separately. Given these disparities, a comprehensive comparison between these two works is limited, except in the context of beamforming strategies. In [136], conventional ZF BF is employed to facilitate each BS in serving its respective users and reducing interference. In contrast, we employ different ZF BF techniques to mitigate interference caused by SN nodes to PN nodes in both the UL and DL states of both scenarios. Subsequent graphs illustrate the divergent outcomes resulting from the application of various ZF BF methods. As evident in both figures, Figs. 4.11(a) and 4.11(b), our beamforming techniques yield improved performance for both the primary and secondary networks. Furthermore, our proposed model and underlying assumptions demonstrate that Scenario B outperforms Scenario A in the SN, whereas in the PN, the reverse holds true. However, when employing conventional ZF BF, based on our assumptions for both the primary and secondary networks, Scenario A has superior performance compared to Scenario B.

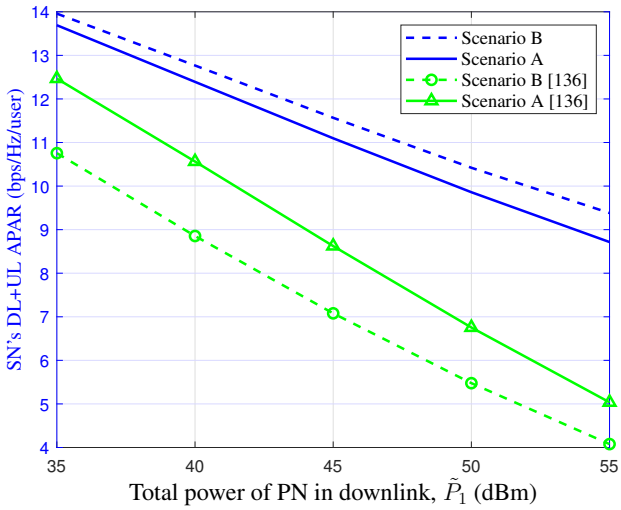

(a) DL+UL APARs of SN.

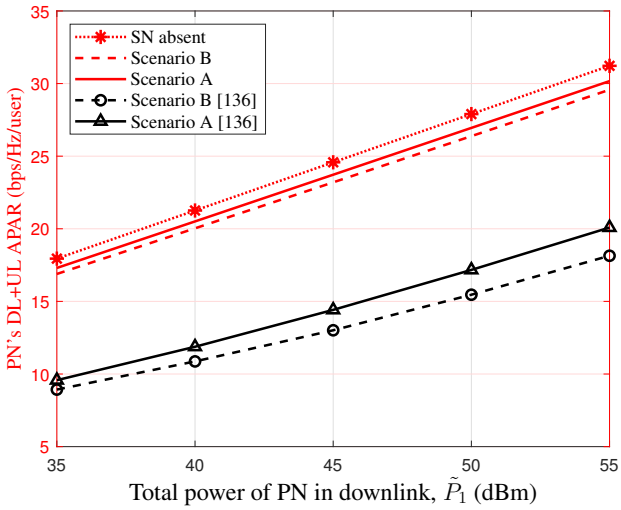

(b) DL+UL APARs of PN.

Figure 4.11: SN's and PN's APARs comparison in both scenarios versus total power of the PN, with $M_{\mathrm{p}} = 32$, $M_{\mathrm{s}} = 20$, $N_{\mathrm{p}} = 4$, $N_{\mathrm{s}} = 4$, $d_{\mathrm{p}} = 1000$ m, $d_{\mathrm{s}} = 500$ m, $\tilde{P}_2 = 20$ dBm, $\eta = 0.5$, $\rho = 0.9$.

Chapter 5

Conclusions and Future Work

In this chapter, we present a summary of the main results obtained in this dissertation and outline some potential directions for future research.

5.1 Conclusions

In Chapter 3 of this dissertation, we conduct an in-depth study on the joint power allocation and beamformer design problem for a single-cell wireless system comprising two multi-user networks. Each network consists of a base station, equipped with massive multi-input-multi-output (MIMO), located at its center, while all users in both networks are single-antenna devices. To enable underlay spectrum sharing (USS), we allow the secondary network (SN), the network with no exclusive frequency spectrum, to opportunistically utilize the spectrum holes of the primary network (PN), license owner of the frequency spectrum, as long as the constraints of both PN and SN are satisfied. In Scenario A, which followed the conventional time-division duplexing (C-TDD) approach, we examine the uplink (UL) and downlink (DL) states of both networks. The study considers the impact of perfect and imperfect channel state information (CSI), where the latter is estimated based on [76]. To minimize disrupting the PN and ensure seamless operation, the SN is required to listen to the PN during the learning phase [76] and to obtain essential information about the locations of the primary nodes and their channel states. Additionally, the PN's parameters are designed without consideration of

the SN's presence. To maximize the total SN's sum-rate and spectral efficiency of the whole network, we employ beamforming techniques for both the primary base station (PBS) and secondary base station (SBS), as well as USS to enhance both spatial and spectral diversity simultaneously. We formulate the total SN's sum-rate maximization problem in both UL and DL, while ensuring the primary users' (PU) individual rate constraints and SN power limitations is guaranteed. The optimization problems and their corresponding constraints can be easily separated and optimal solutions are proposed for each phase. Our solutions result in simplicity and computational efficiency. By employing a zero-forcing (ZF) type receive beamformer at the SN, the SBS is effectively protected from interference caused by the PN's nodes. Additionally, a ZF type transmit beamformer at the SN is designed to protect the PN's nodes, allowing the PN to function independently even in the presence of the SN. Numerical examples demonstrate that our proposed system model significantly increases average per-user achievable rate(APAR) in the presence of the SN, compared to the absence of the SN. Moreover, we observe that changing PN's parameters affects both PN and SN performances. However, altering the SN's parameters had no considerable impact on the PN's performance, mainly affecting the SN's performance in terms of APAR, as we thoroughly investigated. Furthermore, our numerical findings indicate that the performance of the two networks is not remarkably affected by the channel estimation errors.

In Chapter 4, we extend our investigation to the R-TDD mode while maintaining the same system model as in Chapter 3. The joint problem of power allocation and beamformer design is examined under this R-TDD approach, utilizing imperfect CSI as discussed in [76]. Just like in Chapter 3, the PBS shares some of the PN's information with the SBS. As a result, during the learning phase, the SN listens to the PN, gathering important information about the PN nodes. Beamforming techniques are employed for both PBS and SBS, leading to the formulation of the SN's sum-rate maximization problem in both UL and DL while satisfying the individual data rate constraints for PUs in both phases and SN power limitations. Noticeably, the UL and DL optimization prob-

Table 5.1: SN in Uplink

SN	**Scenario A**	**Scenario B**
DoF[a]	$M_{\mathrm{s}} - M_{\mathrm{p}}$	$M_{\mathrm{s}} - N_{\mathrm{p}}$
Affected PN Node[b]	PBS	PUs
Source of Interference (SoI)[c]	PUs (No BF[d])	PBS (BF)
Distance from the SoI[e]	PUs	PBS

[a] SBS Degrees of Freedom to serve SUs
[b] Which PN nodes may be affected by the interference caused from the SUs in each scenario.
[c] Interference caused by the PN to SBS in each scenario.
[d] Beamforming.
[e] Distance of SBS from the PN's SoI.

lems and their respective constraints can be readily separated, facilitating the provision of optimal solutions that are both simple and computationally efficient. In the R-TDD mode, the designed beamformers depend on the subspace spanned by the columns of the MIMO channel matrix between the base stations of the two networks. This approach eliminates the need for downlink training, resulting in improved spectral efficiency for both networks, It is demonstrated that the beamforming and power allocation at the PN are independent of those at the SN. Furthermore, our proposed R-TDD solution requires less cooperation between the PN and SN compared to the C-TDD mode solution. Through numerical experiments, we illustrate that our proposed R-TDD mode generally outperforms the C-TDD mode in terms of the SN's sum-rates. Similar to Chapter 3, our proposed system model significantly enhances spectral efficiency and APAR in the presence of the SN compared to the scenario without the SN. Moreover, variations in the PN's parameters impact both the PN and SN performances, whereas changes in the SN's parameters have minimal effects on the PN's performance, primarily affecting the SN's output in terms of APAR, as previously examined. Tables, 5.1 and 5.2, illustrate significant and comparable parameters of the SN in both UL and DL modes for scenarios A and B. These two tables provide us with information on the degrees of freedom, various

Table 5.2: SN in Downlink

SN	Scenario A	Scenario B
DoF	$M_{\mathrm{s}} - N_{\mathrm{p}}$	$M_{\mathrm{s}} - N_{\mathrm{p}}$
Affected PN Node[a]	PUs	PBS
SoI[b]	PBS (BF)	PUs (No BF)
Distance from the SoI[c]	PBS	PUs

[a] Which PN nodes may be affected by the interference caused from the SBS in each scenario.
[b] Interference caused by the PN to SUs in each scenario.
[c] Distance of SUs from the PN's SoI.

sources of interference, the PN node(s) that must be protected, and their distances from the sources of interference. This aids to track the simulation results easily.

5.2 Future Work

In this section, we outline some potential ways to extend this research:

5.2.1 Multi-Cell System Model

As a potential direction for future research, one could extend this dissertation's investigation from a single-cell wireless communication system to a multi-cell scenario, where the SN operates within the middle cell. This extension would enable the study of interference caused by all PN nodes on the SN nodes. Furthermore, it opens up the opportunity to explore the adverse effects of SN interference on the performance of the PBS and PUs within the middle cell and other neighboring cells. Such an analysis could provide crucial understandings into the complexities of managing spectrum sharing and interference in multi-cell wireless networks.

5.2.2 Multi-Antenna Users

In this study, we have concentrated on the analysis of two wireless communication networks where all users are single-antenna. One opportunity for further research would be to extend the current work by considering multi-antenna user nodes for just one network or both PN and SN. This extension could offer valuable insights into the potential benefits or drawbacks of employing multi-antenna users and its influence on the performances of the PN and SN in both scenarios A and B.

5.2.3 Multi-Carrier Networks

Extending the current research to a multi-carrier orthogonal frequency division multiplexing (OFDM) system holds significant potential for enriching our understanding of wireless communication networks. In the existing single-carrier model, we focused on the joint power allocation and beamforming design for two wireless networks with single-antenna users. By transitioning to a multi-carrier OFDM system, we can investigate the impact of frequency division on the overall performance of both PN and SN in different scenarios. Such an extension would enable us to explore the challenges and opportunities presented by the allocation of subcarriers and the efficient utilization of frequency resources in a single-cell or multi-cell setting. Additionally, studying the interference caused by all PN nodes on the SN nodes in the multi-carrier OFDM system would shed light on the trade-offs between network performance and interference management. Furthermore, we can assess the potential negative effects of SN interference on the PBS and PUs, providing meaningful knowledge into the system's spectral efficiency and capacity. This research extension has the potential to contribute significantly to the advancement of wireless communication networks and inform future design considerations for multi-carrier OFDM-based systems.

Bibliography

[1] A. Briones-Reyes, L. A. Vásquez-Toledo, A. Prieto-Guerrero, and R. Aguilar-Gonzalez, "Mathematical evaluation of spectrum sharing in cognitive radio networks for 5g systems using markov processes," *Computer Networks*, vol. 182, p. 107521, 2020.

[2] J. L. Frauendorf and É. Almeida de Souza, "The different architectures used in 1g, 2g, 3g, 4g, and 5g networks," in *The Architectural and Technological Revolution of 5G*. Springer, 2022, pp. 83–107.

[3] A. S. Shah, A. N. Qasim, M. A. Karabulut, H. Ilhan, and M. B. Islam, "Survey and performance evaluation of multiple access schemes for next-generation wireless communication systems," *IEEE Access*, vol. 9, pp. 113 428–113 442, 2021.

[4] I. Budhiraja, N. Kumar, S. Tyagi, S. Tanwar, Z. Han, M. J. Piran, and D. Y. Suh, "A systematic review on noma variants for 5g and beyond," *IEEE Access*, vol. 9, pp. 85 573–85 644, 2021.

[5] W. H. Chin, Z. Fan, and R. Haines, "Emerging technologies and research challenges for 5g wireless networks," *IEEE Wireless Communications*, vol. 21, no. 2, pp. 106–112, 2014.

[6] R. Zhang, M. Wang, L. X. Cai, Y. Cheng, X. Shen, and L.-L. Xie, "Resource management in sustainable green hetnets with renewable energy sources," *5G Mobile Communications*, pp. 503–529, 2017.

[7] L. Zhao, H. Zhao, K. Zheng, and W. Xiang, *Massive MIMO in 5G networks: selected applications*. Springer, 2018.

[8] S. Mattisson, "An overview of 5g requirements and future wireless networks: Accommodating scaling technology," *IEEE Solid-State Circuits Magazine*, vol. 10, no. 3, pp. 54–60, 2018.

[9] A. S. Shah, "A survey from 1g to 5g including the advent of 6g: architectures, multiple access techniques, and emerging technologies," in *2022 IEEE 12th Annual Computing and Communication Workshop and Conference (CCWC)*. IEEE, 2022, pp. 1117–1123.

[10] A. Dogra, R. K. Jha, and S. Jain, "A survey on beyond 5g network with the advent of 6g: Architecture and emerging technologies," *IEEE Access*, vol. 9, pp. 67 512–67 547, 2020.

[11] M. Sakai, K. Kamohara, H. Iura, H. Nishimoto, K. Ishioka, Y. Murata, M. Yamamoto, A. Okazaki, N. Nonaka, S. Suyama *et al.*, "Experimental field trials on mu-mimo transmissions for high shf wide-band massive mimo in 5g," *IEEE transactions on wireless communications*, vol. 19, no. 4, pp. 2196–2207, 2020.

[12] L. Chettri and R. Bera, "A comprehensive survey on internet of things (iot) toward 5g wireless systems," *IEEE Internet of Things Journal*, vol. 7, no. 1, pp. 16–32, 2019.

[13] R. Hussain, "Shared-aperture slot-based sub-6-ghz and mm-wave iot antenna for 5g applications," *IEEE Internet of Things Journal*, vol. 8, no. 13, pp. 10 807–10 814, 2021.

[14] R. Kaur, A. S. Buttar, and J. Anand, "Spectrum sharing schemes in cognitive radio network: A survey," in *2018 Second International Conference on Electronics, Communication and Aerospace Technology (ICECA)*. IEEE, 2018, pp. 1279–1284.

[15] A. Gupta and R. K. Jha, "A survey of 5g network: Architecture and emerging technologies," *IEEE access*, vol. 3, pp. 1206–1232, 2015.

[16] F. Jameel, M. A. A. Haider, A. A. Butt *et al.*, "Massive mimo: A survey of recent advances, research issues and future directions," in *2017 International Symposium on Recent Advances in Electrical Engineering (RAEE)*. IEEE, 2017, pp. 1–6.

[17] E. Björnson, J. Hoydis, M. Kountouris, and M. Debbah, "Massive mimo systems with non-ideal hardware: Energy efficiency, estimation, and capacity limits," *IEEE Transactions on information theory*, vol. 60, no. 11, pp. 7112–7139, 2014.

[18] E. Björnson, L. Sanguinetti, J. Hoydis, and M. Debbah, "Designing multi-user mimo for energy efficiency: When is massive mimo the answer?" in *2014 IEEE wireless communications and networking conference (WCNC)*. IEEE, 2014, pp. 242–247.

[19] ——, "Optimal design of energy-efficient multi-user mimo systems: Is massive mimo the answer?" *IEEE Transactions on wireless communications*, vol. 14, no. 6, pp. 3059–3075, 2015.

[20] K. S. V. Prasad, E. Hossain, and V. K. Bhargava, "Energy efficiency in massive mimo-based 5g networks: Opportunities and challenges," *IEEE Wireless Communications*, vol. 24, no. 3, pp. 86–94, 2017.

[21] G. J. Foschini, "Layered space-time architecture for wireless communication in a fading environment when using multi-element antennas," *Bell labs technical journal*, vol. 1, no. 2, pp. 41–59, 1996.

[22] R. Chataut and R. Akl, "Massive mimo systems for 5g and beyond networksoverview, recent trends, challenges, and future research direction," *Sensors*, vol. 20, no. 10, p. 2753, 2020.

[23] K. Zheng, S. Ou, X. Yin *et al.*, "Massive mimo channel models: A survey," *International Journal of Antennas and Propagation*, vol. 2014, 2014.

[24] G. N. Kamga, M. Xia, and S. Aïssa, "Spectral-efficiency analysis of massive mimo systems in centralized and distributed schemes," *IEEE Transactions on Communications*, vol. 64, no. 5, pp. 1930–1941, 2016.

[25] P. Rayi and M. Prasad, "Optimization of energy and spectral efficiency of massive mimo-small cell system," in *2015 International Conference on Smart Technologies and Management for Computing, Communication, Controls, Energy and Materials (ICSTM)*. IEEE, 2015, pp. 233–238.

[26] Y. Lin, X. Li, W. Fu, and Y. Hei, "Spectral efficiency analysis for downlink massive mimo systems with mrt precoding," *China Communications*, vol. 12, no. Supplement, pp. 67–73, 2015.

[27] A. Ashikhmin, T. L. Marzetta, and L. Li, "Interference reduction in multi-cell massive mimo systems i: Large-scale fading precoding and decoding," *arXiv preprint arXiv:1411.4182*, 2014.

[28] D. C. Araújo, T. Maksymyuk, A. L. de Almeida, T. Maciel, J. C. Mota, and M. Jo, "Massive mimo: survey and future research topics," *Iet Communications*, vol. 10, no. 15, pp. 1938–1946, 2016.

[29] K. K. Vaigandla and D. N. Venu, "Survey on massive mimo: Technology, challenges, opportunities and benefits," 2021.

[30] Y. Wang and D. Hu, "A left-null-space-based massive access method for cell-free massive mimo iot systems," *Sensors*, vol. 23, no. 11, p. 5285, 2023.

[31] H. Q. Ngo, A. Ashikhmin, H. Yang, E. G. Larsson, and T. L. Marzetta, "Cell-free massive mimo versus small cells," *IEEE Transactions on Wireless Communications*, vol. 16, no. 3, pp. 1834–1850, 2017.

[32] H. Yang and T. L. Marzetta, "Performance of conjugate and zero-forcing beamforming in large-scale antenna systems," *IEEE Journal on Selected Areas in Communications*, vol. 31, no. 2, pp. 172–179, 2013.

[33] H. M. Al-Obiedollah, K. Cumanan, J. Thiyagalingam, A. G. Burr, Z. Ding, and O. A. Dobre, "Energy efficient beamforming design for miso non-orthogonal multiple access systems," *IEEE Transactions on Communications*, vol. 67, no. 6, pp. 4117–4131, 2019.

[34] M. C. Tan, M. Li, Q. H. Abbasi, and M. A. Imran, "A wideband beamforming antenna array for 802.11 ac and 4.9 ghz in modern transportation market," *IEEE Transactions on Vehicular Technology*, vol. 69, no. 3, pp. 2659–2670, 2019.

[35] E. J. Black, B. M. Deutsch, R. J. Hannigan, A. R. Katko, M. Machado, J. H. McCandless, and Y. A. Urzhumov, "Methods and systems for communication with beamforming antennas," Mar. 17 2020, uS Patent 10,595,210.

[36] E. Ali, M. Ismail, R. Nordin, and N. F. Abdulah, "Beamforming techniques for massive mimo systems in 5g: overview, classification, and trends for future research," *Frontiers of Information Technology & Electronic Engineering*, vol. 18, pp. 753–772, 2017.

[37] T. S. Priya, K. Manish, and P. Prakasam, "Hybrid beamforming for massive mimo using rectangular antenna array model in 5g wireless networks," *Wireless Personal Communications*, vol. 120, pp. 2061–2083, 2021.

[38] S. Pandit and G. Singh, "An overview of spectrum sharing techniques in cognitive radio communication system," *Wireless Networks*, vol. 23, pp. 497–518, 2017.

[39] L. Zhang, M. Xiao, G. Wu, M. Alam, Y.-C. Liang, and S. Li, "A survey of advanced techniques for spectrum sharing in 5g networks," *IEEE Wireless Communications*, vol. 24, no. 5, pp. 44–51, 2017.

[40] C. Yang, J. Li, M. Guizani, A. Anpalagan, and M. Elkashlan, "Advanced spectrum sharing in 5g cognitive heterogeneous networks," *IEEE Wireless Communications*, vol. 23, no. 2, pp. 94–101, 2016.

[41] A. Goldsmith, S. A. Jafar, I. Maric, and S. Srinivasa, "Breaking spectrum gridlock with cognitive radios: An information theoretic perspective," *Proceedings of the IEEE*, vol. 97, no. 5, pp. 894–914, 2009.

[42] Q. Zhao and B. M. Sadler, "A survey of dynamic spectrum access," *IEEE signal processing magazine*, vol. 24, no. 3, pp. 79–89, 2007.

[43] L. Luo, P. Zhang, G. Zhang, and J. Qin, "Outage performance for cognitive relay networks with underlay spectrum sharing," *IEEE Communications letters*, vol. 15, no. 7, pp. 710–712, 2011.

[44] S. Srinivasa and S. A. Jafar, "Cognitive radios for dynamic spectrum access-the throughput potential of cognitive radio: A theoretical perspective," *IEEE Communications Magazine*, vol. 45, no. 5, pp. 73–79, 2007.

[45] P. K. Sharma, P. K. Upadhyay, D. B. da Costa, P. S. Bithas, and A. G. Kanatas, "Performance analysis of overlay spectrum sharing in hybrid satellite-terrestrial systems with secondary network selection," *IEEE Transactions on Wireless Communications*, vol. 16, no. 10, pp. 6586–6601, 2017.

[46] S. M. Baby and M. James, "A comparative study on various spectrum sharing techniques," *Procedia Technology*, vol. 25, pp. 613–620, 2016.

[47] L. Li, F. A. Khan, M. Pesavento, and T. Ratnarajah, "Power allocation and beamforming in overlay cognitive radio systems," in *2011 IEEE 73rd Vehicular Technology Conference (VTC Spring)*. IEEE, 2011, pp. 1–5.

[48] S. D. Sumithra and E. A. Shirly, "Interweave dynamic spectrum sharing for cognitive adhoc networks usinggenetic optimization algorithm," in *2021 IEEE 4th*

International Conference on Computing, Power and Communication Technologies (GUCON). IEEE, 2021, pp. 1–6.

[49] D. Li, J. Cheng, and V. C. Leung, "Adaptive spectrum sharing for half-duplex and full-duplex cognitive radios: From the energy efficiency perspective," *IEEE Transactions on Communications*, vol. 66, no. 11, pp. 5067–5080, 2018.

[50] L. Wan, Z. Guo, Y. Wu, W. Bi, J. Yuan, M. Elkashlan, and L. Hanzo, "4g\/5g spectrum sharing: efficient 5g deployment to serve enhanced mobile broadband and internet of things applications," *ieee vehicular technology magazine*, vol. 13, no. 4, pp. 28–39, 2018.

[51] W. S. H. M. W. Ahmad, N. A. M. Radzi, F. Samidi, A. Ismail, F. Abdullah, M. Z. Jamaludin, and M. Zakaria, "5g technology: Towards dynamic spectrum sharing using cognitive radio networks," *IEEE access*, vol. 8, pp. 14 460–14 488, 2020.

[52] R. Esmailzadeh, E. Sourour, and M. Nakagawa, "Prerake diversity combining in time-division duplex cdma mobile communications," *IEEE Transactions on Vehicular Technology*, vol. 48, no. 3, pp. 795–801, 1999.

[53] G. Xu and H. Liu, "An effective transmission beamforming scheme for frequency-division-duplex digital wireless communication systems," in *1995 International Conference on Acoustics, Speech, and Signal Processing*, vol. 3. IEEE, 1995, pp. 1729–1732.

[54] L. Chang and T. Hsing, "Technologies i: Narrowband transmissions," *Handbook of Visual Communications*, p. 421, 1995.

[55] H. Wymeersch and A. Eryilmaz, "Multiple access control in wireless networks," in *Academic Press Library in Mobile and Wireless Communications*. Elsevier, 2016, pp. 435–465.

[56] A. Grami, "Communication networks," *Introduction To Digital Communications*, pp. 457–491, 2016.

[57] L. E. Frenzel, *Electronics Explained: Fundamentals for Engineers, Technicians, and Makers*. Newnes, 2017.

[58] W. S. Jeon and D. G. Jeong, "Comparison of time slot allocation strategies for cdma/tdd systems," *IEEE Journal on Selected Areas in Communications*, vol. 18, no. 7, pp. 1271–1278, 2000.

[59] Y. S. Choi, I. Sohn, and K. B. Lee, "A novel decentralized time slot allocation algorithm in dynamic tdd system," in *CCNC 2006. 2006 3rd IEEE Consumer Communications and Networking Conference, 2006.*, vol. 2. IEEE, 2006, pp. 1268–1272.

[60] H. Minn and A. Khansefid, "Massive mimo systems in noncontiguous bands with asymmetric traffics," *IEEE Transactions on Wireless Communications*, vol. 15, no. 7, pp. 4689–4702, 2016.

[61] H. Celik, "On the performance of dynamic tdd in ultra-dense wireless access networks," Ph.D. dissertation, KTH Royal Institute of Technology, 2017.

[62] A. Hatahet and A. Jain, "Beamforming in lte fdd for multiple antenna systems," 2018.

[63] P. W. Chan, E. S. Lo, R. R. Wang, E. K. Au, V. K. Lau, R. S. Cheng, W. H. Mow, R. D. Murch, and K. B. Letaief, "The evolution path of 4g networks: Fdd or tdd?" *IEEE Communications Magazine*, vol. 44, no. 12, pp. 42–50, 2006.

[64] M. Sauter, *From GSM to LTE: an introduction to mobile networks and mobile broadband*. John Wiley & Sons, 2010.

[65] M. Tolstrup, *Indoor radio planning: a practical guide for GSM, DCS, UMTS, HSPA and LTE*. John Wiley & Sons, 2011.

[66] O. Al-Saadeh and K. W. Sung, "A performance comparison of in-band full duplex and dynamic tdd for 5g indoor wireless networks," *EURASIP Journal on Wireless Communications and Networking*, vol. 2017, pp. 1–14, 2017.

[67] F. Rezaei, A. R. Heidarpour, C. Tellambura, and A. Tadaion, "Underlaid spectrum sharing for cell-free massive mimo-noma," *IEEE Communications Letters*, vol. 24, no. 4, pp. 907–911, 2020.

[68] L. Wang, H. Q. Ngo, M. Elkashlan, T. Q. Duong, and K.-K. Wong, "Massive mimo in spectrum sharing networks: Achievable rate and power efficiency," *IEEE Systems Journal*, vol. 11, no. 1, pp. 20–31, 2015.

[69] X. Zhang, H. Qi, X. Zhang, and L. Han, "Spectral efficiency improvement and power control optimization of massive mimo networks," *IEEE Access*, vol. 9, pp. 11 523–11 532, 2021.

[70] F. Rusek, D. Persson, B. K. Lau, E. G. Larsson, T. L. Marzetta, O. Edfors, and F. Tufvesson, "Scaling up mimo: Opportunities and challenges with very large arrays," *IEEE signal processing magazine*, vol. 30, no. 1, pp. 40–60, 2012.

[71] J. Nam, J.-Y. Ahn, A. Adhikary, and G. Caire, "Joint spatial division and multiplexing: Realizing massive mimo gains with limited channel state information," in *2012 46th annual conference on information sciences and systems (CISS)*. IEEE, 2012, pp. 1–6.

[72] E. G. Larsson, O. Edfors, F. Tufvesson, and T. L. Marzetta, "Massive mimo for next generation wireless systems," *IEEE communications magazine*, vol. 52, no. 2, pp. 186–195, 2014.

[73] M. Cui, B.-J. Hu, J. Tang, and Y. Wang, "Energy-efficient joint power allocation in uplink massive mimo cognitive radio networks with imperfect csi," *IEEE Access*, vol. 5, pp. 27 611–27 621, 2017.

[74] X. Chen and C. Yuen, "Efficient resource allocation in a rateless-coded mu-mimo cognitive radio network with qos provisioning and limited feedback," *IEEE transactions on vehicular technology*, vol. 62, no. 1, pp. 395–399, 2012.

[75] S. Chaudhari and D. Cabric, "QoS aware power allocation and user selection in massive MIMO underlay cognitive radio networks," *IEEE Transactions on Cognitive Communications and Networking*, vol. 4, no. 2, pp. 220–231, 2018.

[76] Z. Pourgharehkhan, S. ShahbazPanahi, M. Bavand, and G. Boudreau, "Channel estimation for spectrum sharing in massive MIMO," *submitted to IEEE Transactions on Cognitive Communications and Networking*, 2022.

[77] R. Saif, Z. Pourgharehkhan, S. ShahbazPanahi, M. Bavand, and G. Boudreau, "Underlay spectrum sharing in massive mimo systems," *IEEE Transactions on Cognitive Communications and Networking*, 2023.

[78] K. Thompson, D. Ritchie, B. Kernighan, D. McIlroy *et al.*, "open-source. uia. web. id 17 hours information services," *History*, vol. 2, no. 2.2, p. 1980s, 1970.

[79] F. Tobagi and L. Kleinrock, "Packet switching in radio channels: Part iii-polling and (dynamic) split-channel reservation multiple access," *IEEE Transactions on Communications*, vol. 24, no. 8, pp. 832–845, 1976.

[80] D. S. ROUP, “Mobile multiple access study,” 1977.

[81] D. Gesbert, M. Kountouris, R. W. Heath, C.-B. Chae, and T. Salzer, “Shifting the mimo paradigm,” *IEEE signal processing magazine*, vol. 24, no. 5, pp. 36–46, 2007.

[82] X. Wang *et al.*, *Wireless communication systems: Advanced techniques for signal reception*. Pearson Education India, 2009.

[83] R. Mahmoudi and K. Iniewski, *Low power emerging wireless technologies*. CRC Press, 2013.

[84] G. Dueck, “Maximal error capacity regions are smaller than average error capacity regions for multi-user channels.” 1978.

[85] D. Tse and P. Viswanath, *Fundamentals of wireless communication*. Cambridge university press, 2005.

[86] A. Chockalingam and B. S. Rajan, *Large MIMO systems*. Cambridge University Press, 2014.

[87] N. R. Challa and K. P. Bagadi, “Design of massive multiuser mimo system to mitigate inter antenna interference and multiuser interference in 5g wireless networks.” *J. Commun.*, vol. 15, no. 9, pp. 693–701, 2020.

[88] F. Meng, P. Chen, and L. Wu, “Power allocation in multi-user cellular networks with deep q learning approach,” in *ICC 2019-2019 IEEE International Conference on Communications (ICC)*. IEEE, 2019, pp. 1–6.

[89] A. A. Khan, R. S. Adve, and W. Yu, “Optimizing downlink resource allocation in multiuser mimo networks via fractional programming and the hungarian algorithm,” *IEEE Transactions on Wireless Communications*, vol. 19, no. 8, pp. 5162–5175, 2020.

[90] N. Akbar, N. Yang, P. Sadeghi, and R. A. Kennedy, “Multi-cell multiuser massive mimo networks: User capacity analysis and pilot design,” *IEEE Transactions on Communications*, vol. 64, no. 12, pp. 5064–5077, 2016.

[91] B. Ning, G. Sun, J. Li, A. Zhang, W. Hao, and S. Yang, “Resource allocation in multi-user cognitive radio network with stackelberg game,” *IEEE Access*, vol. 8, pp. 58 260–58 270, 2020.

[92] X. Wang, S. Ekin, and E. Serpedin, "Joint spectrum sensing and resource allocation in multi-band-multi-user cognitive radio networks," *IEEE Transactions on Communications*, vol. 66, no. 8, pp. 3281–3293, 2018.

[93] C.-X. Wang, F. Haider, X. Gao, X.-H. You, Y. Yang, D. Yuan, H. M. Aggoune, H. Haas, S. Fletcher, and E. Hepsaydir, "Cellular architecture and key technologies for 5g wireless communication networks," *IEEE communications magazine*, vol. 52, no. 2, pp. 122–130, 2014.

[94] S. Haykin, "Cognitive radio: brain-empowered wireless communications," *IEEE journal on selected areas in communications*, vol. 23, no. 2, pp. 201–220, 2005.

[95] S. Stotas and A. Nallanathan, "Enhancing the capacity of spectrum sharing cognitive radio networks," *IEEE Transactions on Vehicular Technology*, vol. 60, no. 8, pp. 3768–3779, 2011.

[96] A. M. Voicu, L. Simić, and M. Petrova, "Survey of spectrum sharing for inter-technology coexistence," *IEEE Communications Surveys & Tutorials*, vol. 21, no. 2, pp. 1112–1144, 2018.

[97] J. Mitola, "Cognitive radio. an integrated agent architecture for software defined radio." 2002.

[98] I. F. Akyildiz, W.-Y. Lee, M. C. Vuran, and S. Mohanty, "A survey on spectrum management in cognitive radio networks," *IEEE Communications magazine*, vol. 46, no. 4, pp. 40–48, 2008.

[99] ——, "Next generation/dynamic spectrum access/cognitive radio wireless networks: A survey," *Computer networks*, vol. 50, no. 13, pp. 2127–2159, 2006.

[100] K. J. Kim, L. Wang, T. Q. Duong, M. Elkashlan, and H. V. Poor, "Cognitive single-carrier systems: Joint impact of multiple licensed transceivers," *IEEE Transactions on Wireless Communications*, vol. 13, no. 12, pp. 6741–6755, 2014.

[101] G. Ding, J. Wang, Q. Wu, Y.-D. Yao, R. Li, H. Zhang, and Y. Zou, "On the limits of predictability in real-world radio spectrum state dynamics: From entropy theory to 5G spectrum sharing," *IEEE Communications Magazine*, vol. 53, no. 7, pp. 178–183, 2015.

[102] F. Hu, B. Chen, and K. Zhu, "Full spectrum sharing in cognitive radio networks toward 5G: A survey," *IEEE Access*, vol. 6, pp. 15 754–15 776, 2018.

[103] A. M. Wyglinski, M. Nekovee, and T. Hou, *Cognitive radio communications and networks: principles and practice*. Academic Press, 2009.

[104] Y. Teng, Y. Zhang, C. Dai, F. Yang, and M. Song, "Dynamic spectrum sharing through double auction mechanism in cognitive radio networks," in *2011 IEEE Wireless Communications and Networking Conference*. IEEE, 2011, pp. 90–95.

[105] O. Amin, W. Abediseid, and M.-S. Alouini, "Overlay spectrum sharing using improper gaussian signaling," *IEEE Journal on Selected Areas in Communications*, vol. 35, no. 1, pp. 50–62, 2016.

[106] M. D. Mueck, S. Srikanteswara, and B. Badic, "Spectrum sharing: Licensed shared access (lsa) and spectrum access system (sas)," *Intel White Paper*, pp. 1–26, 2015.

[107] S. Bhattarai, J.-M. J. Park, B. Gao, K. Bian, and W. Lehr, "An overview of dynamic spectrum sharing: Ongoing initiatives, challenges, and a roadmap for future research," *IEEE Transactions on Cognitive Communications and Networking*, vol. 2, no. 2, pp. 110–128, 2016.

[108] S. K. Sharma, T. E. Bogale, L. B. Le, S. Chatzinotas, X. Wang, and B. Ottersten, "Dynamic spectrum sharing in 5g wireless networks with full-duplex technology: Recent advances and research challenges," *IEEE Communications Surveys & Tutorials*, vol. 20, no. 1, pp. 674–707, 2017.

[109] H. Wang, J. Wang, G. Ding, Z. Xue, L. Zhang, and Y. Xu, "Robust spectrum sharing in air-ground integrated networks: Opportunities and challenges," *IEEE Wireless Communications*, vol. 27, no. 3, pp. 148–155, 2020.

[110] T. L. Marzetta, "Noncooperative cellular wireless with unlimited numbers of base station antennas," *IEEE transactions on wireless communications*, vol. 9, no. 11, pp. 3590–3600, 2010.

[111] T. L. Marzetta and B. M. Hochwald, "Capacity of a mobile multiple-antenna communication link in rayleigh flat fading," *IEEE transactions on Information Theory*, vol. 45, no. 1, pp. 139–157, 1999.

[112] B. M. Hochwald and T. L. Marzetta, "Multiple antenna communication system and method thereof," May 2 2000, uS Patent 6,058,105.

[113] E. Björnson, E. G. Larsson, and M. Debbah, "Massive mimo for maximal spectral efficiency: How many users and pilots should be allocated?" *IEEE Transactions on Wireless Communications*, vol. 15, no. 2, pp. 1293–1308, 2015.

[114] E. Björnson, L. Sanguinetti, H. Wymeersch, J. Hoydis, and T. L. Marzetta, "Massive mimo is a realitywhat is next?: Five promising research directions for antenna arrays," *Digital Signal Processing*, vol. 94, pp. 3–20, 2019.

[115] M. A. Albreem, M. Juntti, and S. Shahabuddin, "Massive MIMO detection techniques: A survey," *IEEE Communications Surveys & Tutorials*, vol. 21, no. 4, pp. 3109–3132, 2019.

[116] T. L. Marzetta and H. Q. Ngo, *Fundamentals of massive MIMO*. Cambridge University Press, 2016.

[117] E. Björnson, J. Hoydis, and L. Sanguinetti, "Massive MIMO networks: Spectral, energy, and hardware efficiency," *Foundations and Trends in Signal Processing*, vol. 11, no. 3-4, pp. 154–655, 2017.

[118] S. Elhoushy, M. Ibrahim, and W. Hamouda, "Cell-free massive mimo: A survey," *IEEE Communications Surveys & Tutorials*, vol. 24, no. 1, pp. 492–523, 2021.

[119] Z. Gao, L. Dai, D. Mi, Z. Wang, M. A. Imran, and M. Z. Shakir, "Mmwave massive-mimo-based wireless backhaul for the 5g ultra-dense network," *IEEE Wireless communications*, vol. 22, no. 5, pp. 13–21, 2015.

[120] Q. Li, G. Li, W. Lee, M.-i. Lee, D. Mazzarese, B. Clerckx, and Z. Li, "Mimo techniques in wimax and lte: a feature overview," *IEEE Communications magazine*, vol. 48, no. 5, pp. 86–92, 2010.

[121] J. Vieira, S. Malkowsky, K. Nieman, Z. Miers, N. Kundargi, L. Liu, I. Wong, V. Öwall, O. Edfors, and F. Tufvesson, "A flexible 100-antenna testbed for massive mimo," in *2014 IEEE Globecom Workshops (GC Wkshps)*. IEEE, 2014, pp. 287–293.

[122] C. Shepard, H. Yu, N. Anand, E. Li, T. Marzetta, R. Yang, and L. Zhong, "Argos: Practical many-antenna base stations," in *Proceedings of the 18th annual international conference on Mobile computing and networking*, 2012, pp. 53–64.

[123] M. Zhou, J. Li, J. Yuan, M. Xie, W. Tan, R. Yin, and L. Yang, "An architecture for aoi and cache hybrid multicast/unicast/d2d with cell-free massive mimo systems," *IEEE Access*, 2023.

[124] J.-H. Lee and O.-S. Shin, "Full-duplex relay based on zero-forcing beamforming," *IEICE transactions on communications*, vol. 94, no. 4, pp. 978–985, 2011.

[125] T. Yoo and A. Goldsmith, "On the optimality of multiantenna broadcast scheduling using zero-forcing beamforming," *IEEE Journal on selected areas in communications*, vol. 24, no. 3, pp. 528–541, 2006.

[126] ——, "Optimality of zero-forcing beamforming with multiuser diversity," in *IEEE International Conference on Communications, 2005. ICC 2005. 2005*, vol. 1. IEEE, 2005, pp. 542–546.

[127] G. Caire and S. Shamai, "On the achievable throughput of a multiantenna gaussian broadcast channel," *IEEE Transactions on Information Theory*, vol. 49, no. 7, pp. 1691–1706, 2003.

[128] T. V. T. Le and Y. H. Kim, "Power and spectral efficiency of multi-pair massive antenna relaying systems with zero-forcing relay beamforming," *IEEE Communications Letters*, vol. 19, no. 2, pp. 243–246, 2014.

[129] S. Timotheou, I. Krikidis, G. Zheng, and B. Ottersten, "Beamforming for miso interference channels with qos and rf energy transfer," *IEEE Transactions on Wireless Communications*, vol. 13, no. 5, pp. 2646–2658, 2014.

[130] L. Wang, H. Q. Ngo, M. Elkashlan, T. Q. Duong, and K.-K. Wong, "Massive MIMO in spectrum sharing networks: Achievable rate and power efficiency," *IEEE Systems Journal*, vol. 11, no. 1, pp. 20–31, 2015.

[131] Y. Li, D. Kudathanthirige, and G. A. A. Baduge, "Massive MIMO relay networks with underlay spectrum sharing," *IEEE Transactions on Cognitive Communications and Networking*, vol. 4, no. 4, pp. 677–691, 2018.

[132] W. Hao, O. Muta, H. Gacanin, and H. Furukawa, "Power allocation for massive MIMO cognitive radio networks with pilot sharing under SINR requirements of primary users," *IEEE Transactions on Vehicular Technology*, vol. 67, no. 2, pp. 1174–1186, 2017.

[133] H. Al-Hraishawi, G. A. A. Baduge, H. Q. Ngo, and E. G. Larsson, "Multi-cell massive MIMO uplink with underlay spectrum sharing," *IEEE Transactions on Cognitive Communications and Networking*, vol. 5, no. 1, pp. 119–137, 2018.

[134] Y. Li and G. A. A. Baduge, "Underlay spectrum-sharing massive MIMO NOMA," *IEEE Communications Letters*, vol. 23, no. 1, pp. 116–119, 2018.

[135] H. Xie, B. Wang, F. Gao, and S. Jin, "A full-space spectrum-sharing strategy for massive MIMO cognitive radio systems," *IEEE Journal on Selected Areas in Communications*, vol. 34, no. 10, pp. 2537–2549, 2016.

[136] D. Kudathanthirige and G. A. A. Baduge, "Reverse TDD-based massive MIMO systems with underlay spectrum sharing," *IEEE Transactions on Wireless Communications*, vol. 18, no. 6, pp. 3142–3160, 2019.

[137] H. Q. Ngo and E. G. Larsson, "No downlink pilots are needed in TDD massive MIMO," *IEEE Transactions on Wireless Communications*, vol. 16, no. 5, pp. 2921–2935, 2017.

[138] J. Niu, G. Y. Li, X. Chen, J. Zheng, D. Fang, and X. Li, "Resource allocation in reverse TDD wireless backhaul HetNets with 3D massive antennas," *IEEE wireless communications letters*, vol. 7, no. 1, pp. 30–33, 2017.

[139] A. Goldsmith, *Wireless communications*.

[140] S. S. Haykin, *Adaptive filter theory*. Pearson Education India, 2002.

[141] S. P. Boyd and L. Vandenberghe, *Convex optimization*. Cambridge university press, 2004.

[142] H. Holma and A. Toskala, *LTE for UMTS: OFDMA and SC-FDMA based radio access*. John Wiley & Sons, 2009.